ELASTICALLY OPERATING LEGS – STRATEGIES AND CONSTRUCTION PRINCIPLES

ELASTISCH ARBEITENDE BEINE - STRATEGIEN UND BAUPRINZIPIEN

Dissertation

zur Erlangung des akademischen Grades

doctor philosophiae (Dr. phil.)

vorgelegt dem Rat der Fakultät für Sozial- und Verhaltenswissenschaften

der Friedrich-Schiller Universität Jena

von André Seyfarth
geboren am 23. März 1970 in Frankfurt (Oder)

Gutachter

1. Prof. Dr. R. Blickhan

2. Prof. Dr. J. L. van Leeuwen

3. Prof. Dr. G. Kluge

Tag des Kolloquiums:

SUMMARY. In this thesis the mechanisms and advantages of spring-like leg operation were investigated. By examining the long jump the general dynamic was described using a hierarchy of simple models taking salient mechanical and muscle-physiological properties into account.

1 GLOBAL SYSTEM PROPERTIES AND THE TIME COURSE OF THE GROUND REACTION FORCE. The shape of the ground reaction force in the long jump is characterised by two clearly separated peaks (Seyfarth et al., 1999). The first **passive peak** takes about $30 - 40$ ms. A comparison of models including distal masses (chapter II and V) and taking muscle properties (stretch enhancement etc., chapter IV and V) into account revealed that this peak is largely generated by deceleration of distal leg masses (soft and bony tissues) during heel strike. Contributions of muscle forces were only minor. The lumped parameters belonging to the distal mass are the result of an adequate description of the time course of the ground reaction force. Nonlinear visco-elastic coupling of distal masses to the skeleton proved to be necessary and represented passive muscle properties, the properties of the heel pad and the deformation of the foot and joints. The **active peak** ($30 - 90$ % of contact time) is characterised by a surprisingly constant leg stiffness with variations of merely 7%. Constant leg stiffness is achieved by synchronous bending of ankle and knee joint. At the joint level, during leg shortening an increase in force of the muscle-tendon complex and during lengthening a decrease is required.

2 CONTRIBUTIONS OF MUSCLE PROPERTIES TO THE LEG OPERATION. The continuous **increase in muscle force** can be attributed to an increase of activation level, the increased force due to muscle lengthening (force-length dependency) and the consequent continuos loading of the tendon and aponeurosis in series. During unloading **decrease in ground reaction force** was achieved by reducing muscle force due to increasing shortening velocity (force-velocity relationship) and muscle shortening (force-length dependency). Thereby, the shortening serial elastic element prolonged the phase of eccentric muscle operation and allowed the highest muscle forces to occur at about midstance. Performance depends on the ability of eccentric force generation. The **elastic behaviour of the system** is a result of fast loading of the muscle-tendon complex and is largely limited by muscle properties (force-length and force-velocity curve). It does not require a sophisticated neural program. In the case of the four-segment model elastic behaviour originated from internal properties and emerged during muscle activation optimised for maximum jumping distances.

3 JUMPING PERFORMANCE AND TECHNIQUES. Taking internal system properties into account a quasi-elastic operation is the optimal strategy for long jumping distances. The elastic behaviour is achieved by synchronous loading of knee and ankle joint (chapter V). To achieve optimal jumping distance at given run-up speed a **minimal leg stiffness** had to be exceeded. Similar results can be obtained by compensating a lower stiffness with a smaller angle of attack (chapter II). The observed strategies (angle of attack and of take-off; Friedrichs et al., in prep.) can only be understood by considering the included muscle properties (chapter IV and V). For such a system the optimal angle of attack is independent of running speed.

4 ADJUSTMENT AND STABILITY OF A DYNAMICALLY LOADED THREE SEGMENTED LEG. Adding a **third leg segment** (like a foot) to a leg consisting of shank and thigh reduces the torque requirements at joint level and the kinetic energy associated with transverse leg segment movements. Simultaneously, it imposes the problems of kinematic redundancy, potential instability and muscular coordination. Optimised leg operation with respect to jumping performance (chapter V), leg stiffness or stability requires a homogeneous bending of both leg joints achieved by rotational stiffnesses adapted to the outer segment lengths (foot and thigh length; chapter III). Nonlinear rotational stiffness behaviour and biarticular structures are alternative (replaceable) strategies to fulfill a safe leg operation for a wide range of initial joint configurations. A short foot with the option of heel contact is a powerful construction to control almost stretched knee positions if elastic joint behaviour is present. By using more flexed ankle joints and an adapted stiffness design the range of safe leg flexion can be extended.

ZUSAMMENFASSUNG. In dieser Dissertation wurden die Mechanismen und Vorteile federartig arbeitender Beine untersucht. Am Beispiel des Weitsprunges wurde die grundlegende Dynamik in einer Hierarchie einfacher mechanischer und muskelphysiologischer Modelle beschrieben.

1 GLOBALE SYSTEMEIGENSCHAFTEN UND DER ZEITLICHE VERLAUF DER BODENREAKTIONSKRAFT. Der Verlauf der Bodenreaktionskraft beim Weitsprung zeichnet sich durch zwei deutlich getrennte Kraftstöße aus (Seyfarth et al., 1999). Der erste **passive Kraftstoß** dauert etwa 30 − 40 ms. Ein Vergleich der Modelle mit distalen Massen (Kapitel II und V) bzw. mit Berücksichtigung von Muskeleigenschaften (Krafterhöhung bei Dehnung usw., Kapitel IV und V) zeigte, daß dieser Kraftstoß maßgeblich durch die Abbremsung distaler Massen (weiche und harte Gewebe) während des Fersenkontaktes hervorgerufen wird. Die Beiträge der Muskelkräfte waren lediglich von untergeordneter Bedeutung. Die Parameter zur Beschreibung der distalen Masse sind das Ergebnis einer angemessenen Beschreibung des Verlaufes der Bodenreaktionskraft. Hierbei war eine nichtlineare viskoelastische Ankopplung der distalen Massen an das Skelett notwendig, welche die passiven Muskeleigenschaften, Eigenschaften des Fersenpolsters sowie die Verformung des Fußes sowie der Gelenke widerspiegelte. Der **aktive Kraftstoß** (30 − 90 % des Kontaktzeit) ist gekennzeichnet durch eine erstaunlich konstante Beinsteifigkeit mit Schwankungen von lediglich 7%. Die konstante Steifigkeit wird erreicht durch eine synchrone Beugung von Sprunggelenk und Knie. Auf muskulärer Ebene erfordert dies einen allmählichen Kraftanstieg im Muskel-Sehnen-Komplex während der Beugung und einen Abfall der Kraft während der Streckung des Beines.

2 EINFLUß DER MUSKELEIGENSCHAFTEN AUF DIE ARBEITSWEISE DES BEINES. Der gleichmäßige **Anstieg der Muskelkraft** kann zurückgeführt werden auf den Anstieg der Muskelaktivierung, den Anstieg in der Kraft-Längen-Funktion sowie der resultierenden Belastung der seriell geschalteten Sehnen und Aponeurosen. Der **Abfall der Bodenreaktionskraft** bei Streckung des Beines wurde erreicht durch eine verminderte Muskelkraft infolge zunehmender Verkürzungsgeschwindigkeit (Kraft-Geschwindigkeits-Beziehung) sowie der Muskelverkürzung (Kraft-Längen-Abhängigkeit). Dabei konnte die Phase der exzentrischen Muskelarbeit durch das sich verkürzende seriell elastische Element verlängert werden, wodurch die größten Kräfte etwa zur halben Kontaktzeit auftreten können. Die Sprungleistung ist entscheidend durch das exzentrische Kraftvermögen gekennzeichnet. Das **elastische Verhalten des Systems** ist eine Folge der schnellen Belastung des Muskel-Sehnen-Komplexes und ist weitgehend beschränkt durch Muskeleigenschaften (Kraft-Längen und Kraft-Geschwindigkeits-Funktion). Es erfordert kein spezielles neuronales Programm. Im Falle des Viersegmentmodells ist das elastische Verhalten eine Folge interner Eigenschaften und tritt bei sprungweitenoptimierter Muskelaktivierung auf.

3 SPRUNGWEITE UND SPRUNGTECHNIK. Unter Berücksichtigung der internen Systemeigenschaften ist die quasielastische Arbeitsweise die optimale Strategie für große Sprungweiten. Das elastische Verhalten wurde durch gleichmäßige Belastung von Knie und Sprunggelenk erreicht (Kapitel V). Um bei gegebener Anlaufgeschwindigkeit die optimale Sprungweite zu erzielen, muß eine **minimale Steifigkeit** überschritten werden. Ähnliche Weiten können erreicht werden durch Ausgleich einer geringeren Steifigkeit durch einen flacheren Anstellwinkel (Kapitel II). Die beobachteten Strategien (Anstell- und Abflugwinkel; Friedrichs et al., in Vorbereitung.) können jedoch nur unter Berücksichtigung von Muskeleigenschaften verstanden werden (Kapitel IV und V). Für solch ein System ist der optimale Anstellwinkel unabhängig von der Anlaufgeschwindigkeit.

4 ABSTIMMUNG UND STABILITÄT EINES DYNAMISCH BELASTETEN DREISEGMENT-BEINES. Das Hinzufügen eines **dritten Beinsegmentes** (wie dem Fuß) zu einem Bein bestehend aus Unter- und Oberschenkel verringert die erforderlichen Drehmomente an den Gelenken sowie die kinetische Energie durch transversale Beinsegment-Bewegungen. Gleichzeitig wirft es die Probleme der kinematischen Redundanz, potentieller Instabilitäten sowie der Muskelsteuerung auf. Eine optimale Arbeitsweise des Beines unter dem Aspekt der Sprungleistung (Kapitel V), einer hohen Beinsteifigkeit und Stabilität erfordert eine gleichmäßige Beugung der beiden Beingelenke, was durch auf die äußeren Segmentlängen (Fuß- und Oberschenkellänge) angepaßte Drehsteifigkeiten erreicht wird (Kapitel III). Nichtlineare Drehsteifigkeiten und zweigelenkige Strukturen sind alternative (austauschbare) Strategien zur Gewährleistung einer sicheren Beinfunktion für einen weiten Bereich von kinematischen Anfangsbedingungen. Ein kurzer Fuß mit der Möglichkeit des Fersenkontaktes ist eine leistungsfähige Konstruktion zur Steuerung stark gestreckter Kniepositionen, wenn die Gelenke elastisch arbeiten. Durch eine stärkere Beugung des Sprunggelenks und einem angepaßten Steifigkeitsdesign kann der Bereich der sicheren Beinflexion erweitert werden.

INTRODUCTION

I
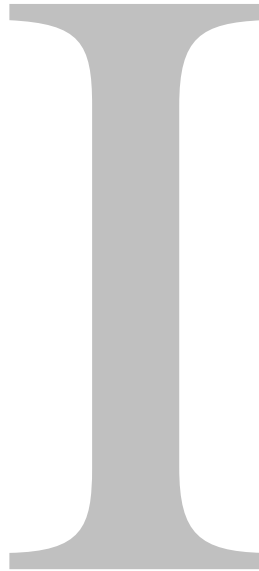
In fast human or animal locomotion a surprisingly stereotype force pattern during the stance phase is present. Forces rise gradually and achieve their peak values at about half the contact time. The whole time series is characterised by an almost sinusoidal shape. Such a behaviour can be described using a harmonically swinging system consisting of a mass supported by a simple linear spring.

This was done several times in the last two decades, first starting with simple one-dimensional models (Alexander, 1986; Özgüven and Berme, 1988) and later extending them to planar spring-mass models (Blickhan, 1989; Mc Mahon and Cheng, 1990). These models were applied to human hopping and running (Farley and González, 1996) and to animal running (Full and Tu, 1991) examining leg stiffnesses at different speeds (Mc Mahon and Cheng, 1990; Farley et al., 1993) and environmental conditions (McMahon and Greene, 1979; Ferris and Farley, 1997). Biological limbs are characterised by a high flexibility in terms of the degrees of freedom (number of joints) and the number of muscles acting across a joint. This results in the motor equivalence problem formulated by Bernstein (1967). The coordination of kinematically

redundant manipulators and the problems due to motor redundancy are also well known in robotics. In biology, a unique activation pattern is found for each particular motor task. But which constraints give rise to unique activation pattern? Biophysical and anatomical constraints, but even psychomotor and cultural factors (Hollerbach, 1990) may coin movement characteristics.

A quasi-elastic operation of a biological limb requires a specific motor program at the muscular level. From physiological studies it is known that muscles are able to work in an almost elastic manner as well. In this case, a quasi-elastic operation at the joint level can be found which corresponds to the total leg stiffness according to the geometrical arrangement of the limb segments. But even spring-like muscle properties do not guarantee stable configurations of the multi-segment system (Dornay et al., 1993). The mathematical relations between global leg stiffness, joint stiffness and muscle stiffness were formulated by Mussa-Ivaldi et al. (1988). It is possible to calculate the resulting leg stiffness assuming a given actuator compliance. Unfortunately, this theory does not predict the stiffness of a particular joint or muscle and may not solve the kinematic redundancy problem.

Limb stability is critically influenced by the geometrical arrangement of the muscles (mono- and biarticular muscles, position-dependent moment arms). Monoarticular muscles control the force amplitude whereas the biarticular muscles are well suited to control force direction (Doorenbosch et al., 1994; Doorenbosch and van Ingen Schenau, 1995). Different muscle activation patterns of mono- and biarticular muscles can be found while optimising the accuracy of force control or position control (Smeets, 1994).

The Equilibrium point hypothesis introduced by Feldman (1966) was based on neuro-physiological findings of spring-like muscle behaviour. It was postulated that equilibrium positions can be adjusted by shifting the rest length of a muscle pair. Thereby, the muscle's force-length relationships stabilise the linkage system at some joint angle. Although this theory was successfully applied to arm movements (Flash, 1987; Shadmer et al., 1993) and to lower limb movements (walking: Günther, 1997) there is no general theory yet to predict the local stiffnesses and nominal positions to solve the kinematic redundancy problem (Gielen et al., 1995).

In this thesis the mechanical and muscle-physiological origins of spring-like leg operation were addressed. Therefore, a series of forward dynamic models was developed to identify the importance of different structures on the leg behaviour in long jump. This type of movement was chosen because a simple optimisation criterion exists. Furthermore, a spring-like leg operation was observed experimentally for a variety of jumping styles. Finally, long jump is still a

8

discipline which was less addressed in forward or inverse dynamic modelling compared to others (running, vertical jump).

The ground reaction forces during the take-off phase of a long jump are characterised by a high impact peak immediately after touch-down which takes up to 25% of the total vertical momentum generated during ground contact. This effect can not be represented by a massless spring. As masses distributed in the distal leg segments play an important role in the dynamics of the long jump, the following questions were addressed in **chapter II** (spring-mass model):

1. How are distal masses represented in lumped parameter model of the long jump?
2. Which techniques result in an optimum jumping distance if the leg operates spring-like?
3. Which role do distal masses play on jumping technique and performance?

A mechanical circuit of at least two masses was necessary to describe the observed pattern of the ground reaction force in sufficient detail. But still the question remained, how spring-like behaviour might be produced within the leg.

In a first approach to this question the segmental alignment of the stance leg was examined. Although a two-segment system (chapter IV) would already be sufficient to allow leg operation, mostly more segments are present in nature. This led us to the following issues investigated in **chapter III** (three-segmental spring-mass model):

1. How can a kinematically redundant three-segment system be controlled?
2. Which advantages compared to a two segment system can be taken?
3. Which concepts are useful to simplify the control of the leg?

The homogeneous loading of the leg joint required an adaptation of the torque control to the segment length design. The human leg design proved to have an almost optimal range of safe leg operation. Elastic joint operation is a smart strategy to handle kinematic redundancy and may result in spring-like leg behaviour.

Unfortunately, there are no structures in the leg which are compliant enough to explain the spring-like leg operation. Leg forces originate largely form muscles spanning the leg joints. The muscle fibres are connected to the skeleton by relatively stiff tendons. Therefore, the dynamics of the muscle-tendon complexes (MTC) was addressed in the following **chapters IV and V**. This allowed to answer the following questions:

1. How does muscle design influence jumping performance?
2. Which jumping technique results in optimal jumping performance?
3. Which muscle stimulation results in optimum jumping distance?
4. How is spring-like behaviour is realised by the musculoskeletal system?

While the first two questions were investigated using a model of a two segmental massless leg with merely one knee extensor muscle the later questions required a more detailed representation of the human body. Therefore, a four segment model based on Van Soest and Bobbert (1993) was used to explore the dynamics of six major leg muscles for optimised jumping performance. Here, again the contributions to the first passive peak (chapter II) and the mechanisms of joint torque adjustment (chapter III) were identified and compared to the former findings.

The spring-like operation of the leg revealed to be a result of optimised muscle operation, muscle properties and leg design. It was found, that synchronised joint action minimised energetic losses and lead to a maximised leg stiffness. Several (partly parallel) mechanisms could be identified which supported this favourable and homogeneous manner of leg loading.

THE SPRING-MASS MODEL

REPRESENTATION OF DISTAL MASSES
DYNAMICS AND TECHNIQUES OF THE LONG JUMP

II
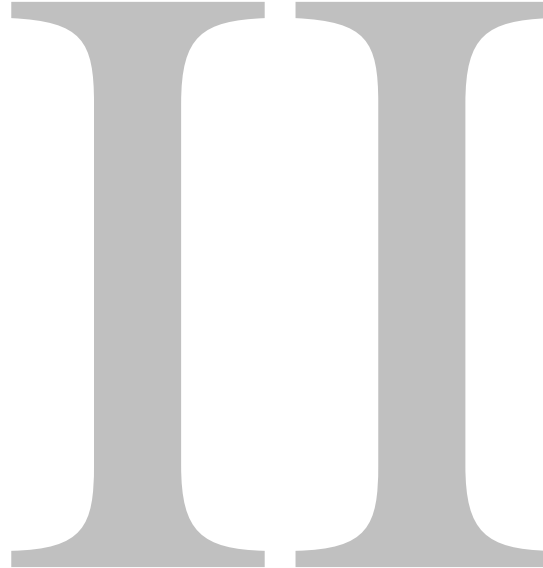
In the present study three questions are addressed:

(1) To what extent can the active peak in long jump be described by a spring-mass model?
(2) Which effects are responsible for the first passive peak in the ground reaction force?
(3) How can the major dynamic mechanisms be embedded into a lumped parameter model?

Therefore, a mechanical model is proposed which quantitatively describes the dynamics of the centre of mass (COM) during the take-off phase of the long jump. The model entails a minimal but necessary number of components: a linear spring with the ability of lengthening to describe the active peak of the force time curve and a distal mass coupled with nonlinear visco-elastic elements to describe the passive peak. The influence of the positions and velocities of the supported body and the jumper's leg as well as of systemic parameters such as leg stiffness and mass distribution on the jumping distance were investigated. Techniques for optimum operation are identified: (1) There is a minimum stiffness for optimum performance. Further increase of the stiffness does not lead to longer jumps. (2) For any given stiffness there is always an optimum angle of attack. (3) The same distance can be achieved by different techniques. (4) The losses due to deceleration of the supporting leg do not result in reduced jumping distance as this deceleration results in a higher vertical momentum. (5) Thus, increasing the touch-down velocity of the jumper's supporting leg increases jumping distance.

SYMBOLS

α angle of the leg to the x-axis

c, d constants in the nonlinear visco-elastic force function

ε leg lengthening constant $\varepsilon = r_+ / (\alpha_E - \alpha_0)$

F_G ground reaction force (GRF)

g gravitational acceleration

k leg stiffness

k_{dyn} generalised dynamic leg stiffness

ℓ relaxed length of the leg (varies from r_0 to r_E)

λ positional relationship, $\lambda = r_2(t_0) / r_1(t_0)$

m total body mass

μ mass ratio $\mu = m_2 / m_1$

ν exponent of the visco-elastic element

ω natural frequency $\omega^2 = k / m$

Δq displacement of swing mass m_2 along r

r leg length (distance between the COM and the ball of the foot)

r_+ leg lengthening $r_+ = r_E - r_0$

Δr leg shortening $\Delta r(t) = \ell(\alpha) - r(t)$

Δs tangential displacement of swing mass (m_2)

v velocity

x horizontal coordinate

y vertical coordinate

Δy displacement in y

INDICES

0 refers to the instant of touch-down

1 refers to the proximal mass m_1

2 refers to the distal swing mass m_2

E refers to the instant of take-off

MAX refers to the instant of maximal leg shortening

q refers to the displacement of the swing mass m_2 along r

r refers to the orientation of the leg

s tangential displacement of the swing mass m_2

INTRODUCTION

Running and jumping are two types of fast saltatoric movements, characterised by a series of alternating aerial and contact phases. The impact occurring during each contact phase serves to negate the vertical momentum. The flight phase is determined by the initial velocity vector of the centre of mass at take-off and the gravitational acceleration.

The function of the leg in repetitive ground contacts at a constant energy level like in hopping or running is comparable to a spring as shown e.g. by Blickhan (1989), Alexander et al. (1986), McMahon and Cheng (1990) and Farley et al. (1993). Modelling the leg as a spring is suited to describe the landing if the body mass, the leg stiffness, and the initial conditions are known.

The spring-mass model is suitable to describe conservative systems. During the human long jump energy is in fact largely conserved (Friedrichs et al., in prep.). Nevertheless, due to the high running speed, the first so called passive impact immediately after touch-down strongly influences the system dynamics. In the long jump this contribution accounts to about 25 percent of the total momentum and can not be neglected.

Alexander (1990) proposed a two-segment model with a Hill-type extensor to predict optimum take-off techniques of the jumpers stance leg in high and long jumping. However, to cope with observed jumping distances unrealistic muscle properties had to be chosen. Even a detailed musculo-skeletal system with 17 segments including all important muscles (Hatze, 1981a) does not describe the complete ground reaction force pattern in sufficient detail.

The understanding of body dynamics during landing or falling was significantly improved by the concept of wobbling masses introduced by Gruber (Gruber, 1997; Gruber et. al. 1998). She showed that the different responses of soft tissues and hard skeleton to impacts are essential for predicting dynamical loads. In long jumping high impacts occur with forces up to ten times body weight.

In this study, the approach to long jumping is to describe the mechanics of the centre of mass and the mechanical function of the supporting leg using a 2D lumped parameter model with a minimum number of mechanical components. The action of the leg is described by a spring, the effect of soft tissues by the introduction of a visco-elastically coupled mass. Thereby, the influence of either initial conditions such as running speed and angle of attack (measured by video analysis) or model properties (like leg stiffness) on the jumping performance are investigated. The quality of the mechanical approach is judged by comparing the experimental force records with the results of the simulation.

METHODS

Experiments

In training competitions in 1995 and 1996, 30 long jumps (distance: $[5.49 \pm 0.86$ SD] m) of 18 male and female sport students (m = $[75.1 \pm 5.13$ SD] kg, body height: $[1.81 \pm 0.06$ SD] m) were filmed for later analysis with a VHS camera (50 half-frames per second). The vertical and horizontal ground reaction forces were recorded with a 3D force plate (IAT, Leipzig). Kinematic input parameters for the dynamic models were obtained by digitising the video sequences (APAS, Ariel).
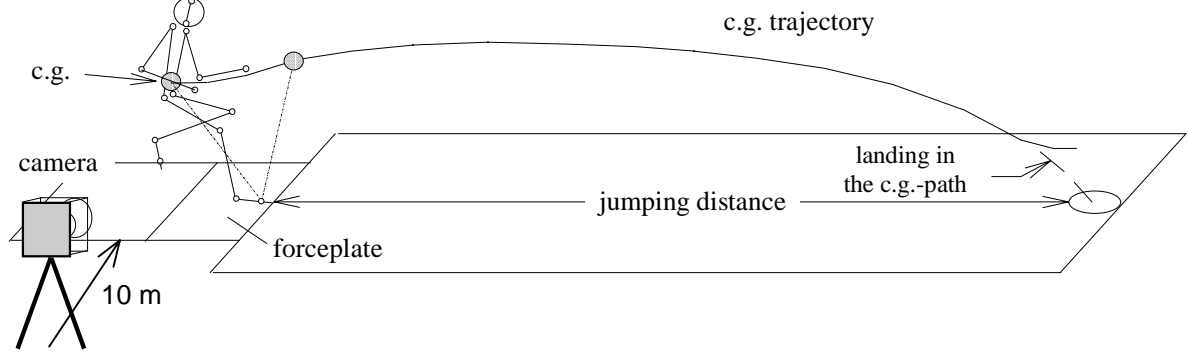
Fig. 1 Experimental set-up for the analysis of the last ground contact in long jumping. The body configuration defined by the positions of the joint markers was used to calculate the c.g. trajectory during the last ground contact and the flight phase. The jumping distance is estimated as the intersection point of the elongated ballistic curve (dashed line) and the ground.

The concept of leg stiffness

The leg length r is defined as the distance of the COM to the ball of the foot as the rotational centre of the system during the stance phase. The initial leg length r_0 and the final leg length r_E are generally not identical. Therefore, the leg lengthening parameter r_+ was introduced as the difference between both leg lengths:

$$r_+ = r_E - r_0. \tag{1}$$

The actual length of the relaxed leg $\ell(\alpha)$ during the contact phase is then defined in a linear approach by (Blickhan et al. 1995; Friedrichs et al., in prep.):

$$\ell(\alpha) = r_0 + r_+ \cdot (\alpha - \alpha_0) / (\alpha_E - \alpha_0)$$
$$= r_0 + \varepsilon \cdot (\alpha - \alpha_0) \tag{2}$$

with ε constant, leg angle α at touch-down α_0, at take-off α_E, initial leg length r_0, change in r by r_+ during contact. Leg shortening $\Delta r(t) = \ell(\alpha(t)) - r(t)$ is zero at the instances of touch-down and take-off.

The force exerted by the leg is related by the stiffness to the shortening of the leg Δr. The leg stiffness is defined by the ratio of the ground reaction force to the leg shortening Δr at maximum knee flexion:
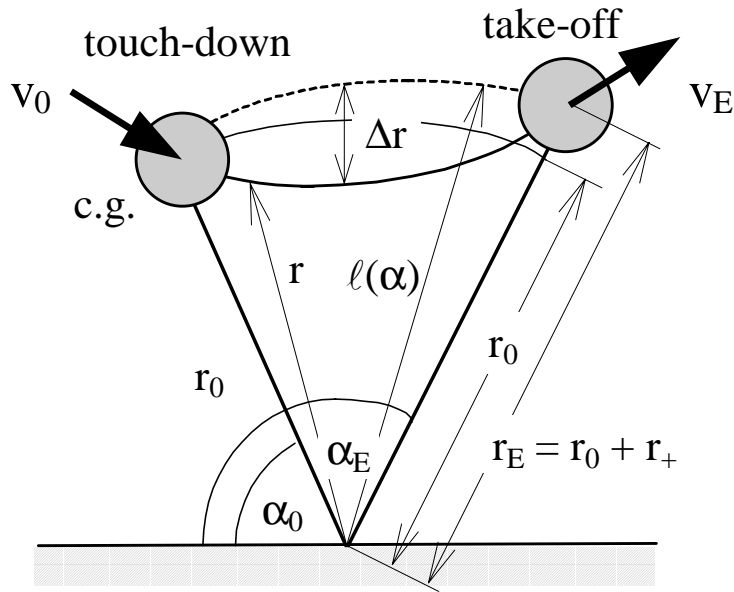
$$k = F_{G,MAX} / \Delta r_{MAX}. \tag{3}$$

14

Fig. 2 Different leg lengths at touch-down and take-off can be described by the leg lengthening r_+. The actual shortening of the leg is Δr, $\ell(\alpha)$ denotes the length of the relaxed leg which increases with α.

The instantaneous ratio in Eq. 3 was generalised as the dynamic leg stiffness:

$$k_{dyn}(t) = F_G(t) / \Delta r(t). \qquad (4)$$

This definition is equal to Eq. 3 for the instant of maximum shortening of the leg and corresponds to the understanding in the literature (Farley and González, 1996).

Numerical methods

The mechanical models were built using standard software packages for dynamic simulations (ALASKA, Institut für Mechatronik; ADAMS, Mechanical Dynamics Inc.). Using given initial conditions, the parameter set was estimated which fulfils the least square criterion between measured and calculated ground reaction forces.

For further parameter studies the models were translated into the equations of motion using the Lagrangian formalism, and solved by a numerical integration procedure using a 4th order Runge-Kutta algorithm (IDL, Creaso). The influence of initial and model specific parameters

on the jumping result were investigated by varying parameter values. The model parameters were first adjusted visually and then calculated using a genetic optimisation algorithm.

MODEL DESCRIPTION AND VERIFICATION

A simple spring-mass system already predicts optimum strategies for the maximum jumping distance. For quantitative descriptions leg lengthening and mass distributions must be taken into account.

The leg as a linear spring

In a first approach to long jumping we a model will be considered in which the leg operates as a spring. This gives basic insights into the influence of geometric parameters and the role of leg stiffness.

It is typical that the ground reaction force during the take-off phase shows a passive and an active peak (Fig. 3). The derived dynamic leg stiffness $k_{dyn}(t)$ has a first peak during the passive phase followed by a relatively constant stiffness during the active phase up to the last 30 ms before the take-off.
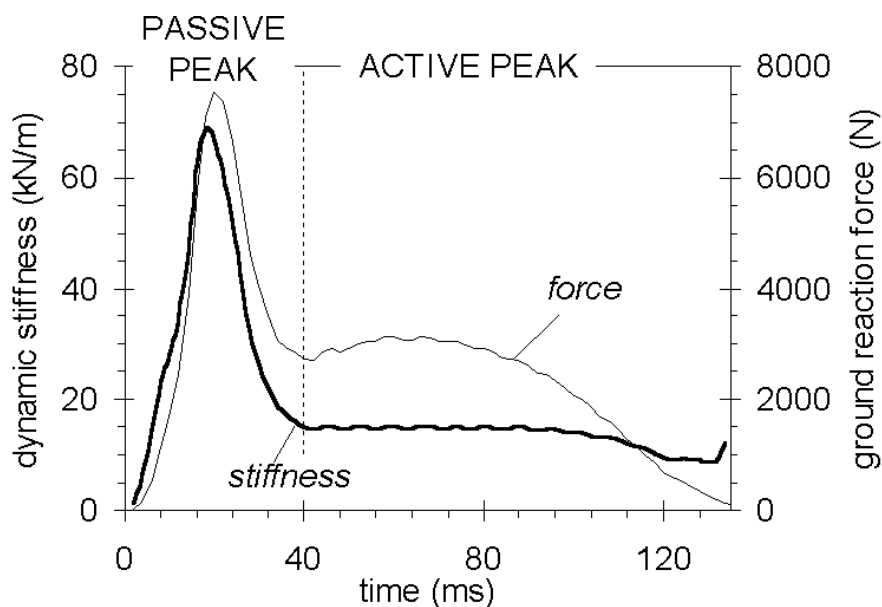

Fig. 3 Experimental result for the ground reaction force F_g and the instantaneous leg stiffness k_{dyn} as a function of the time.

16

Neglecting the passive peak, a simple spring-mass system (Fig. 4) can be used to describe the functionality of the contacting leg during flexion under the assumption of energy conservation. The equations of motion are (Blickhan, 1989):

$$\ddot{x} = x\omega^2 \left(\frac{\ell}{\sqrt{x^2 + y^2}} - 1 \right)$$

$$\ddot{y} = y\omega^2 \left(\frac{\ell}{\sqrt{x^2 + y^2}} - 1 \right) - g$$

(5a, 5b)

where ω is the natural frequency of the system with $\omega^2 = k / m$. The relaxed spring length ℓ corresponds to the initial leg length r_0 which is in this first approach equal to final leg length r_E.
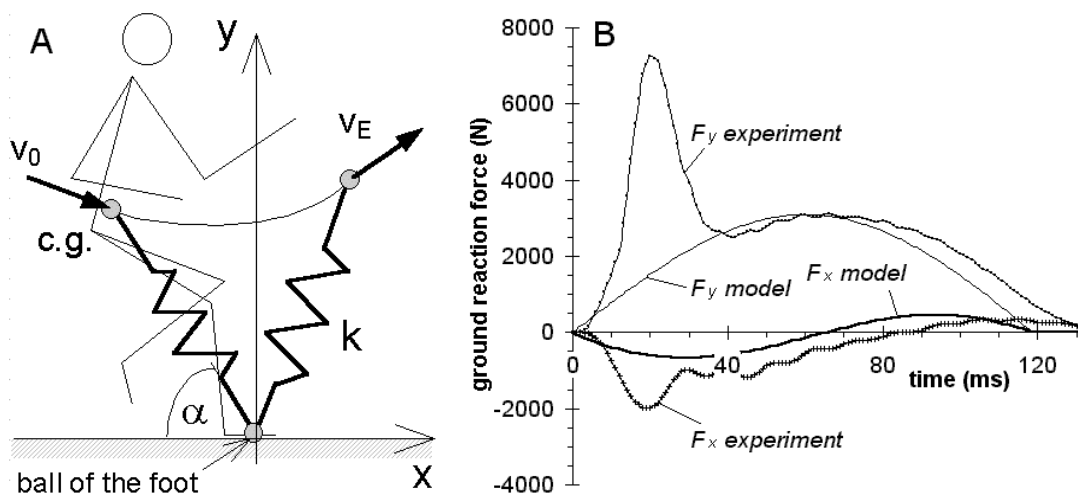

Fig. 4 (A) Schematic drawing showing the planar spring-mass model. The leg spring is defined by the stiffness k. The angle α describes the orientation of the leg with respect to the ground. (B) The model reflects a part of the measured ground reaction forces. The passive peak is missing and the active peak is either to short or to high.

Since the vector of the landing velocity in long jumping has usually only a small vertical component ($|v_{0,Y}| < 1$ m/s), it is sufficient to consider the horizontal approach speed $v_0 = v_{0,X}$. For a given speed the influence of the angle of attack α_0 and the leg stiffness k on the jumping distance can be studied (Fig. 5A).

There is an optimum in jumping distance for a proper angle of attack and the appropriate leg stiffness. At a lower angle of attack the loss in horizontal velocity will prevail the influence of a higher vertical velocity and the jumping distance decreases. A steeper angle leads to overrunning with a smaller vertical impact. This is a general feature observed in all models.
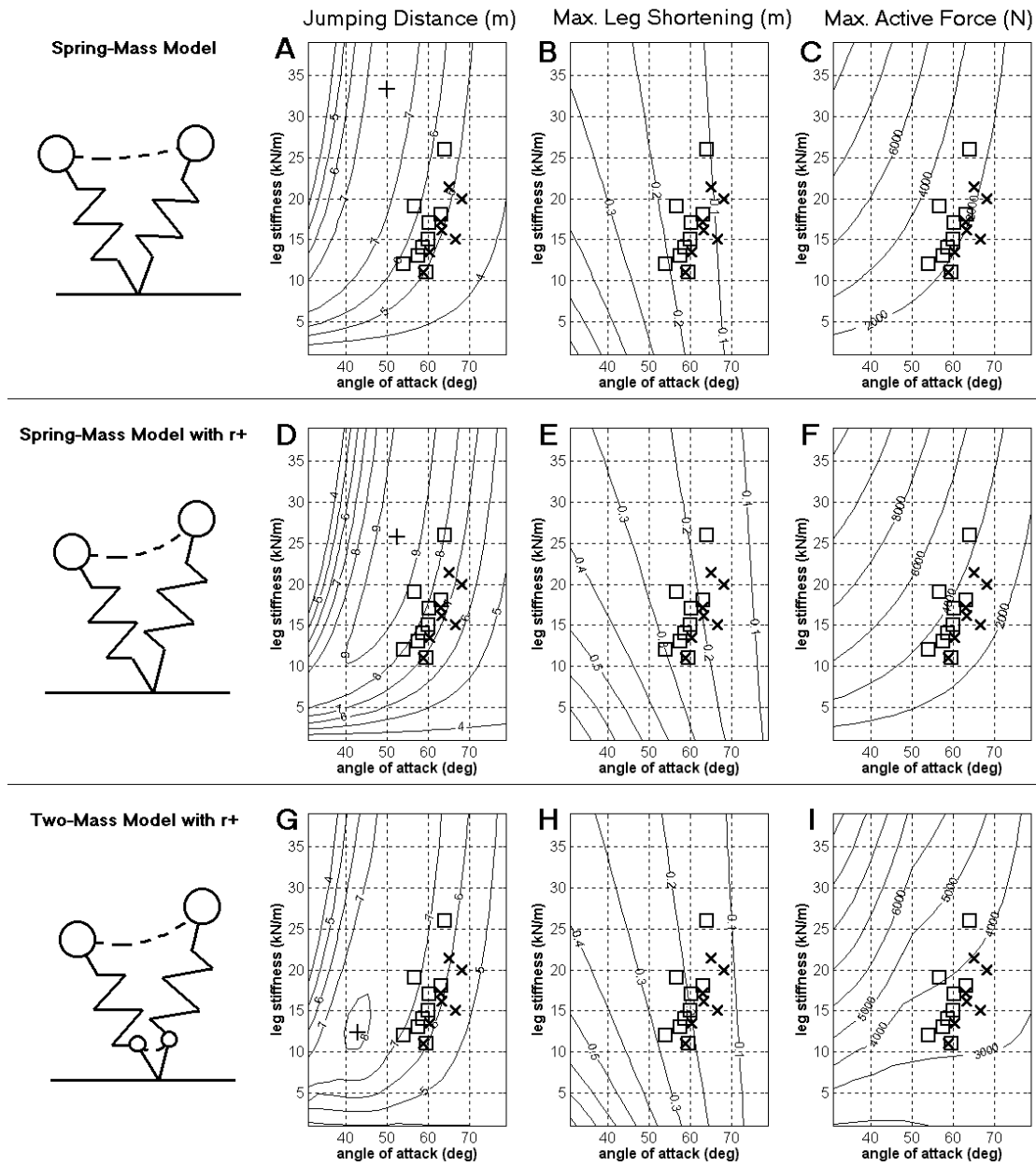
Fig. 5 Influence of angle of attack α_0 and leg stiffness k on jumping distance x_{JUMP} (A, D, G), maximum leg shortening Δr_{MAX} (B, E, H), and maximum active force $F_{MAX,r}$ (C, F, I) predicted using the simple spring-mass model (A, B, C), the spring-mass model with leg lengthening (D, E, F), and the two-mass model for the long jump (G, H, I). The remaining parameters have been chosen according to the mean values for the analysed jumps (m = 75 kg, r_0 = 1.19 m, v_0 = 8.2 m/s, see tab. 1). The contour lines mark values of constant jumping distance x_{JUMP} in meters (A, D, G), maximum leg shortening Δr_{MAX} in meters (B, E, H), and maximum active forces $F_{MAX,r}$ in Newton (C, F, I). The general dependencies are similar for the three models. The jumpers do not reach the optimum because their inability to generate high forces at large leg deflections. The spring-mass model with leg lengthening predicts longer jumps due to the absence of the passive peak (fig. 6).

+ the predicted optimum for jumping distance,

✕ jumps according to their angle of attack and calculated leg stiffness with x_{JUMP} < 5 m, and

☐ jumps with x_{JUMP} > 6 m.

18

The influence of leg stiffness is comparable to that of the angle of attack: A stiffer leg leads to faster repulsion and thus at a lower angle of attack to a loss in horizontal velocity and jumping distance. In contrast, a softer leg can not produce the necessary vertical impact.

A high vertical impact requires a sufficiently high product of the mean vertical ground reaction force and contact time. This is only possible if the leg stiffness achieves a certain minimum value. With a higher stiffness and a corresponding optimal angle of attack (that is steeper angles and shorter contact times) the jumping distance remains nearly constant and even decreases slightly. The better the jump the closer the values come to the range where almost maximum jumping distance can be achieved (Fig. 5A). These features have been observed in all models.

Considering leg lengthening

The simple spring-mass model predicts a significantly shorter active peak than has been measured (Fig. 4). Extending the model by considering lengthening of the relaxed length (i.e., leg length when leg force is zero) during ground contact improves the predictions (Eq. 2, Blickhan et al. 1995). Leg lengthening results on average in a more compliant spring and thus in longer contact times. Note that in order to obtain a similar change in momentum leg lengthening calculated from the active peak force pattern must be less than the cinematographic estimates as long as the passive peak and the corresponding momentum is excluded in the model (Fig. 6B).
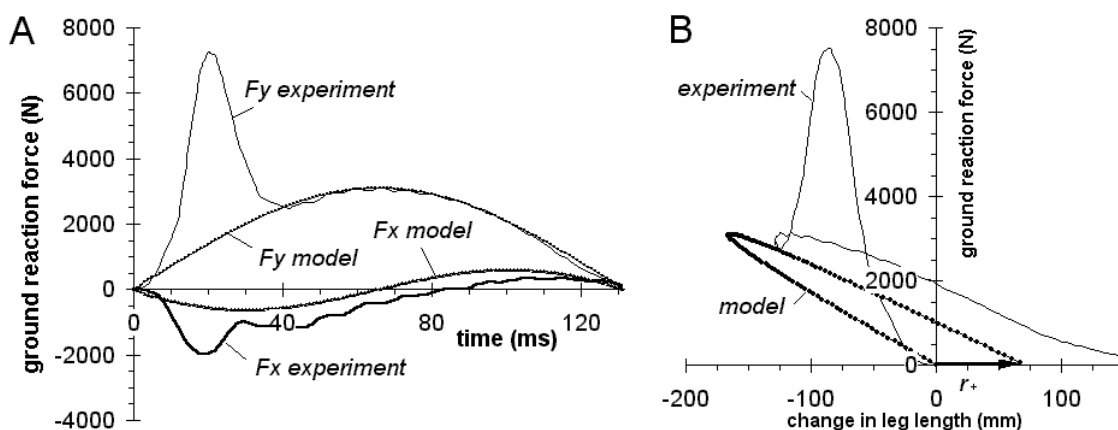

Fig. 6 (A) Ground reaction forces as predicted by the spring-mass model with leg lengthening. (B) Force-leg length relationship of the jumping leg. The measured leg lengthening r_+ can not be reproduced with a spring-mass model with lacking passive peak when the active peak forces should be correct.

Introduction of the leg lengthening shifts the range of close to optimum jumps to larger angles of attack (Fig. 5D). The optimum itself becomes more pronounced and shifts to low stiffness. In general very long jumps require higher active forces (Fig. 5F) and moderate leg shortenings (Fig. 5E). Even elite jumpers are not able to produce the forces and leg compressions to achieve the predicted range of close to optimum operation.

Mechanical model for the passive peak

The passive peak in jumping occurs directly after touch-down of the foot. The measured force pattern can be described accurately when a representative mass is coupled with a nonlinear viscosity to the rigid frame of the spring leg. This mass represents the rigid skeleton and its deceleration during touch-down as well as the relative movement of the soft tissues (muscle etc.) with respect to the rigid frame. The following dependency was used to describe the coupling between soft and hard tissues in one direction (here Δy):

$$F = - (c \cdot sgn\,(\Delta y) + d \cdot v_y) \cdot |\Delta y|^{\,\nu} \qquad (6)$$

where c and d are constants, the exponent ν is about $2.5 - 4.5$, and sgn describes the signum function:

$$sgn\,(\Delta y) = \begin{cases} 1 & for\,\Delta y > 0 \\ 0 & for\,\Delta y = 0 \\ -1 & for\,\Delta y < 0. \end{cases} \qquad (7)$$

The selected visco-elastic coupling fulfils the following requirements:
1. due to the nonlinearity the ground reaction force increases gradually within the first 10 ms,
2. the first peak is symmetric with time, and
3. the active and passive peak are clearly separated.

Assembling with the spring-mass system

A one dimensional description of the vertical component of the ground reaction force during the long jump can now be obtained by combining the linear spring-mass model with the nonlinear visco-elastic system described above. The two force peaks are described by two systems in parallel with different dynamics.

20

A stack of two masses representing the body and the foot respectively (Alexander et al., 1986; Özgüven and Berme, 1988) does not result in realistic dependencies. Nonlinear coupling is necessary. Both masses are effective masses taking the vertical projection and the bending of the leg into account. Depending on the orientation of the leg segments the masses of the leg and the body contribute. The mass of the foot is not sufficient to explain the transferred momentum during the passive impact.

The leg mass can be separated into the masses of the rigid bones, the foot, and of the soft tissues. If the coupling to the ground and the skeleton differs strongly, several damped force oscillations would be present during touch-down. This is not the case during the long jump.

The experimental data can be described accurately with one distal mass and only one type of coupling. In this final model m_2 entails the foot, the skeleton and the wobbling masses distributed all over the body especially in the stance leg. Descriptions with realistic masses are only possible within a planar model.

The planar model for the long jump

By taking planar movements of two distributed masses into account the model is able to describe the relationship between the horizontal and vertical force. Strategies of impact generation or avoidance can now be investigated. By actively hitting the supporting leg onto the board jumpers increase the passive peak and thereby vertical momentum and jumping distance.

In a simple planar spring-mass model the ground reaction force points always in the direction of the spring. During the actual long jump, however, significant deviations in the force direction can be observed within the first 40 ms. These can be attributed to the movement of the distal mass.

In the model the body mass (m_1) is supposed to glide on a massless rod. The orientation of this rod is defined by the position of the ball of the foot and the centre of the body mass. Similar to the simple spring-mass model, the body is coupled to the ground via a linear spring, representing the spring-like operation of the human leg (active peak). At a certain height, a second mass is fixed to the rod by nonlinear visco-elastic elements (Fig. 7).
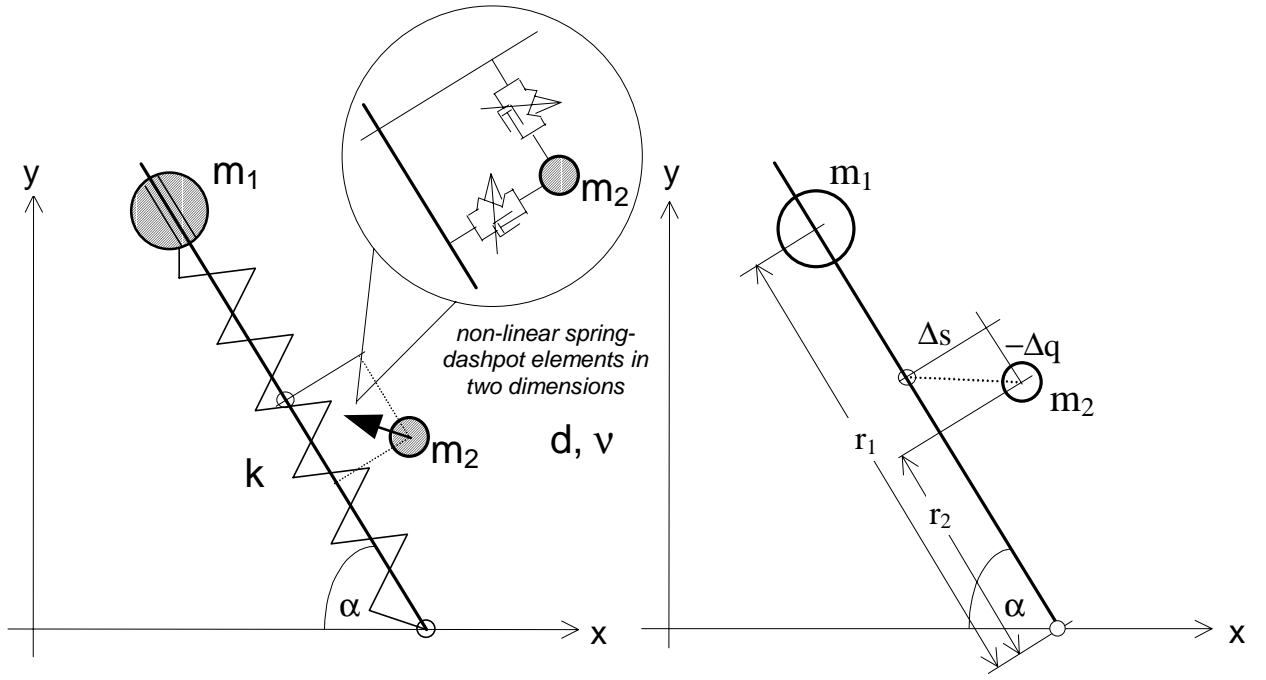
Fig. 7 The planar model for the long jump (schematic drawing with geometric parameters).

The equations of motion are:

$$\ddot{r}_1 = \dot{\alpha}^2 r_1 - \frac{k}{m_1}(r_1 - \ell(\alpha)) - g \cdot \sin\alpha$$

$$\ddot{\alpha} = -\frac{1}{m_1 r_1^2}(r_2 \cdot F_s - \Delta s \cdot F_q) - \frac{1}{r_1}(2\dot{r}_1 \cdot \dot{\alpha} + g \cdot \cos\alpha)$$

$$\Delta\ddot{q} = \Delta s \cdot \ddot{\alpha} + r_2 \cdot \dot{\alpha}^2 + 2\Delta\dot{s} \cdot \dot{\alpha} + (F_q / m_2) - g \cdot \sin\alpha$$

$$\Delta\ddot{s} = -r_2 \cdot \ddot{\alpha} + \Delta s \cdot \dot{\alpha}^2 - 2\Delta\dot{q} \cdot \dot{\alpha} + (F_s / m_2) - g \cdot \cos\alpha$$

(8a-d)

with the nonlinear visco-elastic force functions:

$$F_q(\Delta q, \Delta\dot{q}) = -(c_q \cdot \mathrm{sgn}(\Delta q) + d_q \Delta\dot{q})\Delta q^{\nu_q}$$

$$F_s(\Delta s, \Delta\dot{s}) = -(c_s \cdot \mathrm{sgn}(\Delta s) + d_s \Delta\dot{s})\Delta s^{\nu_s}.$$

(9a,b)

The properties of the element's coupling in radial and tangential direction are assumed to be the same ($c_q = c_s = c$, $d_q = d_s = d$, $\nu_q = \nu_s = \nu$). In addition to the parameters describing the mechanical properties of the simple spring-mass system (k, ε), the mass ratio $\mu = m_2 / m_1$, the positional ratio $\lambda = r_2(t_0) / r_1(t_0)$, and the parameters describing the nonlinear visco-elastic elements must be identified (Eq. 9a,b).

The simulations are calculated for given total mass, its touch-down velocity, given initial leg length and angle of attack. All other parameters including the initial conditions for the distal

22

mass are estimated fitting the time course of the horizontal and vertical component of the ground reaction force (Fig. 8A, 8D and Tab. 1). Some of the parameters can be estimated independently using the experimental data: ε can be obtained from cinematographic data, k can be calculated by dividing the maximal force F_{MAX} during the active peak by the maximum leg shortening Δr_{MAX}.
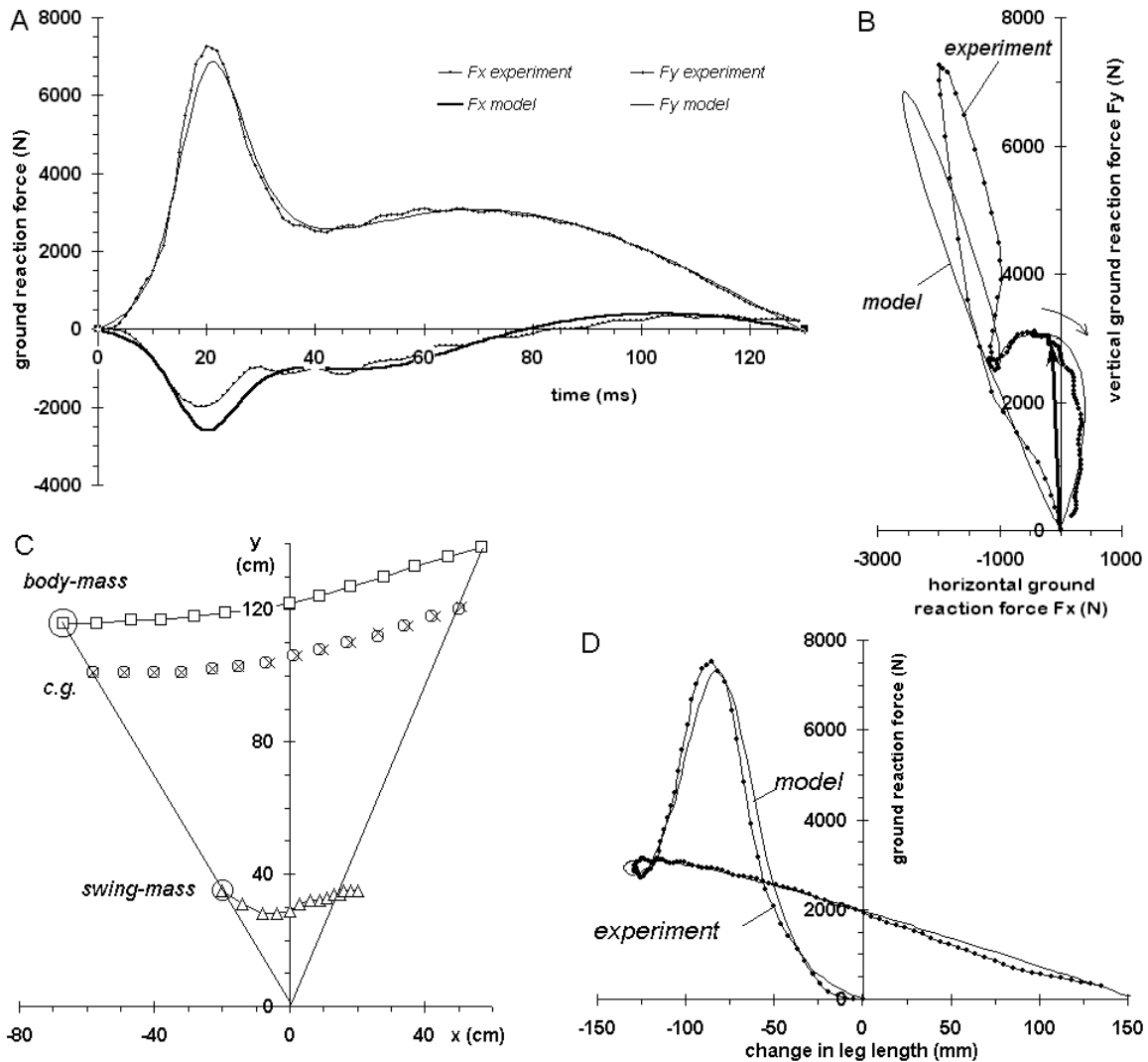
Fig. 8 Comparison between experimental and model results: (A) Ground reaction forces (GRF) in vertical F_y and horizontal F_x components as time series. (B) Tracings of the GRF in the F_x-F_y plane. During heel strike (passive peak) the experimental GRF directs steeper than predicted by the model. (C) The positions of body-mass and swing-mass in the model defines the resulting c.g. (circles). Measured c.g.: crosses. (D) Force-leg length relationship of the jumping leg as simulated by the two-mass model and experimental result.

Remaining systematic differences (Fig. 8B) occur, because the point of centre of pressure shifts during the ground contact which is not realised in the presented model. The results are fairly stable with respect to the position and size of the second mass. The effective distal mass

can be considered to be fixed at about 25 percent of the leg length from the ground (Fig. 8C) and amounts to approximately 27 percent of the body mass.

The parameters specifying the coupling to the skeleton are less sensitive as long as the basic properties described above are fulfilled. Interestingly, the predictions for the initial velocity of the distal mass are similar to the values obtained for the jumpers leg from video-graphic data (Tab. 1). The deviation can be explained by the fact that the average velocity of the leg is higher and less downward orientated than that of the foot.

Measured values for the leg stiffness come fairly close to the predicted optimum (Fig. 5G). The difference in general dependencies of the active force (Fig. 5I) is due to an increasing dominance of the passive peak for larger angles of attack at low leg stiffness.

symbol	parameter	model value (mean ± SD)	experimental result (mean ± SD)	units
k	leg stiffness	14.6 ± 3.72	16.2 ± 3.80	kN/m
ε	leg lengthening constant	3.36 ± 1.44	3.07 ± 1.28	10^{-3} m/deg
λ	positional relation	0.252 ± 0.049	no data available	1
μ	mass relation	0.269 ± 0.064	no data available	1
$\log d_2$	non-linear spring-damper constant	7.45 ± 0.55	no data available	1
$v_2^{(0)}$	initial velocity of swing mass	5.31 ± 0.59	foot: 3.96 ± 1.40	m/s
$\alpha_{v2}^{(0)}$	initial direction of v_2 (downwards)	32.7 ± 4.4	foot: 30.05 ± 11.45	deg

Tab. 1 System properties and initial conditions. Means and standard deviations (SD) are given for the experimental data of 30 trials and the corresponding numerical simulation.

DISCUSSION

The presented mechanical model describes with a minimal set of parameters the dynamics of the long jump. As it is well known (e.g. Hay, 1993), the most influential factor for jumping distance is the running speed. The model predicts also that a certain angle of attack of the leg optimises jumping performance (Alexander, 1990). This optimum requires a relatively low minimal stiffness of the leg.

The controlled musculo-skeleton unit with its connective tissues behaves similarly to a spring with a certain stiffness. This stiffness and the leg shortening (Tab. 1) are not very different from that necessary for running (leg stiffness about 12...15 kN/m, leg shortening in running about 14 cm (Farley and Gonzaléz, 1996), in jumping: ca. 17 cm). To which extent this stiffness can be contributed to intrinsic properties of the participating tissues will be discussed in chapters IV and V.

For sufficient high stiffness values many strategies with different angles of attack are possible to achieve distances which come close (up to 95 percent) to the theoretical maximum. Indeed, several techniques can result in the same jumping distance (Fig. 5). The proper strategy for an athlete depends on his ability to generate stiffness. Differences in stiffness can be compensated by changing the angle of attack of the leg. The kinetic energy of the runner dominates the energetics of the jump (Hay, 1993). To conserve this energy a quasi-elastic strategy is essential for a good performance. The leg largely redirects the movement.

Leg lengthening at take-off is partly an active process. The runner places his leg with the knee slightly bent and takes off with a completely straight leg. This process - facilitated by the special geometry of the human leg - increases the distance over which acceleration takes place. It also compensates partly for the losses which necessarily occur during landing (passive peak).

It is impossible to avoid the impact during touch-down. Jumpers take, however, advantage of the passive peak generated during the impact by actively hitting the jumping leg onto the board. By this measure the passive peak, especially in the vertical component of the ground reaction force, is increased. Despite the fact that the generation of this peak clearly absorbs energy it enhances vertical momentum which is important to achieve long jumping distances. Thus, the new model describes quantitatively the dynamics and mechanisms of the most essential parts of the long jump and helps to understand jumping techniques. For individual jumpers detailed diagnostics are possible about techniques or conditional shortcomings.

General significance

Many models have been proposed to describe human jumping. As jumping in a less extreme form is part of standard locomotion, modelling of jumping is of general significance for human locomotion. Most studies so far have either been descriptive (Hay, 1993; Lees 1994) or alternatively were based on very detailed modelling.

But even extremely detailed models using all major muscles (Hatze, 1981a; Bobbert and Van Soest, 1994) fall short in describing the general dynamics of the process. The major reason is that the landing impact (contributing 25% of the total change in momentum) is not described adequately. The activation dynamics of the musculature precludes active generation of this peak, i.e. even if the musculature was activated and deactivated within 40 ms the muscle could not follow.

Force enhancement due to stretching of the activated muscle (Alexander, 1990) may contribute to the passive peak. The quantitative contribution of muscle forces is treated in

chapters IV and V. A major cause of the impact is the deceleration of distal masses. These masses consist of the skeleton and of soft tissues and are visco-elastically coupled to the ground or to each other.

The comparison between results from the simulations and the experiments reveals that a large fraction of these masses can be identified as muscle masses. The type of coupling as measured for the heel (Gruber, 1987) proves to be necessary for adequate description of the time course of the event. The right damping is necessary to avoid injuries (stiff coupling) or elastic ringing (compliant coupling) making control at least difficult.

The spring-like behaviour of the leg could be replaced by a suitably activated musculo-skeletal system. Nevertheless, it is surprising to which extent the leg performs like a spring. It might be a strategy to simplify control (Bobbert et al., 1996). The shortening of the leg amounts to about 15 percent ($\Delta r_{MAX}/r_0$). A corresponding rotation of the knee results in lengthening of the quadriceps-patella tendon complex by about 35 mm. For the high loads observed the patellar tendon would be stretched by ca. 5 mm. The long aponeuroses of the musculus quadriceps may stretch elastically by about 20 mm. In this case the elastic properties of the passive tissues would largely determine the quasi-elastic operation of the leg and thus its stiffness. At higher knee flexion the conservative operation of the knee can probably not be kept up any longer due to the increasing demand of muscle force and the properties of the connecting tissues. Therefore the limited properties of the human leg do not allow to reach the theoretically possible maximum values. A higher take-off angle will be accompanied by a smaller take-off velocity and thus a shorter jumping distance (chapter IV).

THREE-SEGMENTAL SPRING-MASS MODEL

TORQUE EQUILIBRIUM · STIFFNESS EQUILIBRIUM
SYMMETRICAL LOADING · ASYMMETRICAL LOADING

III
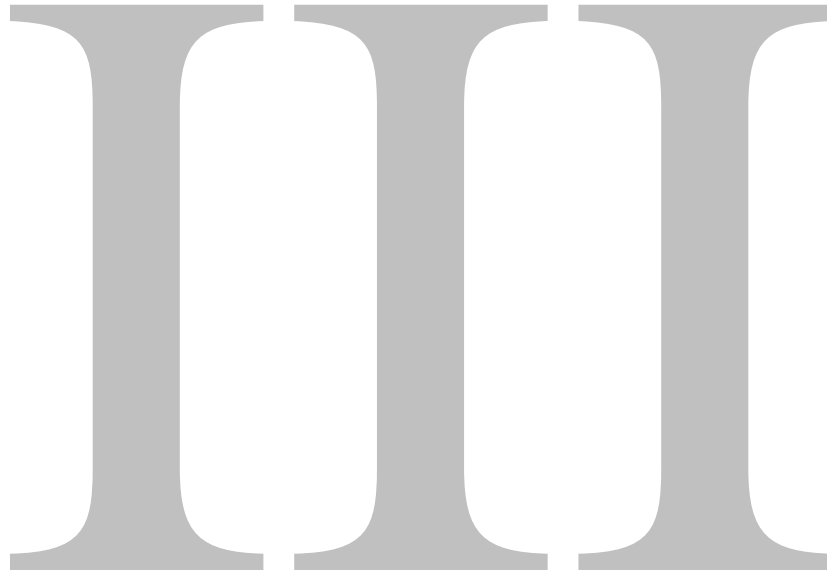
The spring-like behaviour of the leg is now implemented in a multiple segment chain. A simple three-segment model is proposed to investigate the segmental alignment of the leg during repulsive tasks like human running and jumping. The effective operation of the knee and ankle muscles is described in terms of rotational springs.

Following issues were addressed in this study:

(1) How can the joint torques be controlled to result in a spring-like leg operation?
(2) How can rotational stiffnesses be adapted to leg segment geometry?
(3) To what extend can unequal segment lengths be of advantage?

It was found that:

(1) the three-segment leg tends to become unstable at a certain amount of bending,
(2) homogeneous bending requires to adapt rotational stiffnesses to the outer segment lengths,
(3) nonlinear joint torque–displacement behaviour extends the range of stable leg bending and may result in an almost constant leg stiffness,
(4) biarticular structures (like human *m. gastrocnemius*) support homogeneous bending in both joints if nominal angles are properly chosen,
(5) unequal segment lengths enable homogeneous bending when asymmetric nominal angles meet the asymmetry in leg geometry, and
(6) a short foot is useful to enable control of almost stretched knee positions.

Furthermore, general leg design strategies for animals and robots are discussed with respect to the range of safe leg operation.

SYMBOLS

α — ratio R_C / R_λ, stiffness equilibrium requires $\alpha = 1$

$\alpha_{\Delta\varphi}$ — angle of leg shortening in $(\varphi_{12}, \varphi_{23})$-space, $\alpha_{\Delta\varphi} = \arctan(R_{\Delta\varphi}^{-1})$

c_{ij} — rotational stiffness constant

COM — centre of mass

$\vec{d}_{i,j}$ — vector pointing from centre of mass of segment i to joint with segment j

$\Delta\lambda$ — translational working range from nominal to bifurcation length $\Delta\lambda = \lambda_0 - \lambda_B$

$\Delta\varphi, \Delta\varphi_{ij}$ — angular working range from nominal to bifurcation angle $\Delta\varphi_{ij} = \varphi^0_{ij} - \varphi^B_{ij}$

$\Delta\varphi_B, \Delta\lambda_B$ — loss in working range at $\lambda_2 = \lambda_{2,Crit}(\nu)$

$\Delta\varphi_{Crit}$ — angular working range at $\lambda_2 = \lambda_{2,Crit}(\nu)$

$\Delta\lambda_{Crit}$ — translational working range at $\lambda_2 = \lambda_{2,Crit}(\nu)$

$\vec{F}_{i,j}$ — intersegmental force at joint between segments i and j acting on segment j

$\vec{F}_{leg}$ — leg force vector (ground reaction force), components: $F_{leg,x}$, $F_{leg,y}$

$\vec{g}$ — vector of gravitational acceleration

γ — angle between leg axis $\vec{r}$ and middle segment $\vec{\ell}_2$

h_1, h_3 — distance of ankle/knee joint to leg axis, $h_i = \ell_i \sin(\vec{\ell}_i, \vec{r})$

ℓ_1, ℓ_2, ℓ_3 — segment lengths (foot, shank, thigh)

$\vec{\ell}_1, \vec{\ell}_2, \vec{\ell}_3$ — vectors of the leg segments

ℓ_{MAX} — maximum leg length $\ell_{MAX} = \ell_1 + \ell_2 + \ell_3$

$\lambda_1, \lambda_2, \lambda_3$ — relative segment length $\lambda_i = \ell_i / (\ell_1 + \ell_2 + \ell_3)$

λ_0 — nominal leg length corresponding to $(\varphi^0_{12}, \varphi^0_{23})$

λ_B — bifurcation leg length corresponding to $(\varphi^B_{12}, \varphi^B_{23})$

$\lambda_{2,Crit}$ — for $\lambda_2 > \lambda_{2,Crit}(\nu)$ a type II-bifurcation may appear

Λ_2 — substitution $\Lambda_2 = (1-\lambda_2) / \lambda_2$

m — body mass

$M_{ij}, \vec{M}_{i,j}$ — torque acting on segment j at joint between segments i and j, as vector

$\vec{\omega}_i$ — vector of rotational velocity of segment i

ν — exponent of the torque characteristic

$\varphi_1, \varphi_2, \varphi_3$ — segment orientation with respect to the ground

φ_{ij} — inner joint angle between segments i and j (Fig. 1)

$\varphi_0, \varphi^0_{ij}$ — nominal joint angles

$\varphi_{0,Crit}$ — critical nominal joint angle (symmetrical loading)

$\varphi_{0,Extr}$ — nominal angle corresponding to $\varphi_{B,Extr}$

$\varphi_B, \varphi^B_{ij}$ — joint angles of the bifurcation

$\varphi_{B,Extr}$ — extremes of $\varphi_0(\varphi_B)$ in φ_B fulfilling $d\varphi_0 / d\varphi_B = 0$

$\varphi_{ij,Crit}$ — critical joint angle due to $h = 0$ lines

φ_{leg} — leg orientation with respect to the ground

Q — $Q(\varphi_{12}, \varphi_{23})$-function, $Q = 0$ represents torque equilibrium

r — leg length

$\vec{r}$ — leg vector: $\vec{r} = \vec{\ell}_1 + \vec{\ell}_2 + \vec{\ell}_3$

R_C — stiffness ratio $R_C = c_{12} / c_{23}$

$R_{\Delta\varphi}$ — ratio of joint flexions $R_{\Delta\varphi} = \Delta\varphi_{12} / \Delta\varphi_{23}$

R_λ — outer segment length ratio $R_\lambda = \ell_1 / \ell_3 = \lambda_1 / \lambda_3$

$\Theta_i, \underline{\Theta}_i$ — moment of inertia of segment i, as tensor

x, y, z — Cartesian coordinates

INTRODUCTION

Although some movement studies using the leg spring concept (Farley et al., 1996; Seyfarth et al., 1999) can be found in the literature only little is known about the mechanisms and benefits of such a manner of leg operation. The concept of spring-like operation of the total leg can be extended to spring-like operation of joints for exercises as hopping, running, and jumping (Farley and Morgenroth, 1999; Stefanyshyn and Nigg, 1998; Günther et al., in prep.). Depending on the execution characteristics, exhaustion or external constraints changes in joint kinetics and kinematics are found experimentally (e.g. Kovács et al., 1999; Farley et al., 1998; Williams et al., 1991). Thereby elastic operation of joints may disappear for changed

movement criteria, e.g. concerning foot placement (Kovács et al., 1999) or hopping height (Farley and Morgenroth, 1999). An elastic operation of a joint was found to require a significant distance to the acting ground reaction force (Farley et al., 1998). If more than one joint fulfils this condition, the distribution of joint loading has to be realised. With respect of multi-segment legs this evokes the kinematic redundancy problem, i.e. the same leg length can be realised by different joint configurations. This problem was first addressed in Bernstein's motor equivalence problem (Bernstein, 1967). Unfortunately, there is no generally accepted theory yet which could explain the observed behaviour in biological limbs (review in: Gielen et al., 1995).

The approaches found in the literature postulate different optimisation criteria which result in corresponding movement patterns taking physiological, energetic or metabolic aspects into account. Nevertheless, these constraints do not explain the unique motor pattern used by biological systems for an intended movement. However, it is well accepted that biological actuators are adapted to their mechanical environment and to different task-depending requirements (Van Leeuwen, 1992). By their intrinsic properties muscles may stabilise joint rotations to a certain extent (Wagner and Blickhan, 1999).

A key to solve the kinematic redundancy problem is the assumption of spring-like muscle behaviour (Winters, 1995). However, the quasi-elastic muscle operation is not sufficient to guarantee stable joint configurations (Dornay et al., 1993). To investigate the interplay between elastically operating actuators, leg architecture and motor program a mechanical model is required. A simple model recently introduced by Farley et al. (1998) represented torque actuators as linear rotational springs at ankle, knee and hip joint within a four-segment model. The observed leg force tracings, however, require nonlinear torque characteristics according to experimental observations.

The aim of this study is to explore the requirements of elastically operating torque actuators of a kinematically redundant segmented leg. Thereby the influence of the segment length design and different kinematic conditions are taken into account. At least three leg segments are necessary to address kinematic redundancy. The leg design will be judged by investigating the possible kinematic responses to different loading situations. The stability and predictability of the leg operation will be quantified by calculating the configurations of inherent leg instability. This allows to derive criteria for leg length design, motor control (torque adjustment) and kinematic programs. Thereby the effects of leg segmental masses and inertias are neglected, as they are of minor importance in fast types of locomotion (Günther et al., in prep.) if spring-like leg behaviour is present (running, jumping).

METHODS

The three segment model

The planar model (Fig. 1) consists of the following parts: (1) a point mass m representing the total body mass and (2) three massless leg segments (foot, shank and thigh; lengths ℓ_1, ℓ_2, ℓ_3), linked by frictionless rotational joints. The point mass is attached at the top of the thigh (hip). As there is only one point mass the equations of motion are:

$$m\ddot{\vec{r}} = \vec{F}_{leg} + m\vec{g} , \tag{1}$$

where $\vec{r}$ is the position of the point mass, $\vec{F}_{leg}$ is the force due to the operation of the leg segments and $\vec{g}$ is the gravitational acceleration vector. As all segments are massless the force $\vec{F}_{leg}$ acting on the point mass is equal to the external ground reaction force.

Torque equilibrium

To integrate the equations of motion (Eq. 1) the instantaneous leg force $\vec{F}_{leg}$ has to be calculated. The torques at the hinge joints (ball M_{01}, ankle M_{12}, and knee M_{23}) and the orientation of the leg segments $(\vec{\ell}_1, \vec{\ell}_2, \vec{\ell}_3)$ must fulfill the following *static torque equilibrium* (all M_{ij} direct in z; for details see Appendices 1-3):

$$\begin{aligned}
\left. \left(\vec{\ell}_1 \times \vec{F}_{leg}\right)\right|_z &= M_{01} - M_{12} \\
\left. \left(\vec{\ell}_2 \times \vec{F}_{leg}\right)\right|_z &= M_{12} - M_{23} \\
\left. \left(\vec{\ell}_3 \times \vec{F}_{leg}\right)\right|_z &= M_{23}
\end{aligned} \tag{2a-c}$$

where

$$\vec{\ell}_1 + \vec{\ell}_2 + \vec{\ell}_3 = \vec{r} . \tag{2d}$$

These are five algebraic equations to estimate the following five unknowns: the leg force $\vec{F}_{leg}$ (two components) and the segment angles φ_1, φ_2, φ_3. Hereby constant segment lengths $\left|\vec{\ell}_i\right| = \ell_i$, a given leg vector $\vec{r}$ and given torques $M_{ij}(\varphi_1, \varphi_2, \varphi_3; t)$ were assumed.

14
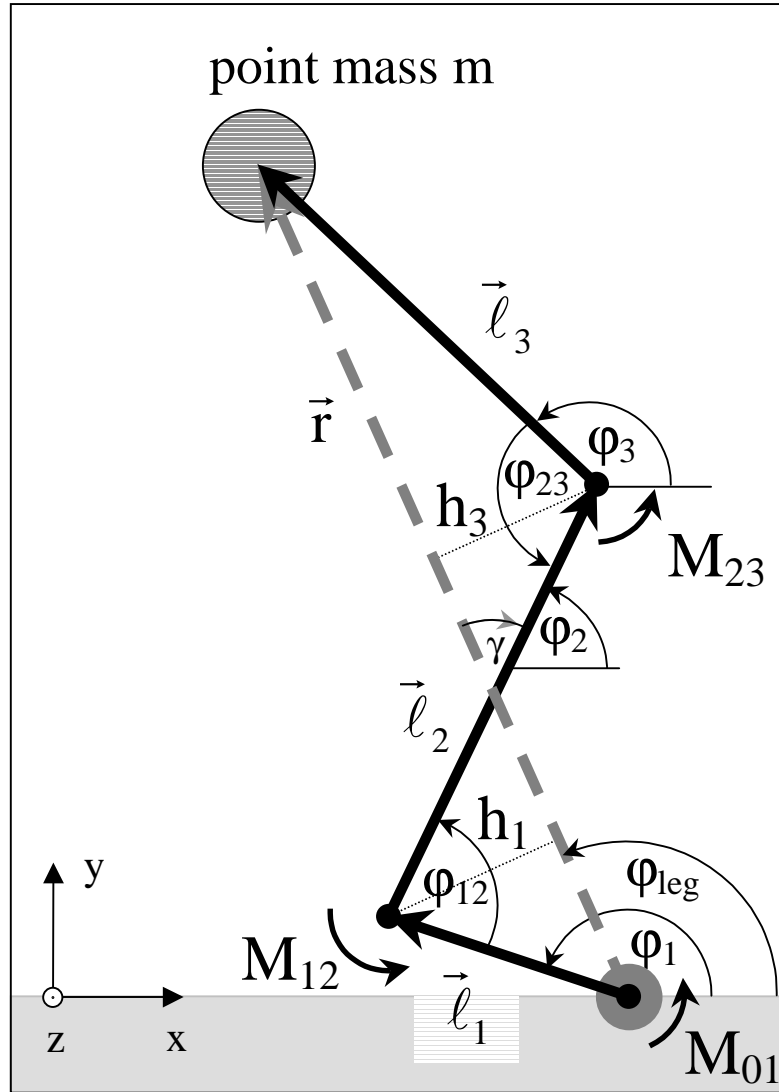
Fig. 1 Three-segment model with one point mass. Torques are applied at ball, ankle, and knee joint (M_{01}, M_{12}, M_{23}). Leg configuration is represented by the inner joint angles (ankle angle: $\varphi_{12} = \varphi_2 + \pi - \varphi_1$, knee angle: $\varphi_{23} = \varphi_2 + \pi - \varphi_3$). The angle γ is defined as the difference between middle segment and leg orientation: $\gamma = \varphi_2 - \varphi_{leg}$ (in this sketch γ is negative).

The segment angles $\varphi_1, \varphi_2, \varphi_3$ may be substituted by the leg angle φ_{leg} and by two variables representing the internal leg configuration (e.g. φ_{12}, φ_{23} or h_1, h_3; Fig. 1). As the leg length $r = |\vec{r}|$ merely depends on the internal leg configuration we separate $\vec{r} = r(\varphi_{12}, \varphi_{23}) \cdot \vec{e}_r(\varphi_{leg})$ where $\vec{e}_r$ represents the unit vector uniquely determined by the leg orientation $\varphi_{leg}(\vec{r})$ and

$$r(\varphi_{12}, \varphi_{23}) = \sqrt{\ell_1^2 + \ell_2^2 + \ell_3^2 - 2\ell_1\ell_2\cos\varphi_{12} - 2\ell_2\ell_3\cos\varphi_{23} + 2\ell_1\ell_3\cos(\varphi_{12} - \varphi_{23})} \,. \qquad (3)$$

After replacing Eq. 2d by Eq. 3 now four equations exist for following unknowns: two components of the leg force $\vec{F}_{leg}$ and two variables representing the internal leg configuration. The internal configuration is a consequence of the chosen torque characteristics at the joints and must fulfill Eq. 3. For torque characteristics only depending on the internal configuration $M_{ij}(\varphi_{12}, \varphi_{23})$ we can identify all configurations $\varphi_{12}, \varphi_{23}$ fulfilling the torque equilibrium (Eq. 2a-c) denoted by $Q(\varphi_{12}, \varphi_{23}) = 0$. In this paper these solutions of $Q(\varphi_{12}, \varphi_{23}) = 0$ will be derived for a simplified situation. After estimating the joint angles using $Q(\varphi_{12}, \varphi_{23}) = 0$ and Eq. 3 the leg forces are simply given by two linearly independent equations of Eq. 2a-c.

Neglect of the external torque M_{01}

To find a first solution of the torque equilibrium the torque at the ball of the foot is neglected: $M_{01} = 0$. This results in leg forces $\vec{F}_{leg}$ always parallel to $\vec{r}$ as we can summarise Eq. 2a-c to $\vec{r} \times \vec{F}_{leg}\big|_z = M_{01}$. For joint torques M_{12}, M_{23} only depending on the internal configuration (φ_{12}, φ_{23}; Fig. 1) the amount of the leg force does also not depend on the leg orientation φ_{leg}. As Eq. 2b becomes the negative sum of Eq. 2a and 2c only two remaining torque equations must be fulfilled:

$$\begin{aligned} -h_1 \cdot F_{leg} &= M_{12} \\ h_3 \cdot F_{leg} &= M_{23} \end{aligned}, \tag{4a,b}$$

or eliminating F_{leg}: $\qquad\qquad M_{12}\, h_3 + M_{23}\, h_1 = 0, \tag{5}$

where $h_1(\varphi_{12}, \varphi_{23})$ and $h_3(\varphi_{12}, \varphi_{23})$ are the distances of the joints to the line of action of the leg force ($h_i = \ell_i \sin(\vec{\ell}_i, \vec{r})$; in Fig. 1: $h_1 < 0$ and $h_3 < 0$). Eq. 5 determines the ratio of ankle to knee torque M_{12} / M_{23} to be equal to $-h_1 / h_3$ as long as the foot contacts the ground at the ball with no external torque ($M_{01} = 0$; no effects of heel or toe contact). In terms of the inner joint angles the simplified torque equilibrium (Eq. 5) results in the requested Q function:

$$Q(\varphi_{12}, \varphi_{23}) = \frac{M_{12}}{\ell_1} \sin\varphi_{23} + \frac{M_{12} - M_{23}}{\ell_2} \sin(\varphi_{12} - \varphi_{23}) + \frac{M_{23}}{\ell_3} \sin\varphi_{12} = 0 \tag{6}$$

The internal leg configuration characterised by Eqs. 3 and 6 requires to know the torques (see below). The amount of leg force F_{leg} remains to be estimated using either Eq. 2a-c or Eq. 4a,b resulting in:

$$F_{leg}(\varphi_{12}, \varphi_{23}) =$$

$$\frac{r(\varphi_{12}, \varphi_{23}) \cdot \left(\dfrac{M_{12}}{\ell_1} \sin \varphi_{23} + \dfrac{M_{12} + M_{23}}{\ell_2} \sin(\varphi_{12} - \varphi_{23}) - \dfrac{M_{23}}{\ell_3} \sin \varphi_{12} \right)}{\ell_1(\cos \varphi_{23} - \cos(2\varphi_{12} - \varphi_{23})) - 2\ell_2 \cos \varphi_{12} \sin \varphi_{23} + \ell_3(\cos \varphi_{12} - \cos(\varphi_{12} - 2\varphi_{23})) - 2\dfrac{\ell_1 \ell_3}{\ell_2} \sin^2(\varphi_{12} - \varphi_{23})}$$

$$(7)$$

where $r(\varphi_{12}, \varphi_{23})$ denotes the instantaneous leg length (Eq. 3).

Symmetrical loading: stiffness equilibrium

To investigate the influence of knee and ankle rotational stiffness, linear ($\nu = 1$) or, more generally, nonlinear ($\nu > 0$, $\nu \neq 1$) rotational springs are introduced:

$$M_{12} = c_{12}(\varphi_{12}^0 - \varphi_{12})^\nu, \qquad (8a)$$

$$M_{23} = -c_{23}(\varphi_{23}^0 - \varphi_{23})^\nu, \qquad (8b)$$

where φ_{12}^0, φ_{23}^0 are the nominal angles of the rotational springs, φ_{12}, φ_{23} are the joint angles (with $\varphi_{ij} < \varphi_{ij}^0$), c_{12}, c_{23} are the rotational stiffnesses and ν is the exponent of nonlinearity. Such a joint torque characteristic is present in humans and several mammals during fast locomotion. The nonlinearity may result from tendon properties and muscle-tendon dynamics (chapter IV).

For the particular case of symmetrical loading with $\varphi_{12}^0 = \varphi_{23}^0$ and $\varphi_{12} = \varphi_{23}$ the torque equilibrium (Eq. 5) results in

$$\frac{c_{12}(\varphi_{12}^0 - \varphi_{12})^\nu}{\ell_1 \sin(\varphi_{12} - \gamma)} = \frac{c_{23}(\varphi_{23}^0 - \varphi_{23})^\nu}{\ell_3 \sin(\varphi_{23} - \gamma)} \qquad (9)$$

which requires:

$$\frac{c_{12}}{\ell_1} = \frac{c_{23}}{\ell_3}, \qquad (10)$$

where $\gamma(\varphi_{12}, \varphi_{23})$ is the intersectional angle between $\vec{\ell}_2$ and $\vec{r}$ (see Fig. 1). Thus, if the ratio of knee to ankle stiffness is equal to the ratio of the thigh to foot segment length a symmetrical loading of the system is a solution of the torque equilibrium (Eqs. 5, 6). The stiffness equilibrium (Eq. 10) does not depend on ℓ_2.

Introduction of normalised segment lengths and the stiffness ratio

As there is no influence of the total leg length, $\ell_{MAX} = \ell_1 + \ell_2 + \ell_3$, neither on the torque equilibrium (Eqs. 5, 6) nor on the stiffness equilibrium (Eq. 10), we can substitute the actual segment lengths by a normalised length $\lambda_i = \ell_i / \ell_{MAX}$ (Fig. 5). Furthermore, to fulfill a symmetrical shortening, only the ratio of the rotational stiffnesses $R_C = c_{12} / c_{23}$ is crucial. The stiffness equilibrium (Eq. 10) requires the ratio R_C to be equal to the length ratio $R_\lambda = \lambda_1 / \lambda_3$, or:

$$\alpha = R_C / R_\lambda = 1. \tag{11}$$

Numerical investigation of the model

Two different approaches were applied to investigate the three segment model: (1) *forward dynamic modelling* of the equations of motion (Eq. 1) and (2) mapping the *solutions of the torque equilibrium* (Eqs. 5, 6) in terms of the possible leg configurations (φ_{12}, φ_{23}) with respect to (a) the nominal angle setup (φ^0_{12}, φ^0_{23}), (b) the segment length design (λ_2, $R_\lambda = \lambda_1 / \lambda_3$), (c) the stiffness ratio R_C, and (d) the torque design (exponent ν). To get an analytical understanding here the second approach was chosen.

Additionally, the influence of nonconservative structures (e.g. heel strike, represented by $M_{01}(\varphi_1, \dot{\varphi}_1)$), segment inertias and continuous changes of the nominal angles on the joint kinematics may be considered.

RESULTS

The solutions of the torque equilibrium (Eq. 2) represent possible joint trajectories during loading of the leg. These solutions allow us to identify critical joint configurations and limitations in the accessibility of the configuration space. The general features of the model (nominal angle setup, segment length design, stiffness ratio, torque characteristic) will be discussed in terms of the

34

torque equilibrium for monoarticular torque generators neglecting external torques (i.e. at the ball $M_{01} = 0$ in Eq. 2 which results in Eqs. 5, 6).

In order to enhance transparency we start with identical segment lengths ($\ell_1 = \ell_2 = \ell_3$, i.e. all $\lambda_i = 1/3$), a stiffness ratio $R_C = 1$ fulfilling the stiffness equilibrium (Eq. 10) and linear torque characteristics ($\nu = 1$). For identical nominal angles $\varphi_{12}^0 = \varphi_{23}^0$ this results in a symmetrical solution (see methods). After exploring this symmetrical segment length design by changing the nominal angles (part 1), different segment length designs, stiffness ratios and torque characteristics will be introduced to explain their influences on the leg operation (part 2). In parts 3 and 4 the segment length design is investigated more profoundly with respect to the location of the h = 0 lines (part 3) and the location of bifurcations in symmetric (part 4.1) and asymmetric loading (part 4.2). The appendix 4 supports the reader with all equations necessary to calculate the location of bifurcations either analytically or numerically.

1 Equal segment length design (1:1:1) and different nominal angle configurations

In Fig. 2A the simple symmetrical condition $\lambda_1 = \lambda_2 = \lambda_3 = 1/3$ and $R_C = 1$ is considered. We start with nominal angle configurations at a constant nominal leg length λ_0 close to a symmetrical condition $\varphi_{12}^0 \approx \varphi_{23}^0$.

1.1 Constant relative nominal leg length $\lambda_0(\varphi_{12}^0, \varphi_{23}^0)$

Leg shortening may lead to multiple pathways: either bending in knee or ankle joint dominates and the other joint will reverse movement direction. At a certain relative leg length λ_B the solutions for exact symmetry ($\varphi_{12}^0 = \varphi_{23}^0$) show a saddle point where three paths of further shortening with Q = 0 (Eq. 6) become possible. From an energetic point of view, a further symmetrical loading of the leg leads to the highest increase in stored elastic energy (i.e. the highest increase in leg force) as compared to both of the nonsymmetrical paths. Therefore, symmetrical loading can not be guaranteed if this *bifurcation* point is reached, i. e. a critical amount of leg shortening $\Delta\lambda = \lambda_0 - \lambda_B$ is exceeded. This relative amount of symmetrical shortening till bifurcation $\Delta\lambda$ is denoted as the *working range*.
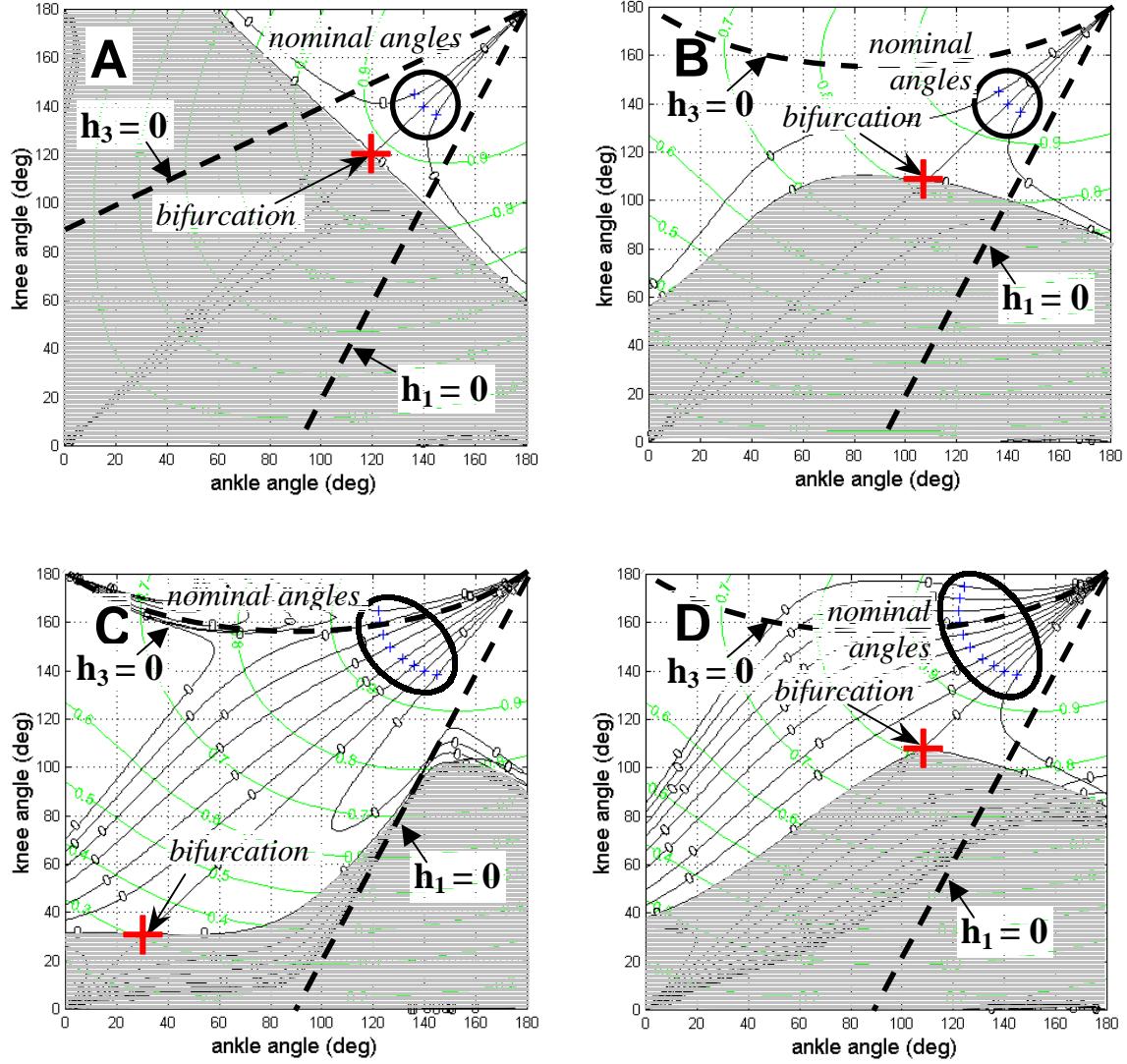
Fig.2 *Solutions of the torque equilibrium (Eq. 6; Q = 0 denoted by thin black lines) in the configuration space (φ$_{12}$, φ$_{23}$) with different leg designs and torque characteristics (see below) fulfilling the stiffness equilibrium (Eq. 11: R$_C$ = R$_λ$) and nominal angles at a relative nominal leg length λ$_0$ = 0.94. The grey areas represent restrictions due to the oblique solution. Configurations with a constant relative leg length λ(φ$_{12}$, φ$_{23}$) = const. are denoted by grey lines with embedded length values (0.2-0.9). Configurations where joints are crossing the leg axis (h$_1$ = 0 or h$_3$ = 0) are denoted schematically by bold dashed lines.*

Leg designs: (A) equal segment lengths 1:1:1 (all λ$_i$ = $^1/_3$), (B, C, D) human-like leg design λ$_1$:λ$_2$:λ$_3$ = 2:5:5. Torque characteristics: (A, B) linear rotational springs at ankle and knee joint, (C) quadratic characteristic (ν = 2: M$_{ij}$ ~ Δφ$_{ij}^2$), (D) linear rotational springs plus a biarticular spring (M$_{13}$ = c$_{13}$ Δφ$_{13}$, c$_{13}$ = 0.05 c$_{23}$).

The configuration space beyond the oblique branch of the symmetrical solution proves to be inaccessible for a given relative nominal leg length λ_0 and a constant R_C. In fact, symmetrical loading of both springs is only possible within a limited range of leg shortening.

Leaving the symmetrical nominal angle configuration leads to solutions either above ($\varphi^0_{12} < \varphi^0_{23}$) or below ($\varphi^0_{12} > \varphi^0_{23}$) the symmetrical solution with a constant R_C. Therefore, the symmetrical solution pointing to the bifurcation separates the configuration space into solutions above and below the symmetrical axis ($\varphi_{12} = \varphi_{23}$). Nevertheless, a conjugate solution branch exists for any nominal setup in the configuration space beyond the oblique solution which is located on the opposite side of the symmetrical axis ($\varphi_{12} = \varphi_{23}$). However, this second branch is not directly accessible starting at the nominal angle configuration (Fig. 2A). An adaptation of R_C in combination with moving the nominal angle configuration (part 4.1) results in a slightly deformed symmetrical solution which may lead to a gain in working range. However, this requires to consider the influence of leg design (R_λ) and the location of foci in the configuration space (part 3).

1.2 Influence of the relative nominal leg length λ_0

Shifting of the relative nominal leg length λ_0 on the symmetrical axis ($\varphi^0_{12} = \varphi^0_{23}$) leads to a corresponding shift of the bifurcation point λ_B without changing the general properties described above. Assuming symmetrical loading a maximum working range $\Delta\lambda$ is found at a certain relative nominal leg length λ_0 (Fig. 5C, D). This dependency $\Delta\lambda(\lambda_0) = \lambda_0(\lambda_B) - \lambda_B$ can be expressed analytically in terms of $\varphi_0(\varphi_B)$ (Appendix 4; Eq. A10, Fig. 5A) and is discussed in part 4.1.

2 Human-like segment length design (2:5:5) and different torque characteristics

The influence of different torque characteristics and a human-like segment length design on the solutions of the torque equilibrium (Eqs. 5, 6) is investigated in Fig. 2B-D. The stiffness ratio R_C equals the ratio of the outer segments $R_\lambda = \lambda_1 / \lambda_3 = 2/5$ (stiffness equilibrium: Eqs. 10, 11). Again nominal angle configurations in the neighbourhood of the symmetrical nominal angle setup ($\varphi^0_{12} \approx \varphi^0_{23}$) are considered.

The bifurcation is shifted to smaller leg lengths due to the changed segment lengths (Fig. 2B). In contrast to an equal segment length design (Fig. 2A), almost homogeneous bending of the joint adjacent to the smaller outer segment (here the ankle joint) becomes possible.

Introducing a nonlinear torque characteristic (exponent $\nu = 2$) shifts the bifurcation to smaller leg lengths (Fig. 2C). The solutions of the torque equilibrium are quite homogeneous in the upper part of the configuration space ($\varphi^0{}_{12} < \varphi^0{}_{23}$). This holds true for a variety of nominal angle configurations as long as the $h_3 = 0$ line is not exceeded.

The effect of biarticular structures acting on knee and ankle joint is shown in Fig. 2D. A linear spring between the outer segments (flexing knee and extending ankle joint) leads again to an almost parallel alignment of solutions for a wide range of different nominal angles. In contrast to Fig. 2C the location of the bifurcation point is not influenced.

3 Intersectional point of solutions (focus)

Certain points of the configuration space (φ_{12}, φ_{23}) are attracting solutions of the torque equilibrium (Eqs. 5, 6) for different nominal angles (φ^0_{12} or φ^0_{23}, respectively), joint stiffness ratios R_C and exponents ν of the torque characteristic. Three different types of such foci are present:

(1) all joints are either completely stretched or bent (joint angle $= n \cdot 180°$, where n is an integer number; fulfils Eq. 5 as $h_1 = h_3 = 0$),

(2) the total leg length is zero (only possible if every segment is smaller than the sum of both the others; fulfils Eq. 2a-c as $M_{01} = 0$), or

(3) one joint lies on the line of action of the leg force and the respective joint angle is the nominal angle (see Figs. 3C, D).

The latter type (3) originates from the fact that (a) both the perpendicular distance of the joint to the force line of action (e.g. h_1) and (b) the respective torque (i.e. M_{12}) vanishes (Eq. 5). As (a) is a purely geometrical condition and (b) only depends on the nominal angle of the joint crossing the force line of action (e. g. φ^0_{12}) there is no influence of neither the remaining nominal angle (Fig. 3C, here $\varphi^0{}_{23}$), the stiffness ratio R_C (Fig. 3D) nor the exponent ν on the location of this focus.
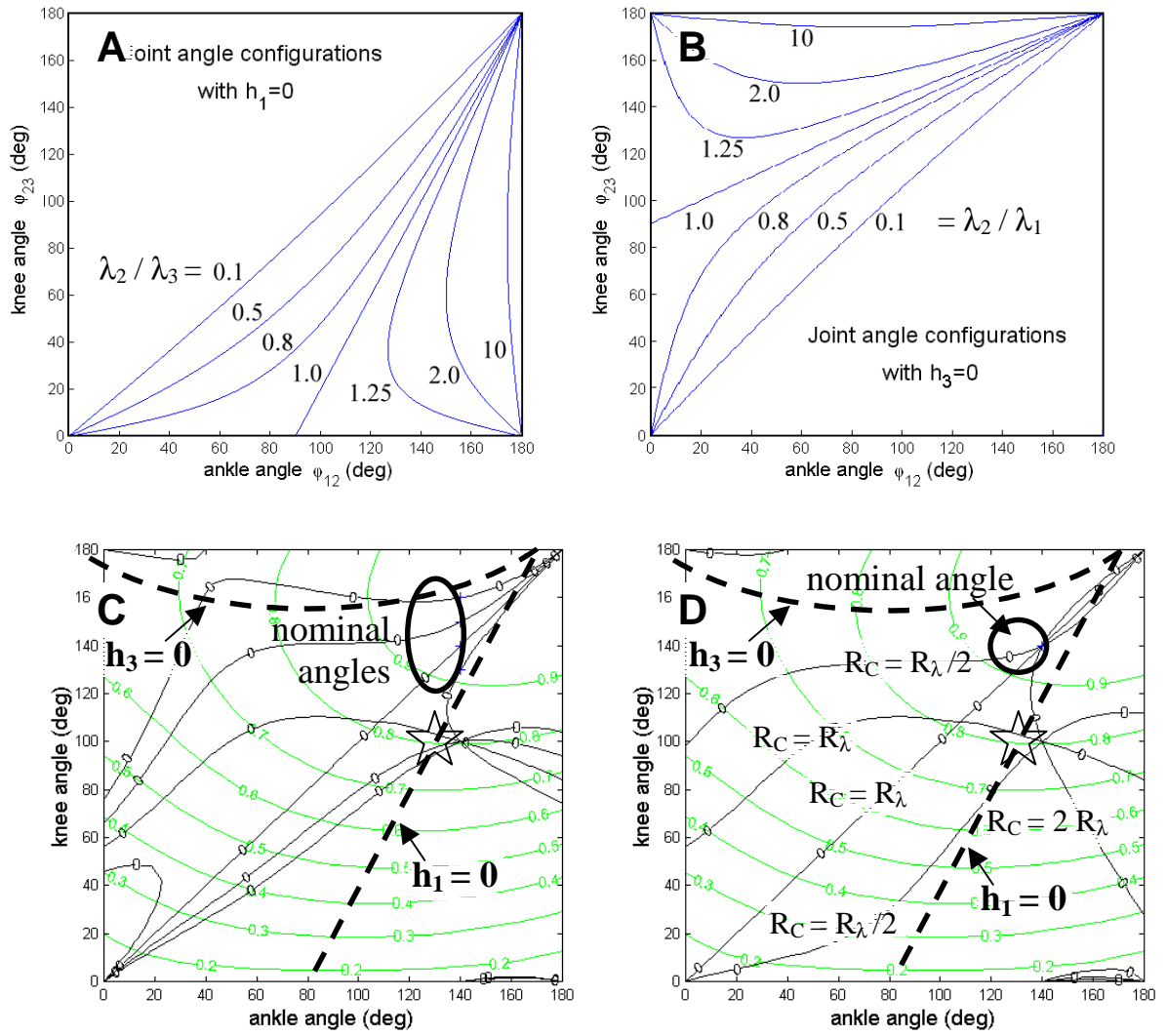
Fig. 3 (A, B) Joint angle configurations where (A) the ankle joint ($h_1 = 0$) and (B) the knee joint ($h_3 = 0$) coincides with the leg axis for different segment length designs (denoted by λ_2 / λ_3 and λ_2 / λ_1; Eq. 12a,b). (C, D) For a given nominal ankle angle φ^0_{12} and arbitrary knee angles φ^0_{23} (C) or arbitrary stiffness ratios R_C (D) a focus at the $h_1 = 0$ line (big star) occurs if $h_1 = 0$ has an intersectional point with $\varphi_{12} = \varphi^0_{12}$. This holds true for different segment lengths λ_1 or different exponents ν of the torque characteristics as long as φ^0_{12} and λ_2 / λ_3 (not shown here) are kept constant. *Note:* There is no focus at $h_3 = 0$ in (D) as $\varphi_{23} = \varphi^0_{23}$ has no intersection with $h_3 = 0$.

The geometrical conditions for angle configurations where the ankle ($h_1 = 0$) or the knee ($h_3 = 0$) joint is crossing the leg axis can be expressed as (Fig. 3A, B):

$$\tan \varphi_{12} = \frac{\sin \varphi_{23}}{\cos \varphi_{23} - \lambda_2 / \lambda_3} \quad (\text{for } h_1 = 0), \tag{12a}$$

$$\tan \varphi_{23} = \frac{\sin \varphi_{12}}{\cos \varphi_{12} - \lambda_2 / \lambda_1} \quad (\text{for } h_3 = 0). \tag{12b}$$

The critical joint angle $\varphi_{ij,Crit}$ (corresponding to the smallest nominal angle for which a focus may occur) results from these equations if the inner to outer segment length ratio is larger than one (e.g. human shank to foot length ratio λ_2 / λ_1; Tab.1, Fig. 2B, C, D and Fig. 3B).

For a homogeneous distribution of the solutions a focus-free area is of advantage. Regarding an equal segment length design (Fig. 2A) this can only be realised for nominal angles smaller than 90°. To allow higher nominal angles the ratio of the length of the inner segment λ_2 to an outer one (λ_1 or λ_3) should be clearly larger than one. This requires the discussion of leg design (part 4). As stated before, it is sufficient to consider only one half of the configuration space (e.g. $\varphi_{12} < \varphi_{23}$) if adequate nominal angles ($\varphi^0_{12} < \varphi^0_{23}$) are chosen. Then, foci in the conjugate configuration space are not of importance for the system behaviour. For example, a human-like segment length design (2:5:5, Figs. 2B–D) allows almost parallel solutions for $\varphi_{12} < \varphi_{23}$ as long as φ^0_{23} smaller than $\varphi_{23,Crit} \approx 156.4°$ (at least for $\nu = 1$: Fig. 3C; Tab. 1).

λ_2 / λ_1	$\varphi_{23,Crit}$	$\varphi_{12,Ref}$
1.0	90°	0°
1.25	126.9°	36.9°
1.5	138.2°	48.1°
2.0	150.0°	58.8°
2.5	156.4°	65.1°
3.0	160.5°	70.1°
10	174.3°	81.2°

Tab. 1 The minimum of the $h_3 = 0$ line expressed as $\varphi_{23}(\varphi_{12})$ is present for a critical knee angle $\varphi_{23,Crit}$ with a corresponding reference angle $\varphi_{12,Ref}$. Solutions may be attracted by a focus at $h_3 = 0$ if nominal angles φ^0_{23} are larger than $\varphi_{23,Crit}$ (Fig. 3B, Fig. 11A).

4 Segment length design (λ_2, $R_\lambda = \lambda_1 / \lambda_3$)

The segment length design, uniquely represented by two relative segment lengths, is illustrated in Fig. 4A as a point within a triangular plane. One aspect of leg design was already discussed in the previous part with respect to focus points. Here, a large ratio of λ_2 / λ_1 or λ_2 / λ_3 was of advantage (Fig. 4B).

Now two further strategies of segment length design will be discussed: variations in the relative length of the middle segment (λ_2-design, Fig. 4C) and the ratio of the outer segment lengths (R_λ-design, Fig. 4D). While the λ_2-design determines the location of the bifurcations in symmetrical loading, the R_λ-design influences the shape of the oblique branch of the symmetrical solution. Taking asymmetric nominal angles into account, this may enhance the working range by suitable R_C adaptations.

40
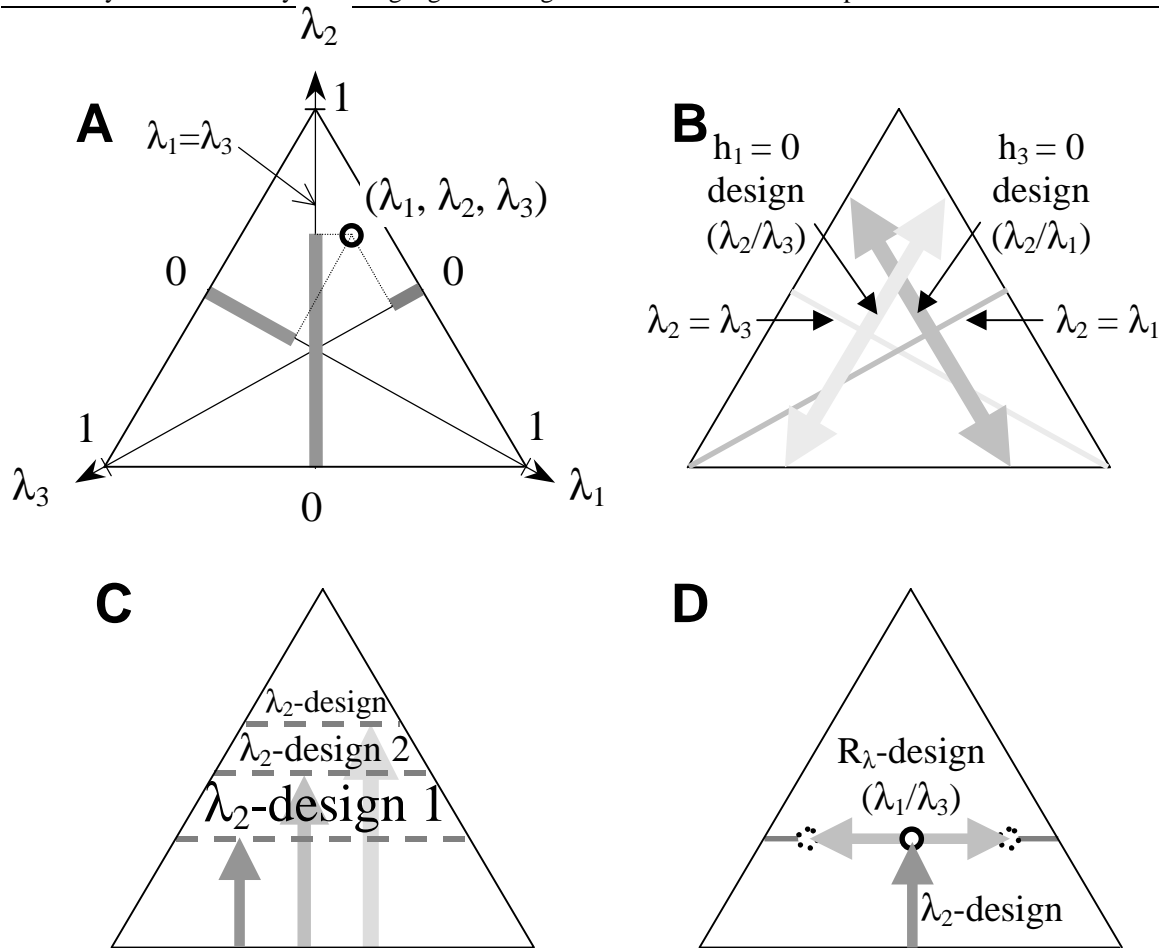
Fig. 4 (A) Segment length design is characterised by a triplet $(\lambda_1, \lambda_2, \lambda_3)$ with $\lambda_1 + \lambda_2 + \lambda_3 = 1$, i.e. a point within the triangle. Different strategies of leg design can be distinguished:
(B) To avoid the attraction of solutions by foci the nominal angle design is restricted by the location of the $h = 0$ line in the chosen half of the configuration space (above or below the symmetrical axis $\varphi_{12} = \varphi_{23}$; Fig. 3C).
(C) λ_2 is locating the bifurcation point(s) in symmetrical loading.
(D) The R_λ-design (ratio λ_1 / λ_3) allows to take advantage of asymmetric leg loading by properly adjusting the joint stiffness ratio R_C.

To investigate the bifurcation behaviour of the leg in general both strategies (λ_2, R_λ) are of importance. Solutions in the neighbourhood of the bifurcation point show divergent paths during leg shortening. Therefore, the locations of existing bifurcation points for different nominal angles and stiffness ratios give a quantitative measure of the leg stability within the configuration space. Although in symmetrical loading the solution directing to the bifurcation is the one and only straight way of leg shortening allowing homogenous loading with respect to joint angles, the existence of a bifurcation also constitutes a possible instability for leg loading.

Almost symmetrical leg loading for a shifted nominal angle configuration can be maintained by an adapted R_C value leading to a new bifurcation point. For asymmetric outer segment length

designs ($R_\lambda \neq 1$) a gain in working range may occur if the joint adjacent to the smaller outer segment is flexed more than the other one.

4.1 Bifurcation behaviour in symmetrical loading: λ_2 – design

The bifurcation angle φ_B for symmetrical loading ($\varphi_0 = \varphi_{12}^0 = \varphi_{23}^0$ and $R_C = R_\lambda$) shifts correspondingly with the nominal angle φ_0 (Fig. 5A, B).

The relationship between φ_0 and φ_B can be expressed analytically as a function $\varphi_0(\varphi_B)$ (Appendix 4: Eq. A10) and has following properties:

(1) $\varphi_0(0) = 0$, $\varphi_0(180°) = 180°$ and $\varphi_0 \neq \varphi_B$ for $0 < \varphi_B < 180°$ and $\nu > 0$,

(2) there is one pole in $\varphi_0(\varphi_B)$ if $\lambda_2 \geq 1/2$, and

(3) there are 0, 1, or 2 local extremes in $0 \leq \varphi_B \leq 180°$.

The inverse function can not be given explicitly as there may exist several values of φ_B for a given φ_0 (Fig. 5A).

The $\varphi_0(\varphi_B)$-dependency is uniquely determined by the relative length of middle segment λ_2 and the exponent of the torque characteristic ν, but not by R_λ (Fig. 10A). In general, there is always a bifurcation within [0, 180°] as long as $\lambda_2 < 1/2$ (type I-bifurcation). Increasing the nominal angle φ_0 there may arise additional solutions for φ_B (type II-bifurcation) for certain constellations of λ_2 and ν (Fig. 5A, B and Fig. 8). Hereby λ_2 must exceed a critical value $\lambda_{2,\text{Crit}}$ which merely depends on the exponent ν (Tab. 2).

ν	$\lambda_{2,\text{Crit}}(\nu)$	$\varphi_{B,\text{Crit}}(\lambda_{2,\text{Crit}},\nu)$	$\varphi_{0,\text{Crit}}(\varphi_{B,\text{Crit}})$
0.5	0.483	36.7°	100.8°
1.0	0.464	54.7°	135.8°
1.5	0.442	71.6°	157.5°
2.0	0.414	90.0°	171.0°
2.5	0.380	114.1°	178.2°

Tab. 2 Critical relative length of the middle segment $\lambda_{2,\text{Crit}}(\nu)$ for given exponents of the torque characteristics ν where for $\lambda_2 \geq \lambda_{2,\text{Crit}}$ a new type II-bifurcation appears (Fig. 5A, B) if the nominal angle φ_0 exceeds a critical nominal angle $\varphi_{0,\text{Crit}}(\lambda_2,\nu)$ (here denoted for $\lambda_2 = \lambda_{2,\text{Crit}}$). This critical nominal angle $\varphi_{0,\text{Crit}}$ corresponds to the bifurcation angle $\varphi_{B,\text{Crit}}$ (denoted again for $\lambda_2 = \lambda_{2,\text{Crit}}$).
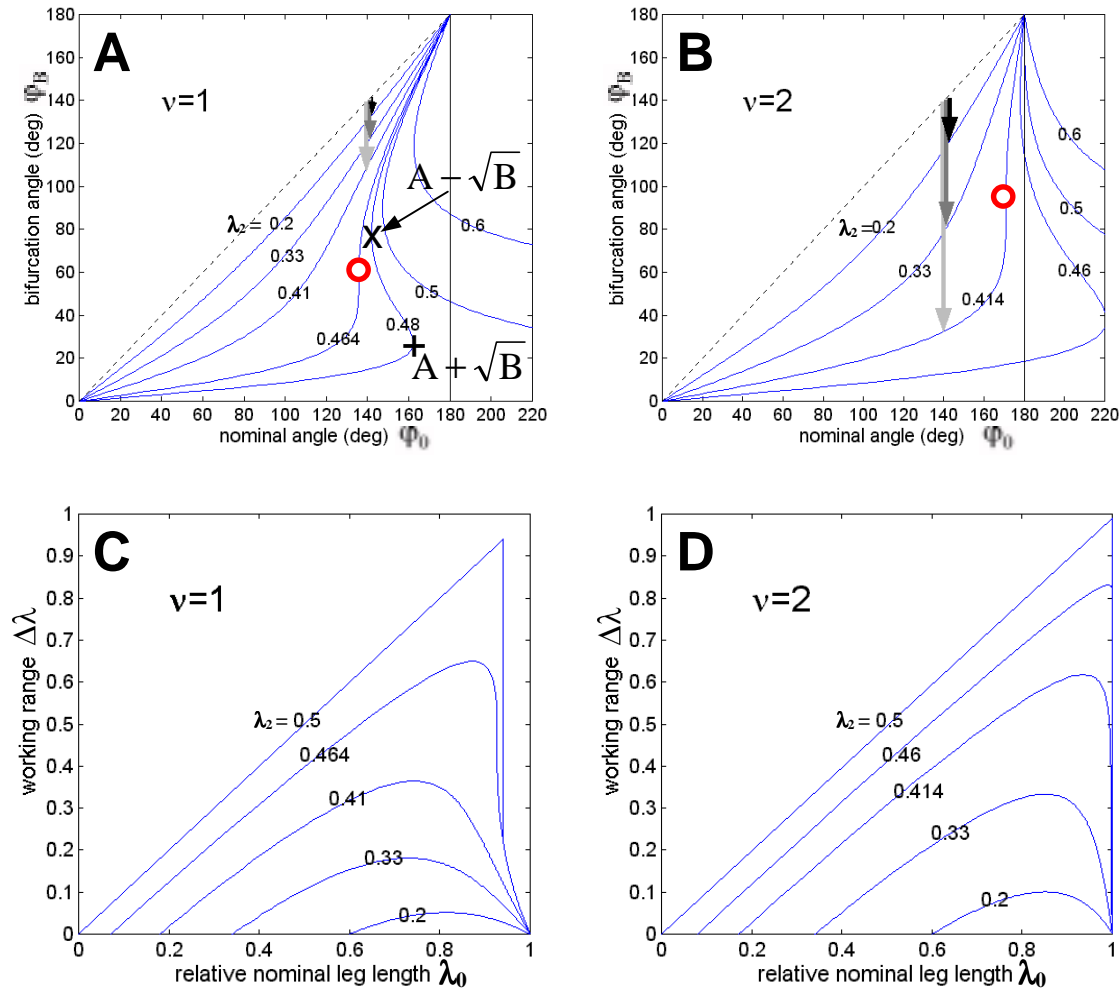
Fig. 5 (A-D) Bifurcations in symmetrical loading. (A, B) For each nominal angle φ_0 and a given exponent ν of the torque characteristic the location of the possible bifurcation angle(s) φ_B depend merely on λ_2 and not on R_λ. If λ_2 exceeds a critical threshold $\lambda_{2,\text{Crit}}(\nu)$ (small circles) a sudden change in φ_B occurs at a corresponding nominal angle $\varphi_{0,\text{Crit}}(\lambda_2, \nu)$. Then, new bifurcations appear for $\varphi_0 > \varphi_{0,\text{Crit}}$ which reduce the working range (small arrows). The local extremes in $\varphi_0(\varphi_B)$ determine the existence of type I (lower extreme '+': $\cos \varphi_{B,\text{Extr}} = A + \sqrt{B}$) or type II (upper extreme 'x': $\cos \varphi_{B,\text{Extr}} = A - \sqrt{B}$) bifurcations.

(C, D) Relative working range $\Delta\lambda = \lambda_0(\varphi_0) - \lambda_B(\varphi_B)$ for different λ_2-designs depending on the relative nominal leg length λ_0 and ν (but not on R_λ). The highest advantage of nonlinear (quadratic) torque design is found for $\lambda_2 = 0.3 - 0.5$ and $\lambda_0 > 0.8$.

In Fig. 5C, D the translational working range $\Delta\lambda = \lambda_0(\varphi_0) - \lambda_B(\varphi_B)$ is shown for different values of λ_2 and ν=1, 2. Two phenomena can be observed:

(1) A type I-bifurcation (present for $\lambda_2 < 1/2$) results in a curved graph $\Delta\lambda(\lambda_0)$.

(2) If a type II-bifurcation occurs, a sudden change in $\Delta\lambda$ appears for a critical $\lambda_{0,\text{Crit}}$ (e.g. Fig. 7C) corresponding to $\varphi_{0,\text{Crit}}(\lambda_2,\nu)$ (e.g. Fig. 7A).
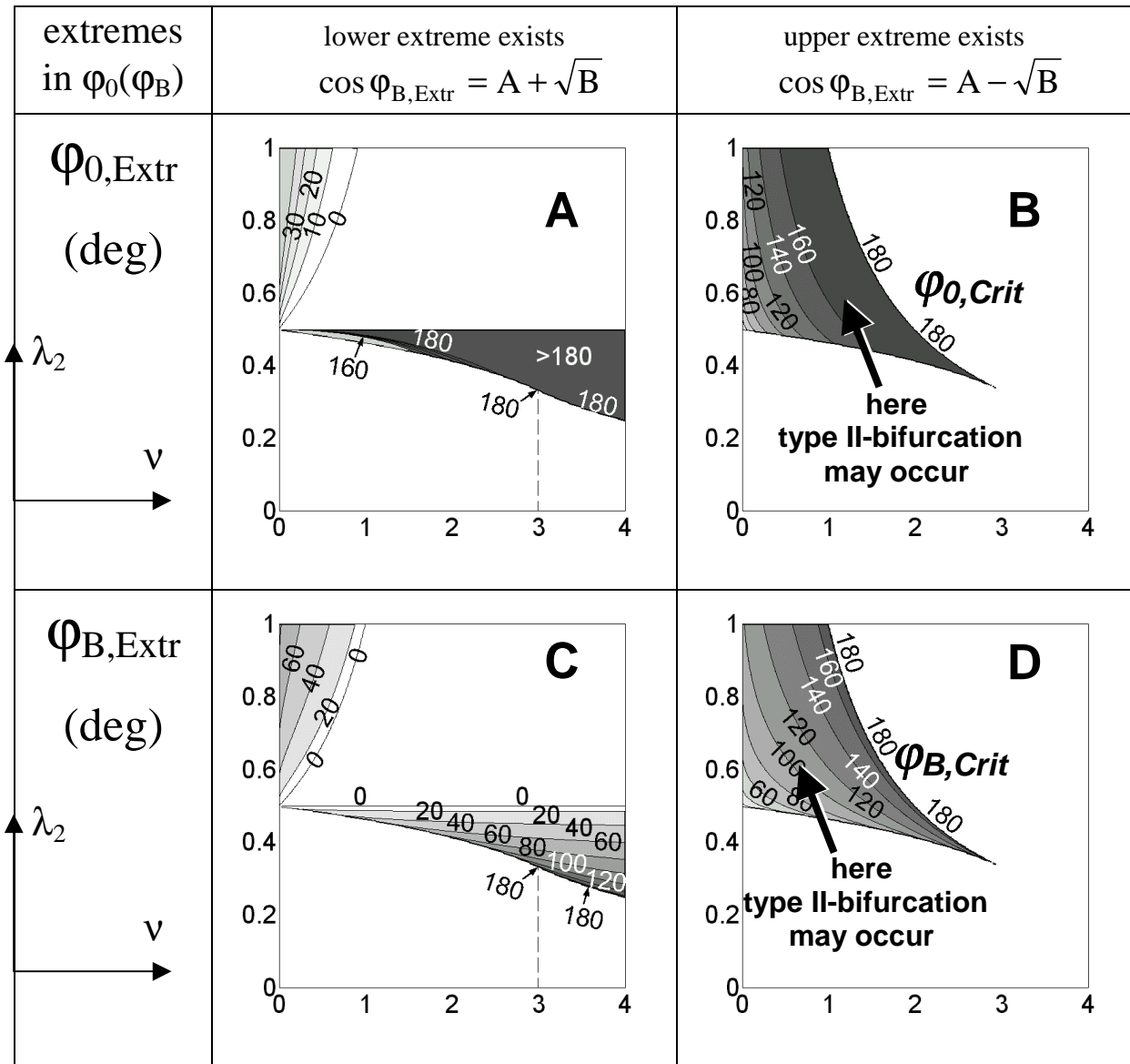
Fig. 6 Regions in (λ_2,ν)-space where according to Eq. A12 extremes in the $\varphi_0(\varphi_B)$ function occur with corresponding nominal (A, B) and bifurcation (C, D) angles.

Solutions of $\cos \varphi_{B,Extr} = A + \sqrt{B}$ (A, C) and $\cos \varphi_{B,Extr} = A - \sqrt{B}$ (B, D) must be within $[-1, 1]$. Only the existence of the upper extreme (compare Fig. 5 A, B) may lead to a sudden decrease in working range if φ_0 exceeds the $\varphi_{0,Crit}$ values shown in (B) with a corresponding $\varphi_{B,Crit}$ shown in (D). For leg lengthening ($\varphi > \varphi_0$) a sudden decrease in working range occurs for all $\varphi_0 \leq \varphi_{0,Extr}$ shown in (A) at a $\varphi_B \leq \varphi_{B,Extr}$ shown in (C) if $\lambda_2 > 1/(2-\nu)$ (upper left corner; Fig. 8). This is not a standard situation for human legs.

With increasing ν from 1 to 2 the working range is significantly enhanced. The risk of a type II-bifurcation remains merely for highly extended nominal angles (higher than 171°, Tab. 2; Fig. 5B).

The existence of a type II-bifurcation is associated with local extremes of the $\varphi_0(\varphi_B)$ function (in Fig. 5A: 'x' and '+', Eq. A11). Then, the derivative of the $\varphi_0(\varphi_B)$ function with respect to φ_B must vanish. This results in following solutions for $\varphi_{B,Extr}$ (Eq. A12):

44

$$\cos \varphi_{B,Extr} = A \pm \sqrt{B} \,, \tag{13}$$

where A and B are functions of λ_2 and ν. A type II-bifurcation may emerge for a critical $\lambda_{2,Crit}(\nu)$ fulfilling B = 0 (Fig. 7A; Tab. 2). Additionally, the right side in Eq. 13 must be within [-1, 1]. In general, a type II-bifurcation exists if the solution $\varphi_{B,Extr}$ according to the upper extreme (negative sign in Eq. 13; Fig. 6D) and the corresponding nominal angle φ_0 (Fig. 6B) are within [0, 180°].
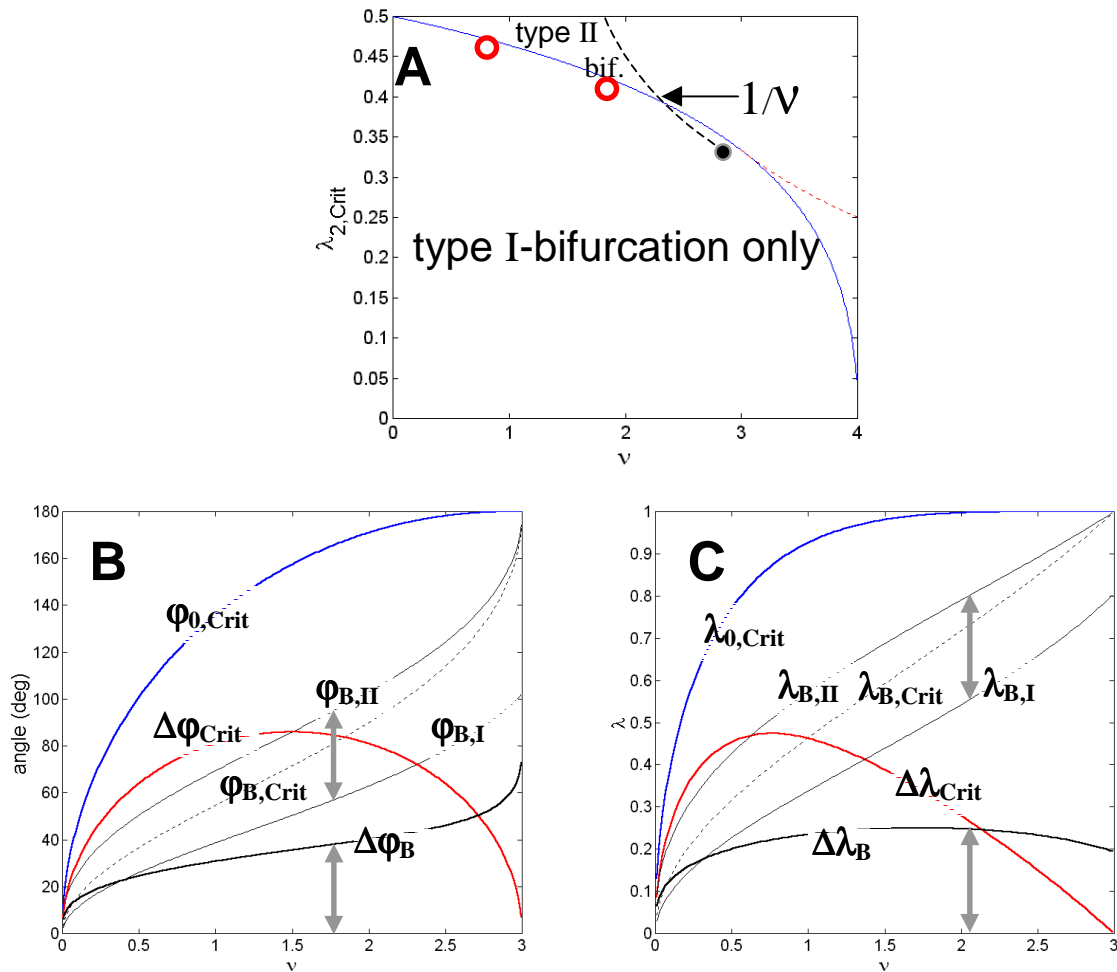
Fig. 7 Symmetrical loading. (A) Critical $\lambda_{2,Crit}(\nu)$ where for $\nu < 3$ a new type II-bifurcation occurs (small circles correspond to Fig. 5A, B), (B) corresponding nominal angle $\varphi_{0,Crit}$ and bifurcation angle $\varphi_{B,Crit}$ resulting in an angular working range $\Delta\varphi_{Crit}$ for $\lambda_2 = \lambda_{2,Crit}(\nu)$, and (C) relative nominal leg length $\lambda_{0,Crit}(\varphi_{0,Crit})$, relative bifurcation length $\lambda_{B,Crit}(\varphi_{B,Crit})$ and corresponding relative working range $\Delta\lambda_{Crit} = \lambda_{0,Crit} - \lambda_{B,Crit}$.

An increase in ν from 0 to 3 leads to smaller $\lambda_{2,Crit}$ (A) and higher $\varphi_{0,Crit}(\lambda_{2,Crit})$ (B). For a satisfactory working range choosing the exponent ν is important. If a critical nominal angle $\varphi_{0,Crit}(\nu)$ (Eqs. A10, A12) is exceeded a sudden decrease in (angular or translational) working range occurs at $\lambda_{2,Crit}(\nu)$ due to the inserted type II-bifurcation. This is shown in (B, C) by $\Delta\varphi_B = \varphi_{B,II} - \varphi_{B,I}$ and $\Delta\lambda_B = \lambda_{B,II} - \lambda_{B,I}$, respectively (I = type I-bifurcation, II = inserted type II-bifurcation; a change in φ_0 of 1.8° is considered between I and II).

(A) For $\nu > 3$ the importance of $\lambda_{2,Crit}(\nu)$ vanishes as the critical nominal angle leaves the considered interval [0, 180°]. For $3 < \nu \leq 4$ no type II-bifurcations occur for λ_2 above $\lambda_{2,Crit}$ (solid line; Fig. 6B, D).

For $\nu > 3$, the $\lambda_{2,\mathrm{Crit}}(\nu)$-line (fulfilling $B = 0$; Fig. 7A) is not an indicator for the appearance of a type II-bifurcation any more as there are no solutions for $\cos\varphi_{B,\mathrm{extr}} = A - \sqrt{B}$ (Fig. 6B, D).

Within $1/\nu < \lambda_2 < 1/2$ (dashed line in Fig. 7A) merely solutions for $\cos\varphi_{B,\mathrm{extr}} = A + \sqrt{B}$ with associated φ_0-values larger than $180°$ (Fig. 6A) are present. This results in not vanishing working ranges $\Delta\varphi$ for $\varphi_0 = 180°$ (Fig. 8).

In Fig. 7B, C effects of an emerging type II bifurcation (for $\lambda_2 = \lambda_{2,\mathrm{Crit}}(\nu)$) on the angular (B) and translational (C) working range are shown for $0 \le \nu \le 3$. To consider the inset of the type II-bifurcation the corresponding critical nominal angles $\varphi_{0,\mathrm{Crit}}$ (or lengths $\lambda_{0,\mathrm{Crit}}$; Tab. 2) were depicted.
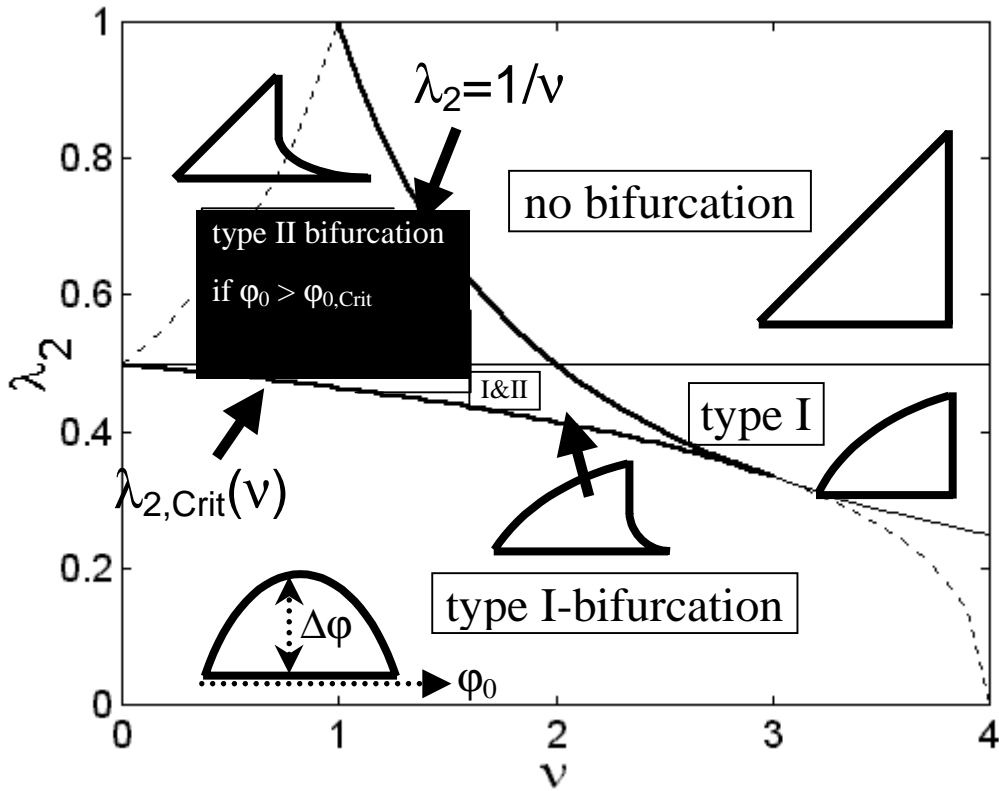
Fig. 8 Regions in (λ_2, ν)-space of different bifurcation behaviour in symmetrical loading.
A type I-bifurcation is present for $\lambda_2 < 1/2$ and any nominal angle φ_0. The type II-bifurcation exists if solutions for φ_B according to the upper extreme $\cos(\varphi_{B,\mathrm{Extr}}) = A - \sqrt{B}$ (Eq. A12) and the corresponding nominal angles φ_0 are within $[0, 180°]$.
With respect to the angular working range $\Delta\varphi(\varphi_0) = \varphi_0 - \varphi_B$ (represented by schematic sketches) the following statements can be made: (1) For $\lambda_2 < 1/2$ the working range is reduced for all nominal angles φ_0 due to type I-bifurcation. This leads to a curved graph in $\Delta\varphi(\varphi_0)$. (2) For $\lambda_2 \ge 1/2$ the working range $\Delta\varphi$ is identical to φ_0 as along as no type II-bifurcation appears. (3) In a region within $\lambda_{2,\mathrm{Crit}}(\nu) < \lambda_2 < 1/\nu$ a sudden decrease in angular working range occurs if φ_0 exceeds the critical nominal angle $\varphi_{0,\mathrm{Crit}}(\lambda_2,\nu)$ (Fig. 6B) which corresponds to a $\varphi_{B,\mathrm{Extr}}$ (Fig. 6D) with $\cos(\varphi_{B,\mathrm{Extr}}) = A - \sqrt{B}$ according to Eq. A12.
For $\nu < 1$ there is a lower extreme $\cos(\varphi_{B,\mathrm{Extr}}) = A + \sqrt{B}$ with $\varphi_B > \varphi_0$ (Fig. 6A, C) if λ_2 exceeds the dashed line $\lambda_2 = 1 / (2-\nu)$. For $\nu > 3$ the dashed $\lambda_{2,\mathrm{Crit}}(\nu)$-line (fulfilling $B = 0$) has no importance any more as there is no corresponding bifurcation angle ($A + \sqrt{B} < -1$; Fig. 6C).

The working range $\Delta\varphi_{Crit}$ (or $\Delta\lambda_{Crit}$, respectively) around such a critical nominal angle (or length) changes dramatically if a nominal angle slightly above or below the critical $\varphi_{0,Crit}$ is chosen (a change in φ_0 of 1.8° is considered). The corresponding bifurcation angles and lengths are denoted by the indices 'B,I' and 'B,II'. At $\nu = 1.75$ there is a maximum loss of $\Delta\lambda_B = 0.25$ in translational working range $\Delta\lambda$ due to the appearance of the type-II bifurcation.

type I bifurcation	maximum angular working range	maximum translational working range
max. working range at nominal angle $\varphi_{0,MAX}$ (deg)		
max. working range $\Delta\varphi_{MAX}$ (deg) or $\Delta\lambda_{MAX}$, respectively		
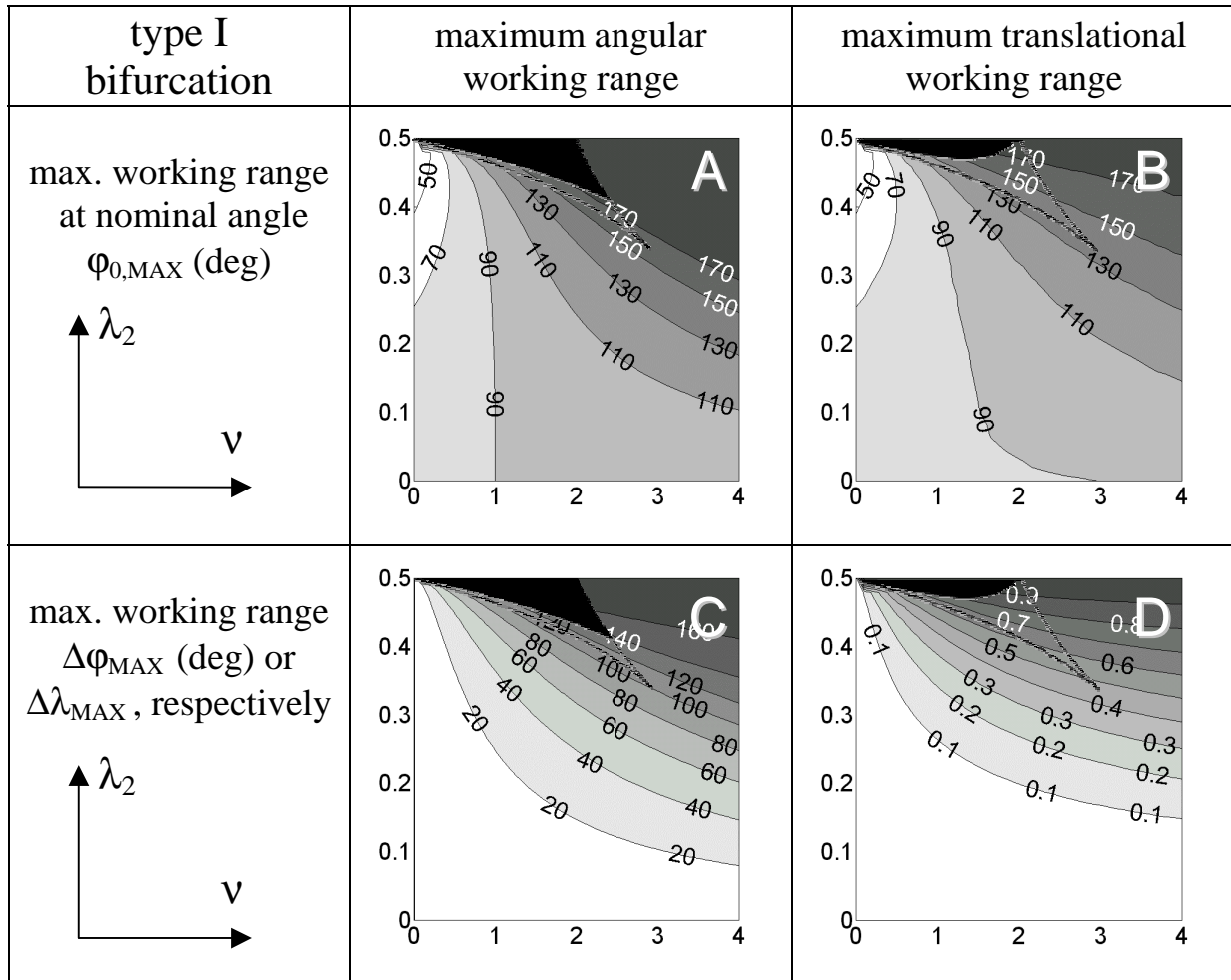
Fig. 9 Maximum angular (A, C) and translational (B, D) working ranges for different leg designs λ_2 and torque characteristics ν. With increasing ν the nominal angle $\varphi_{0,MAX}$ (A, B) and the corresponding maximum working ranges $\Delta\varphi_{MAX}$ (C) or $\Delta\lambda_{MAX}$ (D) are shifted to higher values. Also an increase in λ_2 leads to higher maximum working ranges (C, D) and for about $\nu > 1$ to higher $\varphi_{0,MAX}$ (A, B) as well. For maximum translational working range (D) slightly lower nominal angles (B) are necessary than for maximum angular working range (A, C). For $\lambda_2 > \lambda_{2,Crit}$ a type II-bifurcation is inserted if $\varphi_{0,MAX} > \varphi_{0,Crit}$ is fulfilled (black area). Due to the more flexed leg operation optimising the translational rather than the angular working range, the disturbance by the type II-bifurcation is reduced to a smaller area within the (λ_2,ν)-space.

The possible existence of the two types of bifurcation within the (λ_2,ν)-plane is summarised in Fig. 8. The type I-bifurcation occurs for $\lambda_2 < 1/2$ as a consequence of property (2) of $\varphi_0(\varphi_B)$ (see above). Type II-bifurcations may exist (if $\varphi_0 > \varphi_{0,Crit}$) within an area bordered by the $\lambda_{2,Crit}(\nu)$ and

the $\lambda_2 = 1/\nu$ lines. Approaching the upper limit $\lambda_2 = 1/\nu$ the bifurcation angle and the corresponding nominal angle reach 180° (Fig. 6B, D). Only within a small area of $0 < \nu < 3$ and $\lambda_{2,Crit} < \lambda_2 < \min(1/2, 1/\nu)$ both bifurcation types (I&II) may occur.

In Fig. 9C, D the maximum angular and translational working range limited by the type I-bifurcation (for $0 < \lambda_2 < 1/2$ and $0 < \nu < 4$) is shown. The corresponding nominal angles (Fig. 9A, B) are slightly higher for optimising angular (Fig. 9C) than for optimising translational (Fig. 9D) working range. A large working range can be achieved either by long middle segments (λ_2 near to 1/2) or high exponents of the torque characteristic ν.

The type II-bifurcation reduces the working range if the predicted nominal angle $\varphi_{0,MAX}$ (Fig. 9A, B) exceeds the critical angle $\varphi_{0,Crit}$ shown in Fig. 6B. For a maximised translational working range this region (black area in Fig. 9D) within the (λ_2, ν)-space is clearly smaller than for maximum angular working range (black area in Fig. 9C).
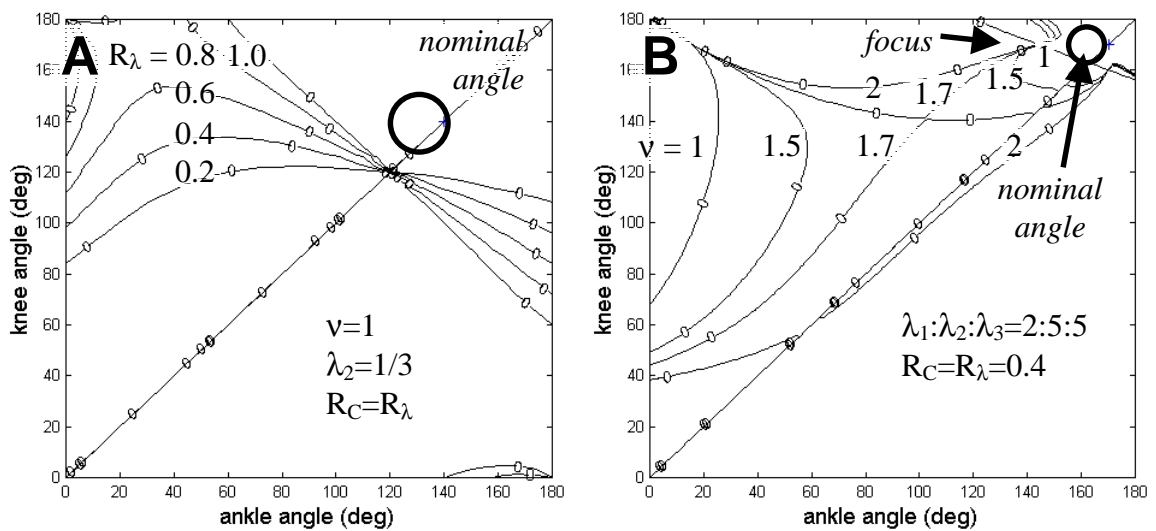
Fig. 10 Influence of (A) R_λ and (B) ν on the oblique branch crossing the symmetrical solution. (A) For a given symmetrical nominal angle φ_0 the location of the bifurcation φ_B remains the same as long as λ_2 and ν are kept constant and the stiffness equilibrium ($R_C = R_\lambda$; Eq. 11) is fulfilled. (B) The oblique branch aligns with the symmetrical branch with increasing ν. Depending on the nominal angle (here 170°) a critical value of ν (here 1.7) must be exceeded to extend the working range significantly (see Fig. 11A, B).

4.2 Bifurcation behaviour in asymmetric loading

So far, exact symmetry ($\varphi_{12} = \varphi_{23}$) for the solutions of the torque equilibrium (Eqs. 5, 6) was assumed requiring the stiffness equilibrium ($R_C = R_\lambda$). These results revealed strategies and possible problems of leg operation with symmetrical nominal configurations. The framework has now to be extended to arbitrary nominal angle setups ($\varphi^0_{12} \neq \varphi^0_{23}$). The bifurcation(s) must be

48

identified within the whole configuration space $(\varphi^B_{12}, \varphi^B_{23})$ with a corresponding stiffness ratio R_C. Three independent parameters must be taken into consideration: λ_2, R_λ, ν.

A non-equal outer segment length design ($R_\lambda \neq 1$) results in oblique branches of the symmetrical solutions which are not mirrored at the symmetrical axis any more (Fig. 10A). This corresponds to different shapes of the $h_1 = 0$ and $h_3 = 0$ lines (Fig. 3A, B; Eq. 12a,b). As a consequence, in one half of the configuration space (e.g. $\varphi_{12} < \varphi_{23}$) the oblique solution may detach from the adjacent focus and align to the symmetrical branch (Fig. 2A, B).

This effect may extend the working range dramatically and is supported by high exponents of the torque characteristic ν (Figs. 2C, 10B).

Starting at asymmetric nominal angles ($\varphi^0_{12} \neq \varphi^0_{23}$) quasi-symmetric solutions characterised by a deformed shape of the solutions for $Q = 0$ and an adapted stiffness ratio R_C still can be found. Now the stiffness equilibrium is disturbed ($R_C \neq R_\lambda$) and the symmetrical axis ($\varphi_{12} = \varphi_{23}$) is not a common solution any more.

To estimate the advantages of an asymmetric outer segment length design the working range for different nominal angle configurations is asked for. The conditions for a bifurcation (saddle point regarding the solutions of a Q function in the configuration space) are $Q(\varphi_{12},\varphi_{23}) = 0$ and $\bar{\nabla}_{\bar{\varphi}} Q(\varphi_{12}, \varphi_{23}) = 0$ (Appendix 4). Using these three equations the bifurcation angles $\varphi_{B,12}$, $\varphi_{B,23}$ and the corresponding stiffness ratio R_C can be solved for numerically.

In Fig. 11 the maximum translational working range $\Delta\lambda$, the corresponding stiffness ratio R_C and the ratio of joint flexions

$$R_{\Delta\varphi} = \frac{\varphi^0_{12} - \varphi^B_{12}}{\varphi^0_{23} - \varphi^B_{23}} \tag{14}$$

are shown for different nominal angles ($\varphi^0_{12}, \varphi^0_{23}$), exponents $\nu = 1, 2$ and a human-like leg design (2:5:5). The working range on the symmetrical axis ($\varphi^0_{12} = \varphi^0_{23}$) corresponds to the findings in Fig. 5C, D fulfilling $R_C = 0.4$ (stiffness equilibrium) and $R_{\Delta\varphi} = 1$ (symmetrical loading: $\alpha_{\Delta\varphi} = 45°$). Here, the working range is merely determined by λ_2 and ν. Leaving the symmetrical axis an increase in working range is observed in the upper half of the configuration space ($\varphi^0_{12} < \varphi^0_{23}$).

For $\nu = 1$ the working range is dramatically reduced if φ^0_{23} exceeds $\varphi_{23,Crit}$ (Tab. 1). This is due to the attraction of the focus at the $h_3 = 0$ line (Fig. 3B,C). Increasing the exponent of the torque characteristic ν from 1 to 2 extends the working range significantly (A, B). In both cases flexing the ankle more than the knee is of advantage. The stiffness ratio R_C must be adjusted according to

the difference in the nominal angles $\varphi^0_{12} - \varphi^0_{23}$ (C, D). For $\nu = 2$ the lines of constant R_C adjustment and constant ratio of joint flexions $R_{\Delta\varphi}$ align (D, F).
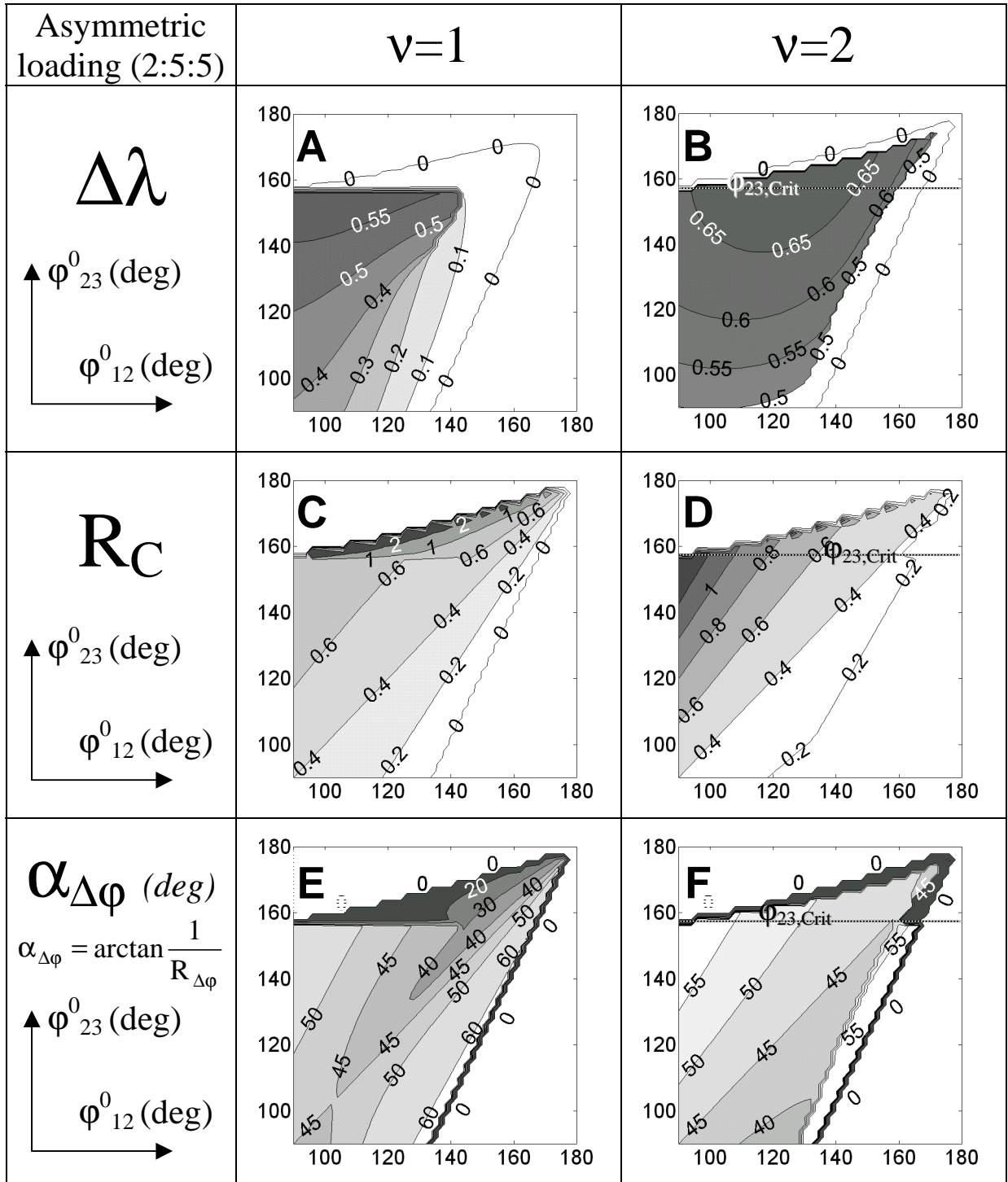
Fig. 11 Asymmetric loading. Influence of the nominal angle configuration (φ^0_{12}, φ^0_{23}) on (A, B) the maximum translational working range $\Delta\lambda$, (C, D) the corresponding stiffness adjustment R_C and (E, F) the ratio of joint flexions $R_{\Delta\varphi} = (\varphi^0_{12} - \varphi^B_{12}) / (\varphi^0_{23} - \varphi^B_{23})$ expressed as an angle $\alpha_{\Delta\varphi}$ for a human-like leg design (2:5:5).

With higher values of ν also solutions near to the symmetrical loading show a high working range (Fig. 11B). But still for $\nu = 2$ the optimum in working range is observed beside the symmetrical axis for $\varphi^0_{12} \approx 120°$, $\varphi^0_{23} \approx 160°$ and $R_C \approx 0.8$. Here the critical knee angle $\varphi_{23,Crit}$ can even be exceeded by φ^0_{23} due to the alignment of the oblique branch with the symmetrical axis (Fig. 10B). An almost optimal working range can be achieved for a wide area of different nominal angles (e.g. $\Delta\lambda > 0.6$ for nominal knee angles higher than about 120° and nominal ankle angles between 90° and 140°). For $\varphi^0_{23} > \varphi_{23,Crit}$, the still present attraction of the $h_3 = 0$ line demands a sensitive R_C adjustment which limits the area of nominal angles that guarantee a safe operation of the leg.

For nominal angle configurations with a considerable working range a simple strategy regarding the rotational stiffness adjustment is observed. The more flexed joint has to be stiffened with respect to the other joint about proportional to the angular differences between both joints (Fig. 11C, D). The stiffness adaptation compensating the asymmetry in nominal angles scales with the exponent of the torque characteristic.

The effect of the predicted optimal R_C-adjustment (Fig. 11C, D) on the joint kinematics is shown in Fig. 11E, F. Here the direction of leg shortening $\alpha_{\Delta\varphi}$ within the configuration space is denoted by the ratio $R_{\Delta\varphi}$ of the differences in ankle and knee joint between nominal and bifurcation position (Eq. 14).

This ratio can be expressed as an angle of leg shortening $\alpha_{\Delta\varphi} = \arctan(R_{\Delta\varphi}^{-1})$ with respect to the φ^0_{12}-axis. At the symmetrical axis an angle of 45° represents equal loading of both joints (i.e. the bifurcation lies on the symmetrical axis as well).

For $\nu = 2$ (Fig. 11F) and unequal nominal angles ($\varphi^0_{12} \neq \varphi^0_{23}$) the ratio $R_{\Delta\varphi}$ reduces the asymmetry in joint angles (e.g. $R_{\Delta\varphi} > 45°$ for $\varphi^0_{12} < \varphi^0_{23}$ and vice versa). For $\nu = 1$ (Fig. 11E) a completely different behaviour is present. For nominal angles near the symmetrical axis and higher than about 100° the ratio of joint flexions $R_{\Delta\varphi}$ indicates an increased asymmetry in joint angles at leg shortening. Only for clearly bent ankle joints (less than about 100°) a reduced asymmetry in joint angles during leg shortening is indicated by angles $\alpha_{\Delta\varphi}$ higher than 45°.

DISCUSSION

The kinematic redundancy problem of a three-segmental leg (with foot, shank, and thigh) can be successfully solved if quasi-elastic torque characteristics are present at the joints (ankle and knee). The requirements to the joint torque characteristic and the leg geometry were identified.

General leg behaviour and leg design

Two different types of leg bending were found: (1) Quasi-symmetric loading where both joints are flexed simultaneously (zigzag alignment) or (2) bow-like loading where both joints tend to stay at the same side with respect to the leg axis.

The first type takes the most advantage of having a third leg segment and results in the highest leg stiffness assuming given rotational stiffnesses. For all leg designs with a middle segment (shank) length less than half of the total leg length ($\lambda_2 < 1/2$) a transition (type I-bifurcation) from the zigzag-mode (1) to bow-like loading (2) occurs at a certain amount of leg shortening. This even holds if the rotational stiffnesses could be adjusted perfectly to the leg geometry.

Making the middle segment (shank) longer than both of the remaining segments (foot and thigh) together results in avoidance of this unfavourable transition in most cases. But even then the system may fall into bow-like loading (type II-bifurcation) for certain nominal angles (Fig. 6) and exponents of the torque characteristics (Fig. 8). Moreover, a very long middle segment reduces the capability of leg shortening due to geometrical constraints. This solution was not chosen by nature. Middle segment lengths of less than half the total leg length are typical. Then, the range of quasi-symmetric leg shortening (i. e. the working range) is always limited. To reach an optimum angular or translational working range relative middle segment lengths higher than 0.4 and exponents of the torque characteristic larger than one are necessary (Fig. 9).

Significance for human legs

In a human leg the relative length of the middle segment (shank) is approximately $\lambda_2 = 0.42$. This is about the region where the inserted type II-bifurcation threatens to reduce the working range dramatically for exponents ν between 1 and 2 (Fig. 7B, C). Increasing the exponent ν the type II-bifurcation (Figs. 6B and 7A) occurs even at smaller middle segment lengths (for $\nu = 2$: $\lambda_{2,Crit} = 0.414$; Tab. 2). Fortunately, here the critical nominal angle is shifted to almost stretched angle positions (for $\nu = 2$: $\varphi_{0,Crit} = 171°$; Tab. 2).

In fact, the human leg design seems to result in a maximum working range for exponents ν between 1 and 2. Such exponents correspond to torque characteristics predicted for highly loaded

muscle-tendon complexes in the human leg (Fig. 3A in chapter IV) and are mainly determined by tendon stress-strain properties.

A longer middle segment (or a shorter foot, see below) would run the risk of a sudden loss in working range for stretched nominal angles (type II-bifurcation). Shortening the middle segment or exponents ν smaller then one would clearly reduce the working range (Fig. 9).

Advantages of operating asymmetrically

The ratio of the outer segment lengths R_λ had no influence on the working range as long as the joints were working in parallel, i.e. the same inner joint angles were present at ankle and knee joint. Such a symmetric operation of the leg was achieved by adapting the joint stiffnesses to the length of the adjacent outer segments (stiffness equilibrium, Eqs. 10, 11) and choosing exactly equal nominal angles.

Leaving the symmetrical axis within the configuration space, different outer segment lengths ($R_\lambda \neq 1$) were of advantage. For instance, a small foot (see below) extended the working range for more stretched nominal knee angles. This was due to the location of the $h_3 = 0$ line where the knee was crossing the leg axis which is shifted to high knee angles (Fig. 3B) and allowed to access almost the whole upper half-space of the configuration space ($\varphi_{12} > \varphi_{23}$). Finally, the attraction of the $h = 0$ lines was reduced using higher exponents ν of the torque equilibrium (e.g. 2; Fig. 10B).

In effect, an asymmetrically operating leg with one joint more flexed than the other was of advantage if the outer segment length design was asymmetric. A homogeneous flexion of both joints was then achieved by adapting the stiffness ratio R_C to the chosen difference in nominal angles (Fig. 11C,D). The nominal angle configurations predicted for maximum working range for a human-like leg design agree with landing conditions in running and hopping (Farley et al., 1998) if an exponent of the torque characteristic of 2 is chosen (Fig. 11B: $\varphi^0_{12} \approx 120°$, $\varphi^0_{23} \approx 160°$).

Role of biarticular muscles

A homogeneous joint loading was also supported by biarticular structures in the leg. Different moment arms of biarticular muscles crossing knee- and ankle joint could help to fulfill the required stiffness ratio. An optimal ratio of the moment arms was found for maximum vertical jumping performance (Fig. 2 in Bobbert and van Zandwijk, 1994). Position dependent moment arms might adapt the ratio to different nominal positions.

As shown in Fig. 2D, only one such muscle (like *m.gastrocnemius*) was necessary to synchronise ankle and knee flexion as only the upper half of the configuration space was of practical interest.

Therefore, no biarticular muscle opposite to *m.gastrocnemius* has to be present in many mammals and humans.

The role of the foot

The introduction of a third leg segment has two major advantages: It reduces the torques required at the leg joints and minimises the energy due to segment rotation (Alexander, 1995).

The foot length design was critical with respect to the range of safe leg operation. Having a small foot compared to the shank length enabled large knee extensions. A small foot compared to the thigh required a reduced stiffness in the ankle joint with respect to the knee. This requires smaller calf muscle cross sections compared to the knee extensors and fits to the generally observed leg design with continuously decreasing masses of the more distal segments.

Nonetheless, very short feet increased the tendency to snap from the zigzag mode into the bow mode due to the now almost two-segmental system. The effective length of the human foot may vary between about 8 and 20 cm changing the point of support from heel to ball. This resulted in a relative length of the middle segment near to the type II-bifurcation. Two mechanisms are involved to avoid the potential instability:

1. Overextension of the ankle joint is prevented by an increase in effective foot length as the centre of pressure is shifted to the tip of the foot. Then, the range of safe leg operation is increased due to a decrease in effective length of the middle segment.

2. Overextension of the knee is avoided by an almost flat touch-down orientation of the foot and the kinematic constraint due to the heel contact. Therefore, the stiffness of the contacting heel pad must be high enough to avoid large deformations which in turn would allow knee overextension. In effect deformations of about 1 cm are allowed due to the highly nonlinear force-displacement characteristic of the human heel pad (Denoth, 1986). This corresponds to a complete leg extension starting at initial knee angles of about $165°$.

Influence of segment masses

The presented model was not able to predict a first impact peak after touch-down (observed e.g. in long jump) even by representing the heel pad by external torques (M_{01}) and replacing the torque characteristics by muscle tendon complexes (see chapters IV, V). This phenomenon requires the representation of leg segment masses (Denoth, 1986). As shown by Gruber (Gruber 1987; Gruber et al., 1998) the proper representation of soft and rigid parts in the human leg is necessary to estimate the internal loads and to predict the observed ground reaction forces. As the leg masses must be decelerated after touch-down, the separation into soft and rigid subsystems allows to realise small foot displacements by reducing the effective mass of the leg (Denoth, 1986). The main part of the leg consists of softly coupled masses (chapter II) which are

54

decelerated delayed to the skeleton. After the impact, the forces predicted by the three-segment model are in agreement with experimental observations for fast types of locomotion (running, long jump).

The leg as a spring?

In this study an elastic joint operation was shown to result in relatively simple strategies for successful leg operation. Nevertheless, there are no structures in the human leg which are compliant enough to account for the observed joint behaviour. Taking the basic muscle properties (force-length and force-velocity relationship, activation dynamics) into account the spring-like behaviour of the leg resulted from muscle stimulation optimised for performance (chapter V). This led to torque characteristics similar to the results from inverse dynamics (Stefanyshyn and Nigg, 1998) and agrees with the assumptions made in this study.

The homogeneous loading of the leg joints enabled the contribution of all major leg muscles to the performance (chapter V). This was achieved by a sensitive control of the leg muscles resulting in stiffness ratios similar to the values predicted by the three-segmental model which results in a high leg stiffness at quasi-symmetric leg operation.

The subtle interplay between rotational stiffnesses and the leg stiffness remains for further investigation. Nevertheless, the linear spring characteristic observed in biological legs is clearly superior to linear rotational springs and can be supported by nonlinear tendon properties with exponents between 1.7 and 2 (chapter IV). Such exponents are sufficient for safe leg operation and show the highest advantage in working range for prevented type II-bifurcations. Higher exponents would lead to nonlinear leg stiffness behaviour and limit the range of joint action.

Further steps

The strategies developed in this study are suitable to be proved in mammalian and human locomotion. The first attempts showed promising predictions of leg kinematics for running and jumping. Hereby the forward dynamic modelling is useful to represent effects of heel strike (to enable geometrical constraints as ground support) or changing nominal angles (to represent energy changes as in drop jump or squat jumps). The later effect corresponds to the neurophysiological understanding of movement control (Feldman, 1966).

Taking the three-segment model as a starting point further effects as

1) the influence of additional leg segments,

2) the influence of segment masses and inertias, or

3) the influence of dissipative joint operation (muscles, heel pad deformation)

can be taken into account.

For (1) the torque equilibrium (Eq. 2a-c) must be extended by introducing equations representing the additional segments (appendix A1-3). For (2) and (3) the joint variables must be integrated using the differential equations which are replacing the corresponding algebraic equations in the torque equilibrium. The influence of external torques (M_{01}) and moments of inertia (e.g. Θ_3) can be estimated by considering peak values as a constant in the torque equilibrium.

APPENDICES

In the first three sections (1-3) the static torque equilibrium of the three segmental spring-mass model (methods, Eq. 2) will be derived. We start with the equations of motion of an arbitrary system of rigid segments (1), then neglecting the inertial properties of the three leg segments (2), and reducing the supported body to a point mass (3).

In section (4) the conditions characterising the bifurcation point in the solutions of the torque equilibrium (Eqs. 5, 6) within the configuration space will be derived. This allows to calculate the working range of the system and results in optimal nominal configurations for different leg designs.

APPENDIX 1: General dynamics of a chain of rigid segments

To derive the equations determining the static configuration of the three leg segments in the sagittal plane we start with the equations of motion of n free rigid bodies (i = 1, 2, ... , n) in the inertial system:

$$m_i \ddot{\vec{r}}_i = \sum_{k(i)} \vec{F}_{k,i}$$
$$\underline{\Theta}_i \dot{\vec{\omega}}_i = \sum_{k(i)} \left(\vec{r}_i + \vec{d}_{i,k} \right) \times \vec{F}_{k,i} + \sum_{j(i)} \vec{M}_{j,i}.$$

(A1a,b)

Here the index k(i) denotes the points of interaction with all forces $\vec{F}_{k,i}$ working on body i (mass: m_i; moment of inertia tensor $\underline{\Theta}_i$), whereas $\ddot{\vec{r}}_i$ is the acceleration vector of the centre of mass (COM) and $\dot{\vec{\omega}}_i$ the rotational acceleration with respect to the inertial system. The force $\vec{F}_{k,i}$ is acting in a distance $\vec{d}_{i,k}$ from the COM. All additional torques (e.g. joint torques) are denoted by $\vec{M}_{j,i}$.

The dynamics of a chain of n rigid bodies connected by n−1 spherical joints additionally requires the following constraint equations (i = 1, 2, ... , n−1):

$$\vec{r}_i + \vec{d}_{i,i+1} = \vec{r}_{i+1} + \vec{d}_{i+1,i}$$
$$\vec{r}_0 = \vec{r}_i + \vec{d}_{1,0}.$$

(A2a,b)

For instance, the vector $\vec{d}_{2,3}$ points from the COM of body 2 to the joint between the bodies 2 and 3, whereas $\vec{d}_{3,2}$ points from the COM of body 3 to the very same joint. Note that $\vec{d}_{1,0}$ (Eq. A2b) is the distance between the COM of body 1 and the point of application of the ground reaction force.

Let us consider a distal (lower) and a proximal (upper) joint for each body i (or segment i). Taking the gravitational acceleration vector $\vec{g}$ into account Eq. A1 can be written as:

$$m_i \ddot{\vec{r}}_i = \vec{F}_{i-1,i} + \vec{F}_{i+1,i} + m_i \vec{g}$$
$$\underline{\Theta}_i \dot{\vec{\omega}}_i = \left(\vec{r}_i + \vec{d}_{i,i-1}\right) \times \vec{F}_{i-1,i} + \left(\vec{r}_i + \vec{d}_{i,i+1}\right) \times \vec{F}_{i+1,i} + \vec{M}_{i-1,i} + \vec{M}_{i+1,i}.$$

(A3a,b)

Except for gravity, ground reaction force $\vec{F}_{0,1}$, and ground torque $\vec{M}_{0,1}$, all forces and torques are internal. For instance, at the joint between the bodies 2 and 3, $\vec{F}_{3,2}$ and $\vec{M}_{3,2}$ are the constraint force and the torque (produced by structures spanning the very same joint) acting on body 2. The corresponding force $\vec{F}_{2,3}$ and torque $\vec{M}_{2,3}$ are pointing in the opposite direction and are acting on body 3, or generally:

$$\vec{F}_{i+1,i} = -\vec{F}_{i,i+1}$$
$$\vec{M}_{i+1,i} = -\vec{M}_{i,i+1}.$$

(A4a,b)

APPENDIX 2: Segment dynamics neglecting inertial contributions (m_i, $\underline{\Theta}_i$) of the leg

The dynamic properties of a segment (body i) will be neglected by setting its mass m_i and moment of inertia $\underline{\Theta}_i$ to zero. This is the case for all leg segments (i = 1, 2, 3). Furthermore, all body weight is shifted to the uppermost segment (body 4). Later on even the moment of inertia of this remaining mass will be neglected.

The assumption of a quasi-static operation of the leg in system (A3a) together with (A4a) leads to (i = 1, 2, ... , n−1) :

$$\vec{F}_{0,1} = \vec{F}_{i,i+1} = -\vec{F}_{i+1,i}.$$

(A5)

57

For a massless leg (segments i = 1, 2, 3) supporting a mass (body 4) at the proximal end of the 3rd leg segment and touching the ground at its distal end (segment 1) we can reduce the system (Eqs. A3a,b) to a planar model (i = 1, 2, 3):

$$\left(\left(\vec{d}_{i,i+1} - \vec{d}_{i,i-1}\right) \times \vec{F}_{0,1}\right)\Big|_z = \vec{M}_{i-1,i}\Big|_z - \vec{M}_{i,i+1}\Big|_z$$

$$m_4 \ddot{\vec{r}}_4 = \vec{F}_{0,1} + m_4 \vec{g}$$

$$\Theta_4 \ddot{\varphi}_4 = \left(\left(\vec{r}_4 + \vec{d}_{4,3}\right) \times \vec{F}_{0,1}\right)\Big|_z + \vec{M}_{3,4}\Big|_z$$

(A6a-c)

where Θ_4 is the principal moment of inertia of body 4 with respect to z. For each leg segment (Eq. A6a) there remains only one equation determining the torque equilibrium. Additionally, we have two equations (Eq. A6b) describing the translational acceleration and one equation (Eq. A6c) representing the rotational acceleration of the supported body. Note that all torques are pointing into the z-direction, perpendicular to the sagittal plane.

APPENDIX 3: Reduction to a point mass model (Θ_4=0)

In order to describe the total body centre of mass dynamics in terms of a point mass, the supported segment has to be reduced to zero length ($d_{4,3} = \left|\vec{d}_{4,3}\right| = 0$) and zero moment of inertia (Θ_4=0). Consequently, there cannot be a torque acting on the supported mass ($M_{34} = \vec{M}_{3,4}\Big|_z = 0$) which leads to:

$$m\ddot{\vec{r}} = \vec{F}_{leg} + m\vec{g}$$

$$\left(\vec{\ell}_1 \times \vec{F}_{leg}\right)\Big|_z = M_{01} - M_{12}$$

$$\left(\vec{\ell}_2 \times \vec{F}_{leg}\right)\Big|_z = M_{12} - M_{23}$$

$$\left(\vec{\ell}_3 \times \vec{F}_{leg}\right)\Big|_z = M_{23}$$

$$\vec{r} = \ell_1 + \ell_2 + \ell_3$$

(A7a-e)

with $\vec{\ell}_i = \vec{d}_{i,i+1} - \vec{d}_{i,i-1}$, $\vec{F}_{leg} = \vec{F}_{0,1}$, m = m$_4$, and $\vec{r} = \vec{r}_4 - \vec{r}_0$. For simplicity, M$_{ji}$ denotes $\vec{M}_{j,i}\Big|_z$. The last equation (Eq. A7e) follows directly from Eq. A2 by subsequently subtracting (Eq. A2a) with i = 1, 2, 3 from (Eq. A2b). With given torques M$_{01}$, M$_{12}$, M$_{23}$ as functions of the leg configuration φ_1, φ_2, φ_3 one can solve the system (Eqs. A7b-e) of five equations for the five unknowns φ_1, φ_2, φ_3, F$_{leg,x}$, F$_{leg,y}$ at any point in time.

For *forward dynamic integration* of equation (Eq. A7a), an initial configuration φ_1, φ_2, φ_3 must be chosen which fulfils the system (Eqs. A7b-e) in accordance to the torque characteristics $M_{ij}(\varphi_1, \varphi_2, \varphi_3)$. E.g. using rotational springs (Eq. 8a,b), this can easily be realised by setting the initial angles to the nominal angles. Then by solving the system (Eqs. A7b-e) at each time step, the acting force, and therefore, the body mass dynamics can be calculated.

APPENDIX 4: Conditions for the bifurcation point

In case of symmetrical nominal angle setup $\varphi_0 = \varphi_{12}^0 = \varphi_{23}^0$ the stiffness equilibrium ($R_C = R_\lambda$) leads to a symmetrical solution ($\varphi_{12} = \varphi_{23}$) of the torque equilibrium (Eqs. 5, 6) which might be crossed by an odd solution. The intersectional point between these solutions of $Q(\varphi_{12}, \varphi_{23}) = 0$ is called a bifurcation point which is determined by the condition $\bar{\nabla}_{\bar{\varphi}} Q(\varphi_{12}, \varphi_{23}) = 0$. It represents a saddle point of the Q-function within the configuration space. The components of the gradient can be expressed for the three segment system as:

$$\frac{\partial Q}{\partial \varphi_{12}} = \lambda_1 \cos\varphi_{12} \cdot M_{23} + \lambda_3 \sin\varphi_{23} \frac{\partial M_{12}}{\partial \varphi_{12}} + \frac{\lambda_1 \lambda_3}{\lambda_2}\left[\frac{\partial M_{12}}{\partial \varphi_{12}} \sin(\varphi_{12} - \varphi_{23}) + (M_{12} - M_{23})\cos(\varphi_{12} - \varphi_{23})\right] = 0$$

$$\frac{\partial Q}{\partial \varphi_{23}} = \lambda_3 \cos\varphi_{23} \cdot M_{12} + \lambda_1 \sin\varphi_{12} \frac{\partial M_{23}}{\partial \varphi_{23}} - \frac{\lambda_1 \lambda_3}{\lambda_2}\left[\frac{\partial M_{23}}{\partial \varphi_{23}} \sin(\varphi_{12} - \varphi_{23}) + (M_{12} - M_{23})\cos(\varphi_{12} - \varphi_{23})\right] = 0 \quad (A$$

8a,b)

In general a bifurcation can be found in an asymmetric nominal angle setup if R_C is properly adapted. Therefore, the solutions of $\bar{\nabla}_{\bar{\varphi}} Q(\varphi_{12}, \varphi_{23}) = 0$ together with $Q(\varphi_{12}, \varphi_{23}) = 0$ do not merely provide the bifurcation point $\varphi_{B,12}$, $\varphi_{B,23}$ but also the corresponding stiffness ratio R_C. For symmetrical loading ($\varphi = \varphi_{12} = \varphi_{23}$ with $\varphi_0 = \varphi_{12}^0 = \varphi_{23}^0$ and $R_C = R_\lambda$) the two equations for the condition $\bar{\nabla}_{\bar{\varphi}} Q(\varphi_{12}, \varphi_{23}) = 0$ (Eq. A8a,b) become linearly dependent and can therefore be simplified to one equation. In the case of rotational springs at the joints (Eq. 8a,b) this leads to:

$$\nu \sin\varphi \cdot (\varphi_0 - \varphi)^{\nu-1} + \left(\cos\varphi - \frac{\lambda_1 + \lambda_3}{\lambda_2}\right) \cdot (\varphi_0 - \varphi)^\nu = 0. \quad (A9)$$

For $\varphi \neq \varphi_0$ this explicitly defines the nominal angle φ_0 as a function of the bifurcation angle φ_B, the relative length of the middle segment λ_2 and the exponent of the torque characteristic ν:

$$\varphi_0(\varphi_B) = \frac{\nu \sin\varphi_B}{\Lambda_2 - \cos\varphi_B} + \varphi_B \quad (A10)$$

with $\Lambda_2 = (1 - \lambda_2) / \lambda_2$. This function implicitly defines all bifurcations φ_B that are present for a given nominal angle φ_0 (see Fig. 5 in results).

For $\lambda_2 < 1 / 2$ there is always at least one bifurcation. For $\lambda_2 > \lambda_{2,Crit}(\nu)$ there may be additional bifurcations (one or two) if φ_0 is larger than the critical $\varphi_0(\lambda_{2,Crit}(\nu))$. To identify the criteria for multiple bifurcations we consider the local extremes of $\varphi_0(\varphi_B)$ which are given by

$$\frac{\partial \varphi_0}{\partial \varphi_B} = \Lambda_2^2 - \nu + \Lambda_2(\nu - 2)\cos \varphi_B + \cos^2 \varphi_B = 0 , \tag{A11}$$

yielding the solutions:

$$\cos \varphi_{B,Extr} = \frac{\Lambda_2(2 - \nu) \pm \sqrt{\Lambda_2^2 \nu(\nu - 4) + 4\nu}}{2} . \tag{A12}$$

Vanishing of the square root defines a condition for a critical $\lambda_{2,Crit}(\nu)$ where additional bifurcations within $0 \leq \varphi \leq \pi$ may appear (see Fig. 7):

$$\lambda_{2,Crit}(\nu) = \frac{1}{1 + \sqrt{\dfrac{1}{1 - \nu / 4}}} . \tag{A13}$$

For $\lambda_2 \geq \lambda_{2,Crit}$ and $\lambda_2 < 1/\nu$ (Fig. 8) an additional type II-bifurcation appears in the configuration space if the nominal angle φ_0 is greater than an angular threshold $\varphi_{0,Crit}(\lambda_2, \nu)$ (Fig. 6). This critical angle results from $\varphi_0(\varphi_B)$ (Eq. A10) with $\cos \varphi_{B,Extr} = A - \sqrt{B}$ (Eq. A12; Figs. 5, 7).

TWO-SEGMENT MODEL WITH ONE LEG MUSCLE

MUSCLE DESIGN AND TECHNIQUES OF THE LONG JUMP

IV

Leg stiffness originates from elastically operating leg joints. The torques are actively generated by leg muscles. At least one leg muscle must be introduced to investigate the interaction between muscle dynamics and leg operation. The aims of this study were:

(1) To identify optimal jumping techniques taking muscle properties into account.

(2) To identify muscle properties influencing jumping performance.

(3) To estimate the maximal muscular contributions to the passive peak.

A two-segment model based on Alexander (1990) was used to investigate the action of knee extensor muscles during long jumps. A more realistic representation of the muscle and tendon properties than implemented previously was necessary to demonstrate the advantages of eccentric force enhancement and non-linear tendon properties.

During the take-off phase of the long jump, highly stretched leg extensor muscles are able to generate the required vertical momentum. Thereby, serially arranged elastic structures enlarge the period of muscle lengthening and dissipative operation, resulting in an enhanced force generation of the muscle-tendon complex. To obtain maximum performance, athletes run at maximum speed and have a net loss in mechanical energy during the take-off phase. The positive work done by the concentrically operating muscle is clearly smaller than the work done by the surrounding system on the muscle during the eccentric phase.

Jumping performance was insensitive to changes in tendon compliance and muscle speed but was greatly influenced by muscle strength and eccentric force enhancement. In agreement with a variety of experimental jumping performances, the optimal jumping technique (angle of attack) was insensitive to the approach speed and muscle properties (muscle mass, muscle fibre to tendon cross-sectional area, relative length of fibres and tendon). The muscle properties restrict the predicted range of the angle of the take-off velocity.

SYMBOLS

α	leg angle	ℓ_f	length of the muscle belly (CE and PE)
α_0	angle of attack (leg angle at touch-down)	ℓ_{LEG}	leg length, distance between point of ground contact and hip
α_{opt}	optimal angle of attack resulting in maximum predicted jumping distance	ℓ_{MTC}	reference length of the muscle-tendon complex
A_{CE}	physiological cross-sectional area of muscle fibres	ℓ_{opt}	optimum fibre length
A_f	physiological cross-sectional area of muscle belly (CE and PE)	ℓ_t	length of serial tendon (SE)
		m	point mass at the hip
A_{PE}	physiological cross-sectional area of parallel element	m_{MTC}	mass of muscle-tendon complex
A_t	physiological cross-sectional area of serial tendon element (SE)	MTC	muscle-tendon complex
		N_{ECC}	eccentric force enhancement (F_{ECC} / F_{MAX})
CE	contractile element	PE	parallel elastic element
$c_1 ... c_4$	constants in the stress-strain relationship of the elastic elements (SE and PE)	r	moment arm of the patella tendon
d	moment arm of the ground reaction force	ρ_{MTC}	density of muscle-tendon complex
ε	strain	R_A	ratio of cross-sectional areas (A_f / A_t) of the muscle
$\dot{\varepsilon}_{MAX}$	maximum muscle fibre strain rate	R_ℓ	relative fibre length (ℓ_f / ℓ_{MTC})
ε_C	critical strain dividing the non-linear and linear behaviour of the tendon	SE	serial elastic component
φ	knee angle	σ	stress
φ_0	initial knee angle at touch-down	σ_{MAX}	maximum isometric stress of muscle fibres
F_{CE}	muscle fibre force	v_0	approach velocity
F_G	ground reaction force	$v_{0,X}, v_{0,Y}$	horizontal and vertical coordinates of the touch-down velocity
$F_{G,EXP}$	experimentally measured ground reaction force from Seyfarth et al. (1999)	v_{CE}	muscle fibre lengthening velocity
		v_{MAX}	maximum shortening velocity of muscle fibres
$F_{G,MOD}$	modelled ground reaction force	V_{MTC}	volume of the muscle-tendon complex
F_{MAX}	maximum isometric force of muscle fibres	$v_{E,X}, v_{E,Y}$	horizontal and vertical coordinates of the take-off velocity
F_{MTC}	muscle force		
F_{ECC}	maximum eccentric force of muscle fibres	x, y	horizontal and vertical co-ordinates of the point mass
F_{PE}	force of parallel elastic element	x_E, y_E	co-ordinates of the point mass at take-off
F_{SE}	force of serial elastic element	x_{JD}	jumping distance
G	constant in Hill-equation (Eq. A1)		
g	gravitational acceleration		
ℓ	length of each leg segment		

INTRODUCTION

Fast saltatoric movements such as human running or jumping are characterised by alternating flight and contact phases. The general dynamics of the body during ground contact represented by the centre of mass trajectory is expressed by the pattern of the ground reaction forces and determines the subsequent flight phase.

Several experimental investigations of the long jump can be found in the literature (e.g. Luhtanen and Komi, 1979; Lees et al., 1994; Stefanyshyn and Nigg, 1998). The limiting

62

factors for attaining greater jumping distances are the ability to increase running speed (Hay, 1993) and the ability to build up large muscle forces (Alexander, 1990). A causal understanding of the contribution of different variables to jumping distance requires a mechanical model of the dynamics during the final support phase before take-off. Obviously, the long jump is a combination of a spring-like elastic operation of the leg and a hammer-like landing shock (Witters et al., 1992). An inverse dynamics approach to the running long jump (Stefanyshyn and Nigg, 1998) used only low run-up speeds, without special attention to impact dynamics. A variety of forward dynamic mechanical models have been developed for human jumps: a mass supported by a simple spring (Alexander et al., 1986; Blickhan, 1989), a two-segment model with a muscle like-torque generator (Alexander, 1990), a four-segment model with a number of muscle-like actuators (e.g. Pandy et al., 1990; Bobbert et al., 1996) or even more detailed models with many more segments and actuators (Hatze, 1981a).

Our goal is to test with a series of models which components are important to describe the dynamics and optimal techniques for the long jump. In a first step, a close fit between measured ground reaction forces and the force predicted by a model was achieved (Seyfarth et al., 1999). This model, an extension of the spring-mass model of Blickhan (1989), was used to describe the spring-like operation of the supporting leg. It predicted an optimal angle of attack of approximately $45 - 55°$ for a leg stiffness of approximately 20 kN/m and an approach speed of 10 m/s. The optimal angle decreased for a higher approach speed and increased for a higher leg stiffness, but was not much influenced by the representation of the distal mass. This model, however, did not take muscle properties into account which, to an unknown extent, contribute to the time course of the force and may shift optimum strategies.

To investigate the role of the muscles in the long jump, the simple model of Alexander (1990) was taken as a starting point. Using a Hill-like torque generator and massless legs, his model predicted the maximum possible approach speed for the long jump to result in an optimal performance. The predicted optimal angle of attack for maximum jumping performance was approximately $70 - 75°$. To describe the first peak in the ground reaction force, the knee extensor muscle was characterised by prestretch without eccentric force enhancement and an extremely high isometric force (approximately 25kN). This resulted in an unrealistic sudden rise in the ground reaction force. In contrast to experimental findings, the passive and active peak were not separated by a local minimum.

In the present study, four questions were addressed: (1) To what extent is the spring-like operation of the leg due to an interaction between leg geometry and muscle-tendon properties? (2) To what extent can a highly activated knee extensor contribute to the first

force peak? (3) What is the role of elastic components and eccentric force enhancement in jumping performance? (4) How does jumping performance depend on muscle architecture? To investigate these issues, a two-segment model was constructed with a Hill-type knee extensor. The extensor muscle was characterised by eccentric force enhancement and included nonlinear serial and parallel elastic components. Distal masses can easily mask the contribution of the musculature under eccentric loading and were therefore neglected in our model. Moreover, only a minor influence of a distal mass representation on the jumping technique was found in our earlier long jump model (Seyfarth et al., 1999).

MATERIAL AND METHODS

Experiments

In an experimental analysis of 30 long jumps by 18 sport students, ground reaction forces and kinematic data were recorded (Seyfarth et al., 1999). The jumping distance was measured as the shortest distance between the take-off position of the foot tip and the landing pit.

Model of the supporting leg

The upper and lower leg were considered as a chain of two rigid segments, each of length ℓ and zero mass. Ground contact was assumed to occur at the distal end of the lower segment. The mass of the jumper was represented as a point mass m at the hip. The distance between the point of ground contact and the hip was the leg length ℓ_{LEG}. The leg angle α was defined as the orientation of the leg ℓ_{LEG} relative to the horizontal plane (Fig. 1).

Representation of knee extensor muscles

To describe the operation of the stance leg, at least one knee extensor muscle must be introduced (Fig. 1). The model of the muscle-tendon complex (MTC) consisted of three elements: (1) the contractile element CE, described by a Hill-like force-velocity relationship with an eccentric force enhancement (Appendix 1: Eqs. A1, A2); (2) a parallel elastic component PE; and (3) a serial elastic component SE. Both elastic elements were characterised by a nonlinear stress-strain relationship (Appendix 2: Eq. A4). Muscle belly force $F_{CE} + F_{PE}$ was equal to the serial tendon force F_{SE}.

During the contact phase, the knee extensor muscle was assumed to be fully activated and had a constant moment arm r at the knee joint. The resulting torque was in equilibrium with the moment generated by the ground reaction force, F_G, with the corresponding variable moment

arm d (Fig. 1, Eq. A5). As distal masses and the foot were neglected, the orientation of the force generated by the leg, i.e. the ground reaction force, was always identical to the leg angle α.
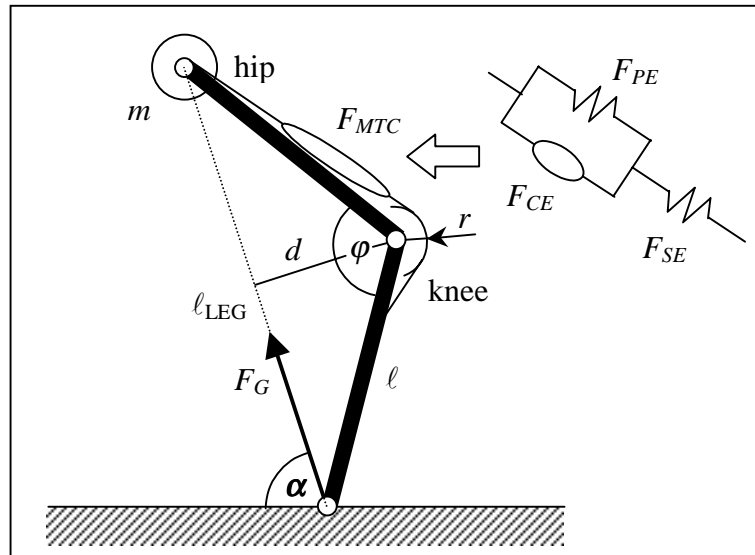

Fig. 1 Two-segment model. Each leg segment is of length ℓ and zero mass. The supported body is represented by a point mass m at the hip. One extensor muscle is acting at the knee joint with constant moment arm r. Muscle force F_{MTC} is equal to the serial tendon force F_{SE} and the sum of the forces produced by CE and PE ($F_{CE}+F_{PE}$). The leg orientation is described in terms of the leg angle α and the knee angle φ. The leg length ℓ_{LEG} is the distance between the point of ground contact and the hip. The distance d is the moment arm of the ground reaction force F_G.

Initial conditions and model variables

The position of the point mass m at touch-down was described by the angle of attack α_0 and the knee angle φ_0 (α_0 approximately $60-65°$, φ_0 approximately $165-170°$; Lees et al., 1994). For elite long jumpers, the initial velocity v_0 is approximately $10-11$ m/s and has only a small vertical component (less than 1m/s; Hay et al., 1986). For an average male athlete, a body mass of 80 kg was assumed (Luhtanen and Komi, 1979).

The height of the centre of mass is approximately 1 m for an upright standing 1.8 m tall male human (Alexander, 1990). A slightly longer leg (segment length $\ell = 0.6$ m) was assumed because (1) the centre of rotation during ground contact shifts form the heel to the ball of the foot and (2) the leg (including the foot) is almost stretched at touch-down and take-off.

Muscle design

The MTC was represented by the CE and two elastic components SE and PE (Fig. 1). Its mass m_{MTC} was not included within the calculations of the dynamics. The reference length of the MTC (ℓ_{MTC}) was approximately the length of the real leg segment (0.5 m). The muscle design was described by (1) the ratio R_ℓ of the fibre length ℓ_f to the total MTC length ℓ_{MTC} : $R_\ell = \ell_f / \ell_{MTC}$ and (2) the ratio R_A of the physiological cross-sectional area of the muscle fibres A_f to the serial tendon cross-sectional area A_t : $R_A = A_f / A_t$.

Assuming an average MTC density ρ_{MTC} of approximately 1100 kg/m^3 (Spector et al., 1980; Winters and Woo, 1990), the geometry of the fibres and tendons (cross-sectional areas and lengths) could be expressed in terms of m_{MTC}, R_A and R_ℓ (Eqs. A8 and A9, Appendix 4). The cross-sectional area of the parallel element A_{PE} accounted for a small part (1%) of the muscle fibre area A_f, the remaining area belonged to the fibres themselves: $A_{CE} = 0.99 \, A_f$.

The maximum isometric force of the muscle fibres F_{MAX} was defined assuming a muscle fibre maximum isometric stress σ_{MAX} of 300 kPa (Alexander and Vernon, 1975; Close, 1972; Eq. A3). The maximum shortening velocity v_{MAX} is the product of the fibre length ℓ_f and the maximum fibre strain rate $\dot{\varepsilon}_{MAX}$ and was assumed to be 14 $\ell_f \cdot \text{s}^{-1}$ (Spector et al., 1980).

In reality, the moment arm d of the ground reaction force is much shorter than described in a two-segment model (Fig. 1). After the first 40 ms of the ground contact, the centre of pressure shifts from the ankle joint to the ball of the foot. Therefore, to generate realistic values of the ground reaction force an unrealistically high maximum isometric muscle force F_{MAX} of approximately 13 kN had to be assumed (see also Alexander, 1990).

Numerical procedure

The trajectory of the point mass, given by the leg force and the gravitational force, was obtained by integrating the equations of motion (Eqs. A6 and A7) numerically with a constant time step (0.01 ms). The calculation was terminated at the instant of take-off, i.e. when the ground reaction force became zero. The resulting jumping distance was calculated assuming a frictionless parabolic flight trajectory and landing at the intersection of the centre of mass trajectory with the ground (Eq. A10).

Parameter studies

The optimal angle of attack α_{opt} leading to a maximum jumping distance was investigated with respect to (1) the running speed at touch-down v_0, (2) the total MTC mass m_{MTC}, (3) the ratio of muscle fibres to serial tendon cross-sectional areas R_A, and (4) the relative fibre length R_ℓ. During take-off phase, a maximum activation of the muscle was assumed because this resulted in the longest jumps and agrees with experimental observations (Kyröläinen et al., 1987).

RESULTS

Forces and work output by muscle and leg

Fig. 2A shows an example of predicted force patterns (modelled ground reaction force $F_{G,MOD}$ and MTC force $F_{MTC,MOD}$) due to a fully activated knee extensor muscle compared to a measured ground reaction force $F_{G,EXP}$ of a 6.9 m jump at 9 m/s approach speed from Seyfarth et al. (1999). This curve can be taken as an example for the other tracings. The simulated jump resulted in a jumping distance of 6.3 m at an angle of the take-off velocity of approximately 14° (measured angle: 21°).

No preactivation was assumed before the moment of touch-down. The general pattern of the predicted dynamics agreed with the experimental result. In both cases, a sharp rise in ground reaction force (first peak) was followed by a prolonged force at a lower level (second peak), but the two peaks were not separated by a local minimum in the simulation. In Fig. 2A, the measured force curve starts 10 ms earlier than the simulated curve because there was no segment representing the foot in the model that would be decelerated first (Seyfarth et al., 1999).

The predicted muscle force had achieved the maximum value by 15 ms after touch-down, when the muscle fibres were at their maximum stretching velocity. The serial tendon had a positive strain during the whole ground contact period (SE in Fig. 2B). It was stretched rapidly immediately after touch-down, shortened very slightly during the next approximately 30 ms (plateau phase) and shortened continuously over the second half of ground contact. The muscle fibres were shortening during the first few milliseconds and during the last 35 ms before take-off (CE in Fig. 2B), when the muscle force was less than the maximum isometric force F_{MAX} (neglecting the force of the parallel elastic element). During most of the ground contact period (approximately $10 - 80$ ms), the muscle fibres were lengthening and therefore absorbing energy.
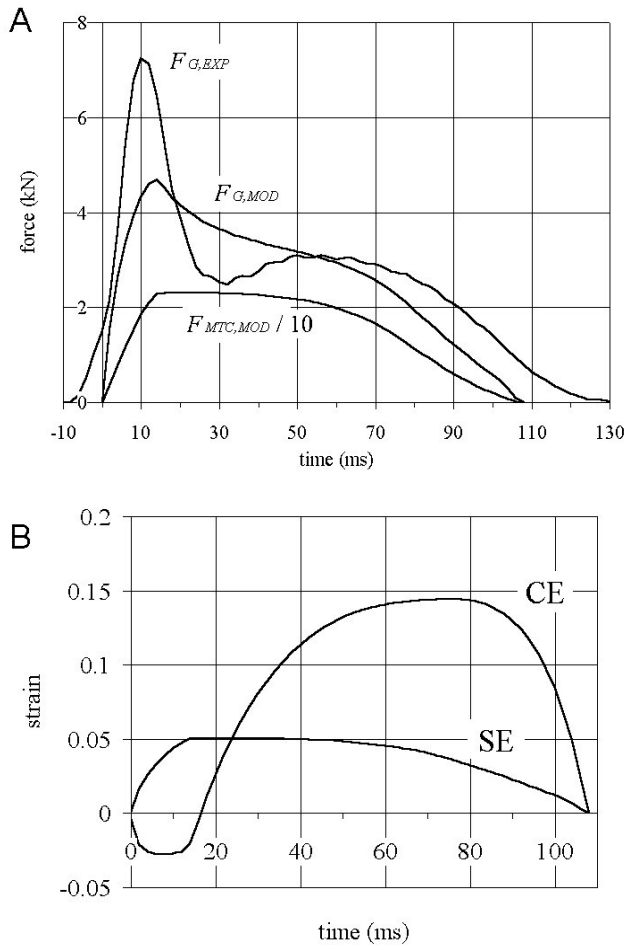
Fig. 2 Dynamics of the two-segment model. (A) Predicted ground reaction force $F_{G,MOD}$ compared with an experimental result $F_{G,EXP}$ (taken from Seyfarth *et al.*, 1999) and predicted internal muscle force $F_{MTC,MOD}$. (B) Strain ε of contractile element (CE) and serial tendon (SE) during ground contact. Concentric contraction takes place only within the first 10 ms and within the last 30 ms. Lengthening of the muscle-tendon complex (MTC) is largely taken up by tendon elongation (see below: R_ℓ).

Model variables (for definition see list of symbols): $m = 80$ kg, $\ell = 0.6$ m, $m_{MTC} = 4$ kg, $\ell_{MTC} = 0.5$ m, $\sigma_{MAX} = 300$ kPa, $R_A = 100$, $R_\ell = 16\%$ ($\ell_f = 0.08$ m); initial variables: $v_{0,X} = 9$ m/s, $v_{0,Y} = -0.4$ m/s, $\alpha_0 = 60°$, $\varphi_0 = 170°$.

Due to a high ground reaction force (up to approximately 5 kN) during the first 20 ms of ground contact, the leg showed a negative work loop (Fig. 3B). After maximum knee flexion, the path of the force-length curve was almost linear (Fig. 3B) in contrast to the nonlinear operation of the extensor muscle (MTC, Fig. 3A). The total energy lost (approximately 280 J, i.e. 44 % of the total muscle work or 9 % of the initial kinetic energy) was absorbed by the muscle fibres (Fig. 4).

The shape of the CE work loop was almost rectangular (Fig. 3A). Only 8 % of the energy transferred to the CE was given back to the point mass during the concentric phase (Fig. 4). In contrast, in the SE approximately 80 % of the stored energy was reusable as mechanical energy. The remainder was absorbed by the CE.
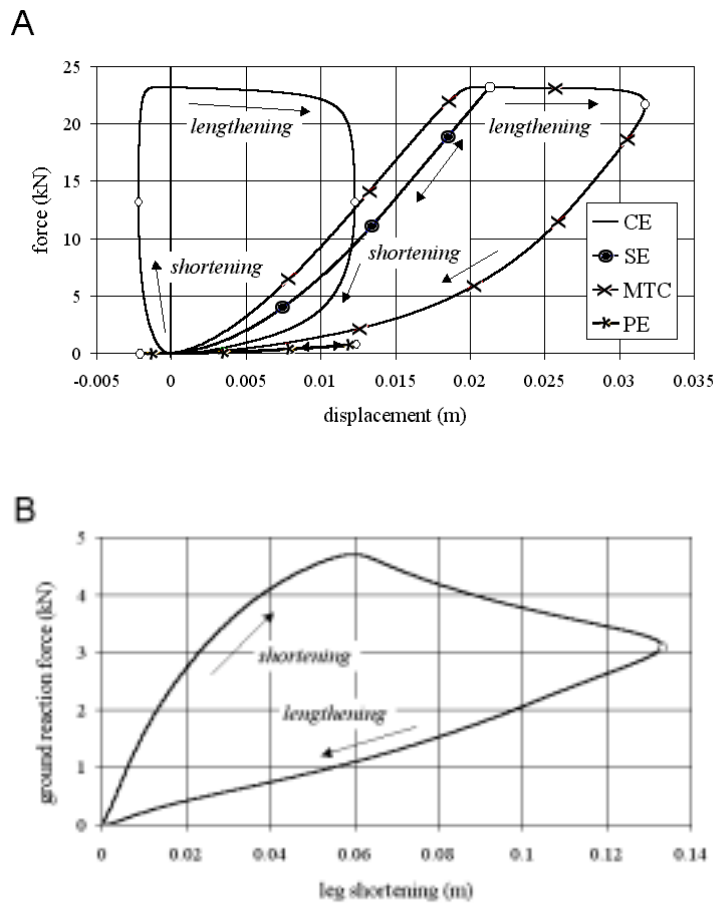
A

B

Fig. 3 Predicted work loops of (A) the muscle-tendon complex (MTC) including the contractile element (CE), serial element (SE) and parallel element (PE), and (B) the supporting leg according to the situation in Fig. 2. Leg shortening is defined as difference of actual leg length ℓ_{LEG} to the leg length at the instant of touch-down. (B) During lengthening the leg shows almost linear behaviour. The small circles represent the transitions between shortening and lengthening.
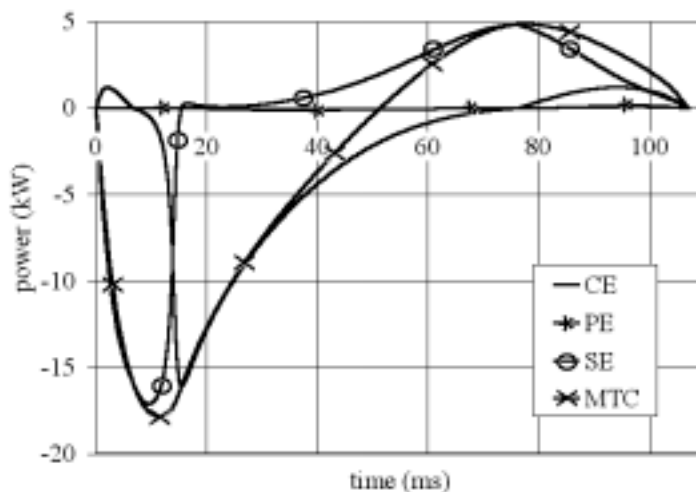
Fig. 4 Predicted power delivered by muscle tendon complex (MTC) with the contractile element (CE), serial element (SE) and parallel element (PE). Power is largely absorbed by the tendon (SE) and the muscle fibres (CE) during the first half of the step whereas only the tendon delivers power during take-off.

Optimal jumping techniques

Approach speed and angle of attack. In Fig. 5, the influence of the angle of attack α_0 and the running speed v_0 on the jumping distance, the percentage of mechanical energy of the point mass at take-off relative to the instant of touch-down, and the angle of the take-off velocity is shown. For high approach speeds (greater than 6 m/s), the optimal angle of attack (approximately $65-70°$) was insensitive to the approach speed (Fig. 5A). The change in

69

mechanical energy during the take-off phase was approximately ± 5 % while using an optimal angle of attack (Fig. 5B). For running speeds greater than 5 m/s optimal performance required a net loss of energy. At lower approach velocities, the leg generated net positive work for optimal performance. This required optimum angles of attack that were steeper than 70° (Fig. 5B).

The angle of the velocity vector at take-off relative to the horizontal plane (take-off velocity angle, Fig. 5C) increased for decreased angles of attack if the running speed was less than 8 m/s. At higher speeds, the angle of take-off velocity was insensitive to the angle of attack or even decreased slightly for small angles of attack.
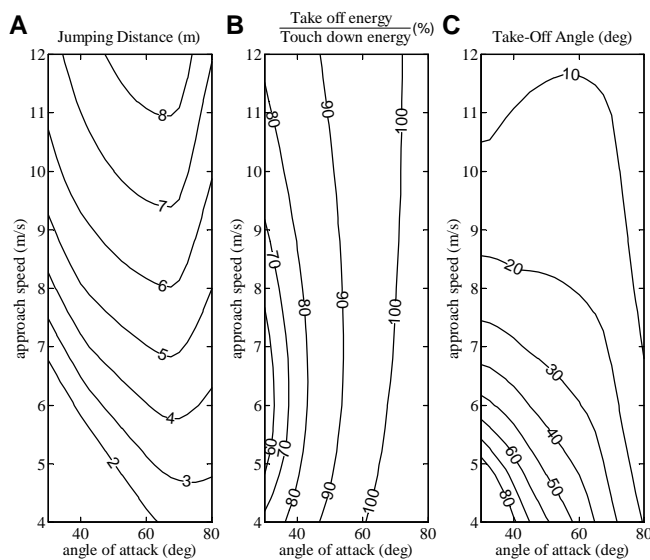

Fig. 5 Influence of the angle of attack at touch-down α_0 and the approach speed v_0 on (A) the jumping distance (contour lines, in m), (B) the percentage of take-off to touch-down mechanical energy (contour lines, in %), and (C) the angle of the velocity vector at take-off relative to the horizontal plane (contour lines, in degree). The optimal angle of attack $(65 - 70°)$ for the long jump is insensitive to the approach speed for velocities higher than 6m/s. The optimal jumping distance (A) is achieved with a nearly complete energy recovery (B). At high running speeds only flat take-off velocity angles can be realised (C) and flatter angles of attack do not lead necessarily to steeper take-off angles. Model variables are given in Fig. 2, in all studies the vertical touch-down velocity was zero.
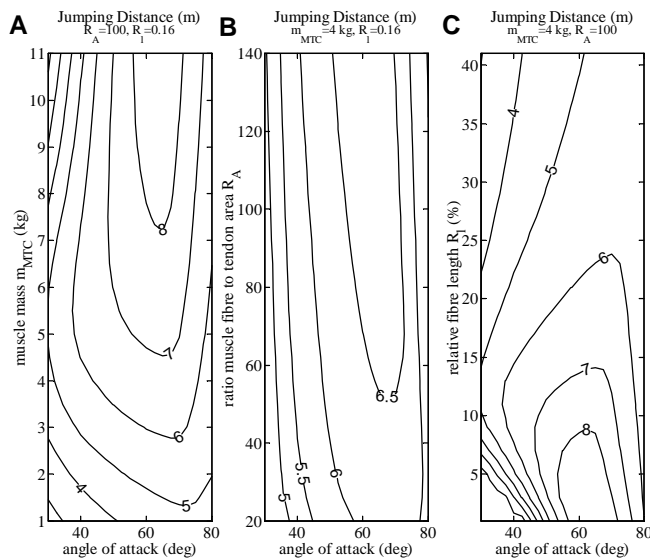
Fig. 6 Influence of the angle of attack at touch-down α_0 and (A) the total muscle mass m_{MTC}, (B) the ratio of fibre to tendon cross sectional areas R_A, and (C) the relative fibre length R_ℓ on jumping distance (contour lines, in m). Jumping distance depends strongly on muscle mass (A) and much less on the partitioning between elastic and contractile tissues (B, C). The optimal angle of attack $(65 - 70°)$ is largely insensitive to the muscle mass m_{MTC} (A), slightly dependent on the ratio of the cross-sectional areas R_A (B), and the relative fibre length R_ℓ (C). For longer fibres (larger R_ℓ) the optimum for α_0 becomes more pronounced. Model and initial variables are given in Fig. 2, in all studies the vertical touch-down velocity was zero.

The influence of the initial knee angle φ_0. Compared to the situation in Fig. 2 (initial knee angle 170°), a smaller knee angle φ_0 led to a shorter jumping distance (for $\varphi_0 = 160°$ a difference of −19 cm and for $\varphi_0 = 150°$ a difference of −38 cm) and a decreased angle of take-off velocity (for $\varphi_0 = 160°$ a difference of −2° and for $\varphi_0 = 150°$ a difference of −4°). Nevertheless, the percentage of the take-off to touch-down mechanical energy increased for smaller knee angles φ_0 (for $\varphi_0 = 160°$ a difference of +1.7 % and for $\varphi_0 = 150°$ a difference of +3.2 %).

Optimal muscle design

Muscle design and angle of attack. The influence of the angle of attack and the total muscle mass m_{MTC}, the ratio of muscle fibres to tendon cross-section area R_A, and the relative fibre length R_ℓ on the jumping distance is shown in Fig. 6.

Keeping the architectural variables (R_A, R_ℓ) constant, the muscle mass determined the maximum force exerted by the leg and had a strong influence on the jumping distance (Fig. 6A). For masses higher than 4 kg, the optimal angle of attack (approximately 65°) was fairly insensitive to changes in muscle mass. Note that the muscle mass is not part of the accelerated mass, it simply represents the volume of the musculature.

For a realistic ratio of the fibre to tendon cross-sectional area of approximately 100 (Winters and Woo, 1990; Pierrynowski, 1985) the optimal angle of attack was approximately 65 − 70° (Fig. 6B). At high ratios ($R_A > 140$) and angles of attack less than 65° slightly higher distances can be achieved. The muscle can produce higher forces and the tendon becomes more compliant. In contrast, for thick tendons ($R_A < 30$) this optimum shifted to steeper angles (more than 70°). However, the jumping performance was not influenced much by R_A.

The influence of the length ratio R_ℓ proved to be more complex (Fig. 6C). Very short muscle fibres ($R_\ell = 1 \%$) led to unrealistically large jumping distances (for humans more than 9 m at 9 m/s approach speed) at realistic optimal angles of attack α_{opt} of 60 − 65°. A relative fibre length of approximately 5 % predicted the smallest α_{opt} of approximately 60° and a jumping distance of approximately 9 m. For longer fibres, α_{opt} increased. For example, at $R_\ell = 15 \%$ a realistic jumping distance (6.7 m) with an α_{opt} of 65 − 70° was calculated.

Compared to the situation in Fig. 2, the predicted jumping distance was quite insensitive to changes in maximum shortening speed of the muscle fibres v_{max} (less than 1% change in distance for twice or half the original speed). Halving or doubling of the tendon compliance

led to a surprisingly small change in jumping distance (less than 3%) as well. Thus, jumping distance is insensitive to muscle speed and the serial tendon compliance.

In contrast, changes of the total MTC mass m_{MTC} (to 50 % or 200 %), of the maximum isometric muscle fibres stress σ_{MAX} (to 50 % or 200 %), and of eccentric force enhancement N_{ECC} (defined as the ratio between maximum eccentric force F_{ECC} to maximum isometric force F_{MAX}; from 1.8 to 1.4 or 2.2, respectively), led to a considerable change in jumping distance (m_{MTC}: −24 % or +25 %, σ_{MAX} : −22 % or +35 %, N_{ECC}: −8 % or +8 %). Thus, jumping distance is sensitive to muscle strength and to eccentric force enhancement.

DISCUSSION

The model presented here predicted the angle of attack used in long jump to be insensitive to running speed (> 6 m/s) and muscle design. The angles agreed with the experimental observations of Seyfarth et al. (1999) within a range of approximately 5°. Furthermore, the model gave a reasonable explanation of why long jumpers use relatively low angles of the take-off velocity and of the extent to which they take advantage of energy losses in leg muscle. Although the model was very simple, it provided insights into muscular dynamics at high stretching velocities and the contribution of a fully activated knee extensor muscle to the shape of the ground reaction force time series in running and jumping.

To what extent is the spring-like operation of the leg due to an interaction of leg geometry and muscle-tendon properties? Due to relatively short muscle fibres ($R_\ell = 0.16$) and high muscle activation (shown experimentally by Kyröläinen et al., 1987) lengthening of the muscle-tendon complex largely takes place within the serial tendon. Therefore, the MTC work loop was strongly influenced by the J-shaped nonlinear stress-strain curve of the tendon (Fig. 3A). The geometry function, given by the ratio of ground reaction force to MTC force, was high for an almost stretched knee joint exactly at the instant where tendon stiffness was low (for small deflections). Furthermore, during muscle shortening before take-off the maximum force was decreasing continuously with increasing shortening velocity. This resulted in an almost linear period of the work loop during unloading (Fig. 3B). The period of linear behaviour could be extended by elastic components in other leg muscles with more compliant tendons (e.g. the Achilles tendon) or by reducing the muscle activation just before the active peak as observed experimentally (Kyröläinen et al., 1987) and it possibly simplifies the control of jumps.

72

In contrast to a spring-mass system with a constant leg stiffness (Seyfarth et al., 1999), a realistic muscle automatically adapts its stiffness at different leg shortening velocities which keeps the optimal jumping techniques robust (Fig. 7). Characterisation of this effect requires a proper description of the muscle eccentric force enhancement together with suitable compliance characteristics of the serial elastic tendon.

Taking the force-length relationship of the knee extensor into account (Fig. 7), the spring-like behaviour of the leg would be slightly enhanced. Depending on the initial fibre length ℓ_f with respect to the optimal fibre length ℓ_{opt} this leads to a slightly increased dependency of the predicted optimal angle on running speed ($\ell_f = \ell_{opt} / 1.4$ in Fig. 7). Nevertheless, for maximum performance the muscle was assumed to work at near the maximum ($\ell_f > \ell_{opt} / 1.2$) within the force-length curve.
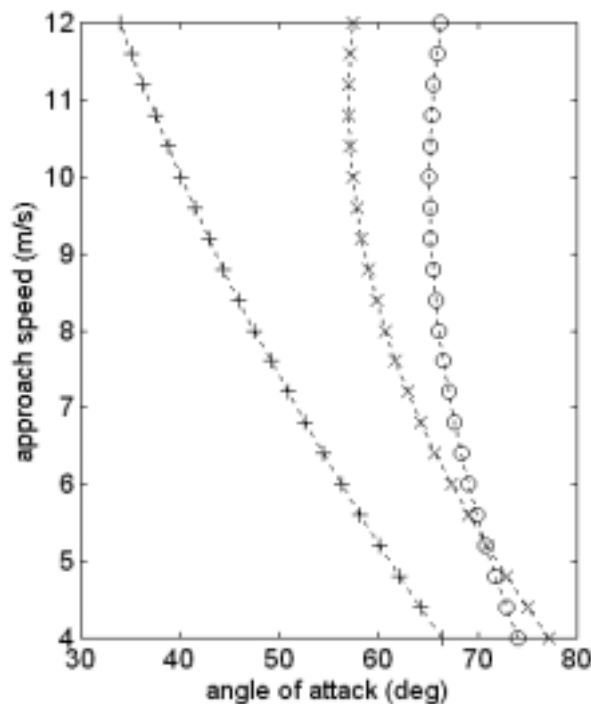

Fig. 7 Predicted optimal angle of attack for different approach velocities using (+) a spring-mass model (leg stiffness: 16 kN/m), (o) the present two-segment model with one extensor muscle (see Fig. 5), and (×) the same model extended by an extensor force-length characteristic with $\ell_{opt} = 1.4\,\ell_f$ where ℓ_f is the muscle fibre length and ℓ_{opt} is the optimal fibre length.

To what extent can a highly activated knee extensor contribute to the first force peak? How does jumping performance depend on muscle architecture? In our model, prestretch was excluded because no antagonist was present. An antagonist muscle would reduce the net knee torque. Assuming a maximum isometric force of the extensor muscle of 10 kN, a realistic preactivation of 60 % did not reproduce the high force peak observed experimentally of approximately $7 - 8$ kN (see Fig. 2A). Only the unrealistic assumption of a completely preactivated extensor without an antagonist produced an appropriate initial peak in amplitude. The shape of this first force peak was characterised by a rapid rise followed by a steady

decent similar to that described by Alexander (1990). However, the shape of the curve in Alexander's (1990) model was not due to force enhancement by eccentric operation of the muscle but was instead a direct consequence of the geometric conditions and an assumed prestretch of the series elastic component (geometry function of the leg, see Eq. A5; Van Ingen Schenau, 1989) which resulted in a rapid rise in ground reaction force (force increases from zero to maximum within one time step).

So including realistic tendon properties and eccentric muscle load in a model are not sufficient to describe the initial peak in force. To achieve this inclusion of a combination of passive properties due to the distributed mass of the system (Seyfarth et al., 1999) and muscle properties is necessary.

What is the role of elastic components and eccentric force enhancement in jumping performance? Jumping performance was not much dependent on tendon compliance. At high approach speeds high eccentric forces are an important feature that increase the vertical momentum at the expense of mechanical energy loss. This requires stiff tendons to profit from high stretching velocities immediately after touch-down. In contrast, low tendon stiffness allows a higher amount of elastically stored energy and results in a prolonged period during which the activated muscle fibres are stretched. As shown in vertical jumping (Zajac, 1993), energy storage and muscle work output are compensating effects. Thinner tendons could improve mechanical efficiency but prevent muscle fibres from making use of high eccentric forces.
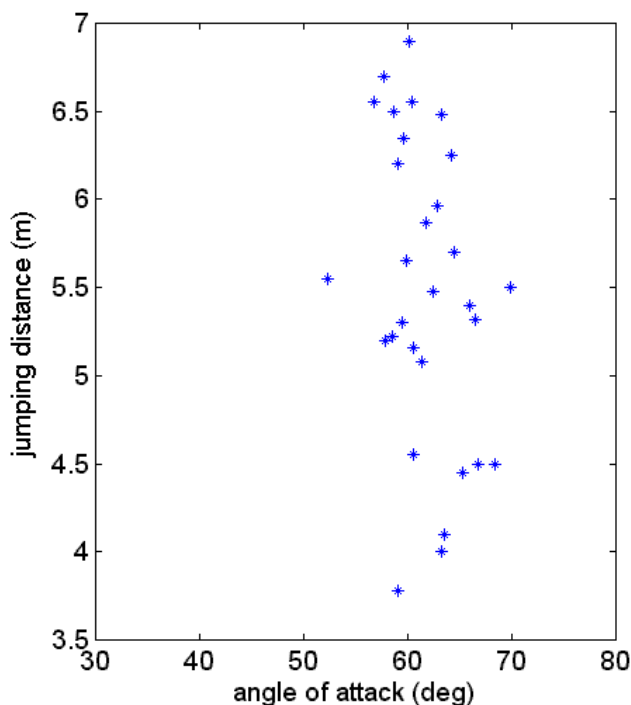

Fig. 8 Experimental analysis of variation in the chosen angle of attack with jumping distance in 30 long jumps by 18 individuals.

How does jumping performance depend on muscle architecture? Jumping distance was more sensitive to changes in length ratio R_ℓ than to the ratio of tendon to muscle fibre cross-sectional areas R_A (Fig. 6). Good jumpers benefit from short muscle fibres and long tendons. This is a well-known architectural feature of animals specialised on jumping (Alexander, 1988; Ettema, 1996). Nevertheless, the optimal angle of attack did not depend much on the actual muscle design (Fig. 6). Exactly this observation was found in an experimental analysis of long jumpers with a variety of abilities (Fig. 8).

Furthermore, the maximum muscle velocity v_{MAX} did not play a crucial role in the performance of the take-off phase because the muscle produces only very little positive work (Fig. 4). Therefore, maximum performance has been observed for the shortest fibres. Nevertheless, intrinsic muscle velocity v_{MAX} could have a positive influence on running speed.

Shortcomings of the model and further directions

It was not possible to reproduce accurately the magnitude of the first force peak because no distributed masses corresponding to those of the supporting leg were included in the present model (Seyfarth et al., 1999). This results in shorter jumps (-9 %) and somewhat flatter angles of the take-off velocity (-7°) than observed experimentally.

Furthermore, a foot is not included and thus the sequence of impacts generated by the contact of the heel pad and the ball of the foot was not represented in our model (see Hatze, 1981a). The lack of the foot also resulted in unrealistically high muscle forces and a shorter contact time (Stefanyshyn and Nigg, 1998). Furthermore, plantar flexion, swing leg movement, and arm lifting lead to a higher take-off position of the body centre of mass (Hay and Nohara, 1990; Seyfarth et al., 1999).

Our model can not simulate the details of prestretch because no antagonists are present and the segments have zero mass. In reality, preactivation before touch-down is present (Kyröläinen et al., 1987). This was compensated to some degree by introducing an instantaneous rise in the activation state.

Very short muscle fibres require a specific muscle architecture (e.g. characterised by large pennation angles) and reduce the range of muscle lengths over which high forces can be produced (due to the force-length relationship). This was not included in our model.

The model could be improved by introducing other leg muscles. For example, the biarticular gastrocnemius muscle couples knee extension to plantar flexion (Van Ingen Schenau, 1989) and improves the utilisation of the work capacity of the extensor muscle. On the other hand, through the simultaneous activation of other muscles not spanning the knee (e.g. hip extensors

and plantar flexors) the net knee torque can be increased (Zajac, 1993). Inclusion of these muscles and their influence of the operation of the knee extensors is investigated in chapter V. To keep the tendon strain less than the critical value for rupture, a high stiffness of the serial tendon had to be assumed. This meant that with a fully activated muscle spring-like sinusoidal patterns of the ground reaction force were not possible. To represent the spring-like behaviour during ground contact, additional elastic structures (deformation of the foot, Achilles tendon, ligaments) should be introduced into the model. With regard to the spring-mass model (Blickhan, 1989; Seyfarth et al., 1999) the leg can produce only a certain maximum force and has therefore a limited ability to operate like a spring. Thus, accurate production of the limited take-off velocity angle of human long jumps can only be achieved by taking the muscle properties into account.

APPENDIX 1: The force-velocity relationship of the muscle fibres

For shortening ($v_{CE} \leq 0$):

$$F_{CE} = F_{MAX} \frac{v_{MAX} + v_{CE}}{v_{MAX} - G \cdot v_{CE}}, \tag{A1}$$

and for lengthening ($v_{CE} \geq 0$):

$$F_{CE} = F_{MAX} \left(1.8 + 0.8 \frac{v_{CE} - v_{MAX}}{7.56 G \cdot v_{CE} + v_{MAX}} \right), \tag{A2}$$

where v_{CE} is the muscle fibre lengthening velocity, F_{CE} is the muscle fibre force, F_{MAX} is the maximum isometric force, v_{MAX} is the maximum shortening velocity and G is a constant (here $G = 5$) (Van Leeuwen, 1992; Otten, 1987). The muscle fibres maximum isometric stress σ_{MAX} and cross-sectional area A_{CE} determined the maximum isometric force F_{MAX}:

$$F_{MAX} = \sigma_{MAX} A_{CE}. \tag{A3}$$

APPENDIX 2: Stress-strain relationship of the elastic components:

$$\sigma = \begin{cases} c_1 \varepsilon^{c_2} & for\ \varepsilon \leq \varepsilon_c \\ c_3 \varepsilon + c_4 & for\ \varepsilon \geq \varepsilon_c \end{cases}, \tag{A4}$$

where σ is stress, c_1-c_4 are constants, ε is strain and ε_C is critical strain . The elastic components behave nonlinearly until a certain specific critical strain $\varepsilon \leq \varepsilon_c$ and linearly for

higher strains $\varepsilon \geq \varepsilon_C$. The exponent c_2 was 1.75, the tangent modulus of the linear part c_3 was 1.5 GPa. The critical strain ε_C was 0.035 for the serial tendon and 0.1 for the parallel element (Van Leeuwen, 1992 referring to measurements of Ker, 1981). The remaining variables c_1 and c_4 are calculated from the given variables c_2 and c_3.

APPENDIX 3: The ground reaction force

The ground reaction force F_G caused by the muscle-tendon complex force F_{MTC} was given by:

$$F_G = r\, F_{MTC}\,/\,d, \tag{A5}$$

where r was the moment arm of the knee extensor muscle and d was the moment arm of the ground reaction force (Fig.1). During ground contact, the equations of motion of the point mass m were:

$$\ddot{x} = -(\,F_G\,/\,m\,)\cos\alpha, \tag{A6}$$

$$\ddot{y} = (\,F_G\,/\,m\,)\sin\alpha - g, \tag{A7}$$

where g is the gravitational acceleration, α is the leg angle, and $\ddot{x}, \ddot{y}$ are the horizontal and vertical accelerations.

APPENDIX 4: Muscle design variables

The ratios $R_A = A_f\,/\,A_t$ and $R_\ell = \ell_f\,/\,\ell_{MTC}$ where A_f and A_t are the physiological cross-sectional areas of the muscle fibres and serial tendon, respectively, and ℓ_f and ℓ_{MTC} are the lengths of the fibres and MTC, respectively, were used to calculate the tendon cross-sectional area using the total MTC mass m_{MTC}, mean density ρ_{MTC}, and the total MTC length $\ell_{MTC} = \ell_f + \ell_t$ where ℓ_t is tendon length:

$$m_{MTC} = \rho_{MTC} V_{MTC} = \rho_{MTC}\left(A_f l_f + A_t l_t\right), \tag{A8}$$

where V_{MTC} is the volume of the muscle-tendon complex. Note that the muscle pennation angle was neglected in this approach. Introducing the design variables R_A and R_ℓ we obtain:

$$A_t = \frac{m_{MTC}}{\ell_{MTC}\rho_{MTC}} \cdot \frac{1}{R_\ell(R_A - 1) + 1}. \tag{A9}$$

At this stage the subscript f denotes the muscle belly including both the parallel element and the muscle fibres themselves, whose lengths are identical. The parallel element takes up only a small part of the cross-sectional area: $A_{PE} = 0.01 \cdot A_f$.

APPENDIX 5: Jumping distance.

Given the take-off variables (position x_E, y_E and velocity $v_{E,X}$, $v_{E,Y}$), from numerical integration, the jumping distance x_{JD} is:

$$x_{JD} = \frac{v_{E,X}}{g}\left(v_{E,Y} + \sqrt{v_{E,Y}^2 + 2g \cdot y_E}\right) + x_E .$$
(A10)

FOUR-SEGMENT MODEL WITH SIX LEG MUSCLES

THE ORIGIN OF SPRING-LIKE LEG BEHAVIOUR

V

In this study the origin of spring-like leg behaviour in long jump is addressed. Therefore, a forward dynamic model of the human musculoskeletal system was used to study the interaction between segment dynamics and muscle dynamics. The model consists of four rigid segments representing the upper body (head, both arms, trunk and swing leg: HATL) and the stance leg (foot, shank and thigh) and six major muscle-tendon complexes (MTCs) acting on the intersegmental hinge joints. Muscle stimulation STIM(t) was optimised for maximum jumping distance whereas each muscle was allowed to switch on only once.

This allowed us to investigate the following aspects:
(1) To what extend is spring-like operation supported by inherent MTC properties?
(2) How is spring-like operation supported by segmental arrangement during leg loading?
(3) Which effects are contributing to the passive force peak?

It was found that:
(1) Optimising jumping performance leads to spring-like leg behaviour.
(2) Thereby, synchronous and quasi-elastic ankle and knee joint loading occurred.
(3) Leg stiffness is an overall behaviour of the whole body and originates from a synchronised, quasi-elastic muscle operation reducing intermuscular and interarticular energy losses.
(4) Highly activated MTCs show quasi-elastic behaviour at fast loading speeds due to intrinsic muscle properties (force-length, force-velocity, activation dynamics) and loading of serial elements.
(5) During passive peak, elastic leg operation was superimposed by distal mass deceleration.

A_{REL} Hill parameter corresponding to $G = 1 / A_{REL}$

B_{REL} Hill parameter with $v_{MAX} = B_{REL} / A_{REL} \cdot \ell_{CE,OPT}$

c_{ij} rotational stiffness at a joint connecting segments i and j

COM   centre of mass

d_X, d_Y constants of the foot force-displacement relationship

$\Delta\varphi_{ij}$ angular displacement with respect to a nominal angle $\varphi_{0,ij}$

$\Delta\ell$ instantaneous amount of leg shortening $\Delta\ell(t) = \ell_0 - \ell(t)$

$\Delta x, \Delta y$ horizontal, vertical displacement of the ball of the foot

ε_{MAX} tendon strain at maximum isometric force F_{MAX}

F_G ground reaction force

F_{MLS} ground reaction force at maximum leg shortening

F_{MAX} maximum isometric muscle force

F_{TD} muscle force at touch down

F_X, F_Y horizontal, vertical component of the ground reaction force F_G

φ_i orientation of segment i (1: foot, 2: shank, 3: thigh, 4: HATL) with respect to the ground

φ_{ij} inner joint angle between segments i and j

$\varphi_{0,ij}$ nominal joint angle

G curvature of the force-velocity curve

HATL   upper body including head, both arms, trunk and swing leg

JD   jumping distance

k_{ACT} mean leg stiffness during active peak

k_{LEG} instantaneous leg stiffness ($F_{LEG} / \Delta\ell_{LEG}$)

ℓ leg length (distance form the ball to the centre of mass)

ℓ_0 rest length of the leg

ℓ_{CE} muscle fibre length

$\ell_{CE,OPT}$ optimal muscle fibre length

$\ell_{SE,0}$ serial tendon slack length

N_{PREACT} level of muscle preactivation $N_{PREACT} = F_{TD} / F_{MAX}$

M_{ij} torque acting at the joint between segments i and j

MLS   maximum leg shortening

MTC   muscle-tendon complex

$\vec{r}_B$ position of the ball of the foot $\vec{r}_B = (\Delta x, \Delta y)$

R_C stiffness ratio c_{12} / c_{23}

STIM(t)   muscle stimulation, switches from 0 to 1 at t_{START}

STV   variation in leg stiffness during active peak

t_C contact time

t_{START} if $t_{START} \geq 0$: time where STIM(t) switches from 0 to 1
if $t_{START} < 0$: level of muscle preactivation $N_{PREACT} = -t_{START}$

v_{MAX} maximum muscle fibre shortening velocity

v_Y vertical velocity of the ball of the foot

INTRODUCTION

In the literature many papers are found focussing on the 'leg stiffness' during different activities and its adaptation to speed and environmental conditions (e.g. Mc Mahon and Cheng, 1990; Farley et al., 1998). The leg may behave as a spring, but it is not a spring. The tendons are not compliant enough to account for the joint excursions and consequently the muscle fibres must lengthen and shorten during the stance phase. But these muscle fibres are very complex elements which have among other properties a force-velocity relationship which causes energy absorption. Moreover, there is a highly nonlinear geometry function involved in the transfer from joint moments to 'leg force'.

This leads to the question: How can such a complex system display spring-like behaviour? What is causing the increase in force during leg shortening and the decrease in leg force

during lengthening? Is the spring-like behaviour caused by some ingenious control mechanisms, or does it simply follow from the intrinsic properties of the system?

In order to study such questions for running with an optimal control model optimisation criteria are needed. These are complex for this type of exercise. Fortunately, stiffness behaviour similar to that found in running is found in the long jump, and there is a clear optimisation goal: the longest jump. There is one drawback: the initial part of the stance phase is dominated by the impact of the distal segments (chapter II), but with the model this can be separated out and the 'active' behaviour of the leg itself can be investigated.

In this study the muscle stimulation histories for a forward dynamic model that represents the salient properties of the real system were optimised using the jumping distance as optimisation criterion. If it turns out that the optimal solution displays spring-like behaviour, subsequently the origins of this behaviour can be identified.

METHODS

Experimental data.

To acquire initial conditions for simulations and to evaluate simulation results, kinematic data (Fig. 1A) and ground reaction forces (Fig. 2B) obtained from 18 sport students performing long jumps were used. These data were collected in a study described elsewhere (Friedrichs et al., in prep.; Seyfarth et al., 1999). In total, 30 long jumps were analysed. Jumping distance was defined as the shortest distance between the take-off position of the tip of the foot and the rear end of the landing pit.

Planar model of the human body.

For simulations the two-dimensional forward dynamic model of the human musculo-skeletal system shown in Fig. 1B was used. The model, which calculates the motion of body segments corresponding to muscle stimulation input, was based on a model described in detail elsewhere (Van Soest and Bobbert, 1993). It consisted of four rigid segments representing the right foot, lower leg, upper leg (the right leg was used in the one-legged push-off) and a HATL segment representing head, arms, trunk and left leg. These segments were interconnected in hinge joints representing hip, knee and ankle joints. The orientation of the segments (angles φ_i, i=1...4) defines the joint angles (φ_{ij}). The contact between the ball of the foot ($\vec{r}_B$) and ground was described by two nonlinear force functions:

$$F_Y = \begin{cases} -d_Y(\text{sgn}(\Delta y) + v_Y)|\Delta y|^3 & \text{if } \Delta y < 0 \\ 0 & \text{else} \end{cases}$$

$$F_X = \begin{cases} -d_X \Delta x |\Delta y|^3 & \text{if } F_Y > 0 \\ 0 & \text{else} \end{cases}$$

(1a,b)

where Δx and Δy were the horizontal and vertical displacements of the ball of the foot, v_Y was the vertical ball velocity divided by 1 m/s, d_X and d_Y were constants ($d_X = 5 \cdot 10^6$ N/m^4 and $d_Y = 10^7$ N/m^3) and 'sgn' denotes the signum function (chapter II). Heel contact was described by fixation of the foot rotation ($\varphi_1 = \text{const}$) resulting in a negative external moment at the ball of the foot M_{01}. If the ball torque became positive ($M_{01} > 0$) the unilateral constraint ($\ddot{\varphi}_1 = 0$) was cancelled (for notation see Fig. 1 in chapter III).

In the skeletal submodel, the following six major muscle-tendon complexes (MTCs) contributing to extension of the lower extremity were embedded: hamstrings (HAM), gluteus maximus (GLM), rectus femoris (RF), vasti (VAS), gastrocnemius (GAS) and soleus (SOL). A Hill-type muscle model was used to represent each of these six MTCs. It consisted of a contractile element (CE), a series elastic element (SE) and a parallel elastic element (PE), and was also described in full detail elsewhere (Van Soest and Bobbert, 1993). Behaviour of SE and PE was determined by a nonlinear force-length relationship. SE was characterised by a slack length $\ell_{SE,0}$ (Tab. 1) and a maximum strain $\varepsilon_{MAX} = 0.04$ corresponding to the maximum isometric muscle force F_{MAX}. Behaviour of CE was more complex: contraction velocity depended on active state, CE length, and force, with force being directly related to the length of SE. This length could be calculated at any instant from the state variables CE lengths and joint angles, because the latter directly determine MTC lengths. Following Hatze (1981b) the relationship between active state, representing the fraction of cross-bridges attached, and muscle stimulation STIM was modelled as a first order process. STIM, ranging between 0 and 1, is a one-dimensional representation of the effects of recruitment and firing frequency of α-motoneurons.

Because in this study only one-legged push-offs with the stance leg were investigated, a decision had to be made concerning the behaviour of swing leg. It was decided to simply create one rigid head-arms-trunk-leg segment (HATL), so that only the muscles of the stance leg could be used for the push-off. To set parameter values of the HATL segment, the trunk moment of inertia was scaled by taking the masses of the remaining body segments into account. To meet the strength of long jumpers the maximum isometric force of the muscles of

the right leg were set to 65% of the values used for two legs in vertical jumping (Tab.1 and Fig. 1B; Van Soest and Bobbert, 1993).

MTC	SOL	GAS	VAS	RF	GLM	HAM
F_{MAX} (N)	5200	2600	5850	1950	3250	2600
$\ell_{CE,OPT}$ (m)	0.055	0.055	0.093	0.081	0.2	0.104
$\ell_{SE,0}$ (m)	0.2356	0.376	0.16	0.34	0.15	0.37
$\ell_{CE,OPT}$ / $\ell_{SE,0}$	1 : 4.28	1 : 6.84	1 : 1.72	1 : 4.2	1 : 0.75	1 : 3.56

Tab. 1 Specific parameters of the six leg muscles (adapted from: Van Soest, 1992).

Optimisation of STIM(t)

For each of the conditions to be studied, a dynamic optimisation had to be formulated. Dynamic optimisation of maximum height jumping was studied in its full complexity by Pandy et al. (1990). Partly based on their results, the following restrictions were imposed on STIM: First, STIM was allowed to take on either the initial value of zero or the maximal value of 1.0. Second, STIM was allowed to switch to the maximum value just once, and thereafter had to remain maximal until take-off. Under these restrictions, STIM(t) of each of the six muscle groups of the push-off leg is described by a single parameter: the instant t_{START} at which it switches from initial value to its maximal value. Third, an initial level of preactivation was allowed for touch-down. The preactivation level N_{PREACT} was defined as the ratio of the muscle's force at touch-down F_{TD} to its maximum isometric force F_{MAX}. Preactivation was included into the optimisation of STIM(t) by interpreting negative STIM inset times ($t_{START} < 0$) as a positive level of preactivation at touch-down. The optimisation problem is thus reduced to find the combination of six switching times that produces the maximum jumping distance JD calculated as the distance between the ball position at take-off and the intersection of the ballistic flight trajectory with the ground (details in chapter II and IV).

Leg stiffness and joint stiffness

The leg length ℓ is given by the distance of the ball of the foot to the body centre of mass (COM). The rest length of the leg ℓ_0 is defined by the leg length where leg force is zero. If the leg length varies between touch-down and take-off an instantaneous representation of $\ell_0(t)$ may be required to fulfill zero forces at both conditions (Seyfarth et al., 1999). The difference of the actual leg length $\ell(t)$ to the rest length $\ell_0(t)$ defines the leg shortening $\Delta\ell = \ell_0 - \ell$. This

allows to define the instantaneous leg stiffness k_{LEG} given by the ratio of the amount of the ground reaction force F_G to instantaneous amount of leg shortening $\Delta\ell$ (Seyfarth et al., 1999):

$$k_{LEG}(t) = \frac{F_G(t)}{\Delta\ell(t)}.$$ (2)

This is a generalisation of the leg stiffness which fits to the leg stiffness at maximum leg shortening $k_{MLS} = F_{MLS} / \Delta\ell_{MLS}$ assuming that the highest active leg force occurs at maximum leg shortening (e.g. McMahon and Cheng, 1990; Farley et al., 1993). A constant leg stiffness $k_{LEG}(t)$ represents an ideal linear spring. In reality, increasing or decreasing stiffness time series may occur (Fig. 3C) denoting higher force during either leg shortening or lengthening. During active peak ($0.3-0.9\ t_C$), the constancy of the leg stiffness $k_{LEG}(t_i)$ was characterised by the stiffness variation STV given by

$$STV = \frac{SD(k_{LEG}(t_i))}{mean(k_{LEG}(t_i))},$$ (3)

where discrete time steps t_i were assumed ($0.3\ t_C < t_i < 0.9\ t_C$). At joint level, the ratio of the joint torque M_{ij} to the corresponding joint angular displacement $\Delta\varphi_{ij} = \varphi^0_{ij} - \varphi_{ij}$ defined the instantaneous joint stiffness:

$$c_{ij}(t) = \frac{M_{ij}(t)}{\Delta\varphi_{ij}(t)}.$$ (4)

Here again the nominal angle φ^0_{ij} was given by the angular positions at touch-down and take-off. Similar to the rest length of the leg ℓ_0, differences may also be present in the angular configurations between touch-down and take-off. Therefore, an assumption had to be made. The simplest approach is to postulate linear changes of the nominal positions with respect to time (chapter II). Changes in nominal joint configurations were postulated the first time in Feldman's equilibrium point hypothesis (1966). Thereby, the spring-like muscle operation was reduced to two control parameters: a stiffness and a nominal position (reviews in Winters, 1995 and Gielen et al., 1995).

As joint torques do not necessarily vanish at touch-down or take-off infinite joint stiffnesses may be present at this situations, e.g. if muscular preactivation is assumed. The ratio of ankle to knee rotational stiffness defines the instantaneous stiffness ratio R_C:

$$R_C(t) = \frac{c_{12}(t)}{c_{23}(t)} . \tag{5}$$

The adjustment of the rotational stiffnesses to nominal configurations and the segment length design is discussed in detail in chapter III.

Numerical procedure

The equations of motion of the four-segment system together with the additional equations representing the internal muscle dynamics were integrated using a numerical variable order Adams-Bashforth-Moulton solver (`ode113` in Matlab, The Mathworks). The optimisation algorithm (`fmins` in Matlab, The Mathworks) used the simplex search method of Lagarias et al. (1997).

RESULTS

Experimental data

In the experiments distances between 3.78 and 6.90 m were observed. The contact times varied between 120 and 176 ms. The leg kinematics during the take-off phase of a long jump is shown in Fig. 1A. Hereby, the best jump was taken as an representative example of a long jump for further investigation as the optimised performance is considered in the simulation study.
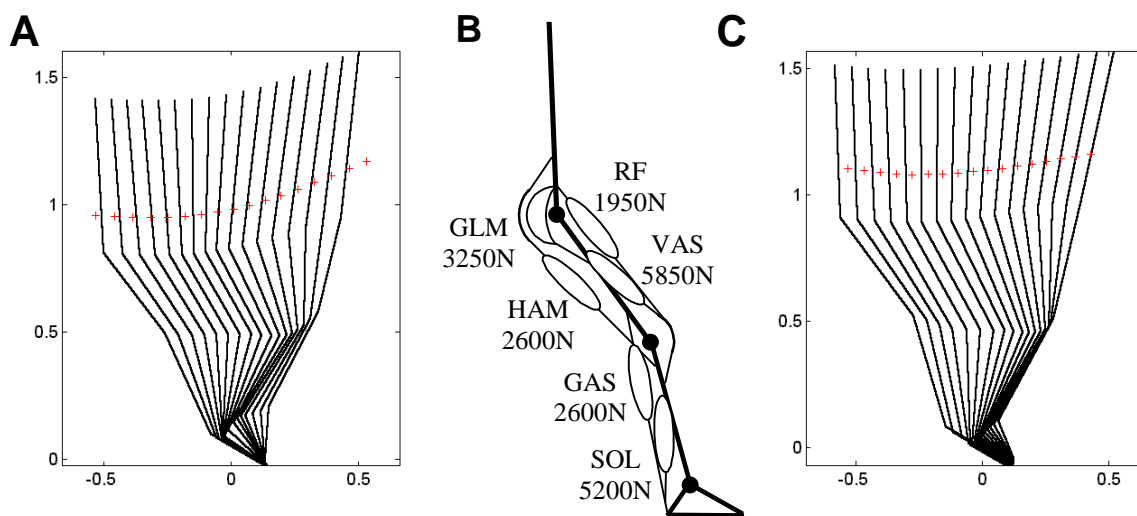

Fig. 1 Kinematics of the take-off phase of a 6.9 m jump. (A) Experimental centre of mass position (+) and segment orientation defined by ball, ankle, knee, hip and shoulder landmarks. (C) Output of the simulation using a four-segment model (B) optimised for jumping distance.

The stance leg touched down with a knee angle of approximately 160° and an angle of attack (orientation of the leg with respect to the ground) of about 61 degree. During the ground contact knee and ankle joints were bent by about 30° before they returned to the stretched position at take-off. The centre of mass moved to a forward upper position with respect to the trunk (Fig. 1A) mainly due to the arm and swing-leg movement (not shown in this figure). The tracing of the ground reaction force corresponding to the selected jump in Fig. 1A is shown in Fig. 2. A first high force peak (4000 − 8000 N) was observed within the first 30 − 40 ms followed by a prolonged second peak. The sinusoidal second force peak reached a maximum of 2500 − 4500 N at about half contact time (chapter II, Friedrichs et al., in prep.). The experimental tracing of the leg force-length relationship is shown in Fig. 3A. After the first peak, a steady descend of the leg force with increasing leg length was found. The leg length increased by about 12.6% from touch-down to take-off. The instantaneous leg stiffness $k_{LEG}(t)$ (Fig. 3B, C) showed a maximum during passive peak which was 3 to 8 times higher than the leg stiffness during active peak ($k_{ACT} = 16.6 \pm 3.0$ kN/m). The instantaneous leg stiffness varied by STV = $6.6 \pm 3.7\%$ during this time ($0.3 − 0.9\ t_C$).
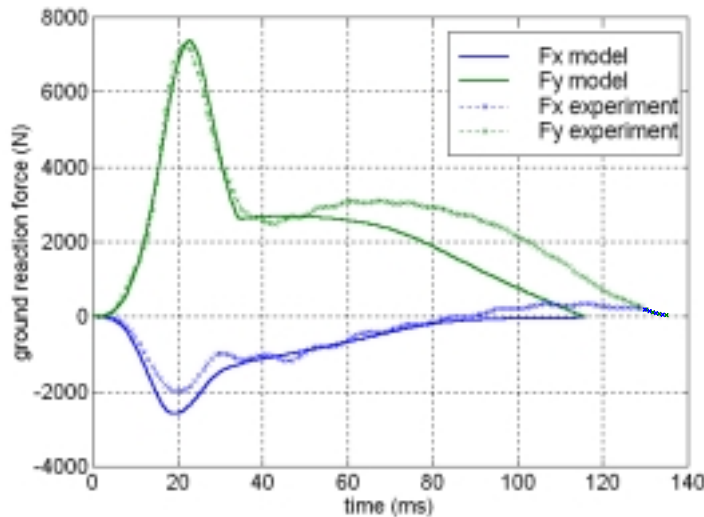

Fig. 2 Simulated and experimental ground reaction forces of a 6.9 m jump corresponding to Fig. 1. In the model muscle stimulation was optimised for maximum jumping distance. Predicted jumping distance: 5.72 m.

Optimal long jump predicted by the model

In the optimal solution all muscles were either already switched on at touch-down (SOL, VAS, GLM, RF) or completely dropped out during the whole stance phase (GAS and HAM). The maximum level of preactivation N_{PREACT} was observed in VAS (32%) and SOL (23%), followed by GLM (12.5%) and RF (7.1%). The remaining biarticular muscles (GAS and

HAM) did not contribute to the vertical momentum generation. Using the muscular configuration shown in Fig. 1B and Tab. 1a jumping distance of 5.72 m was predicted. The predicted segment kinematics (Fig. 1C) was similar to the experimental findings. During the optimisation process ankle and knee joint kinematics became almost synchronised with a similar range of flexion (knee: 25°; ankle: 30°). The orientation of the HATL segment aligned with the leg axis.

The pattern of the predicted ground reaction force was similar to the experimental findings (Fig. 2). During the passive peak a precise description of the ground reaction force was achieved. The active force peak had an almost sinusoidal shape with a maximum somewhat earlier than measured. The contact time was about 115 ms and therefore about 17% shorter than in the experiment.
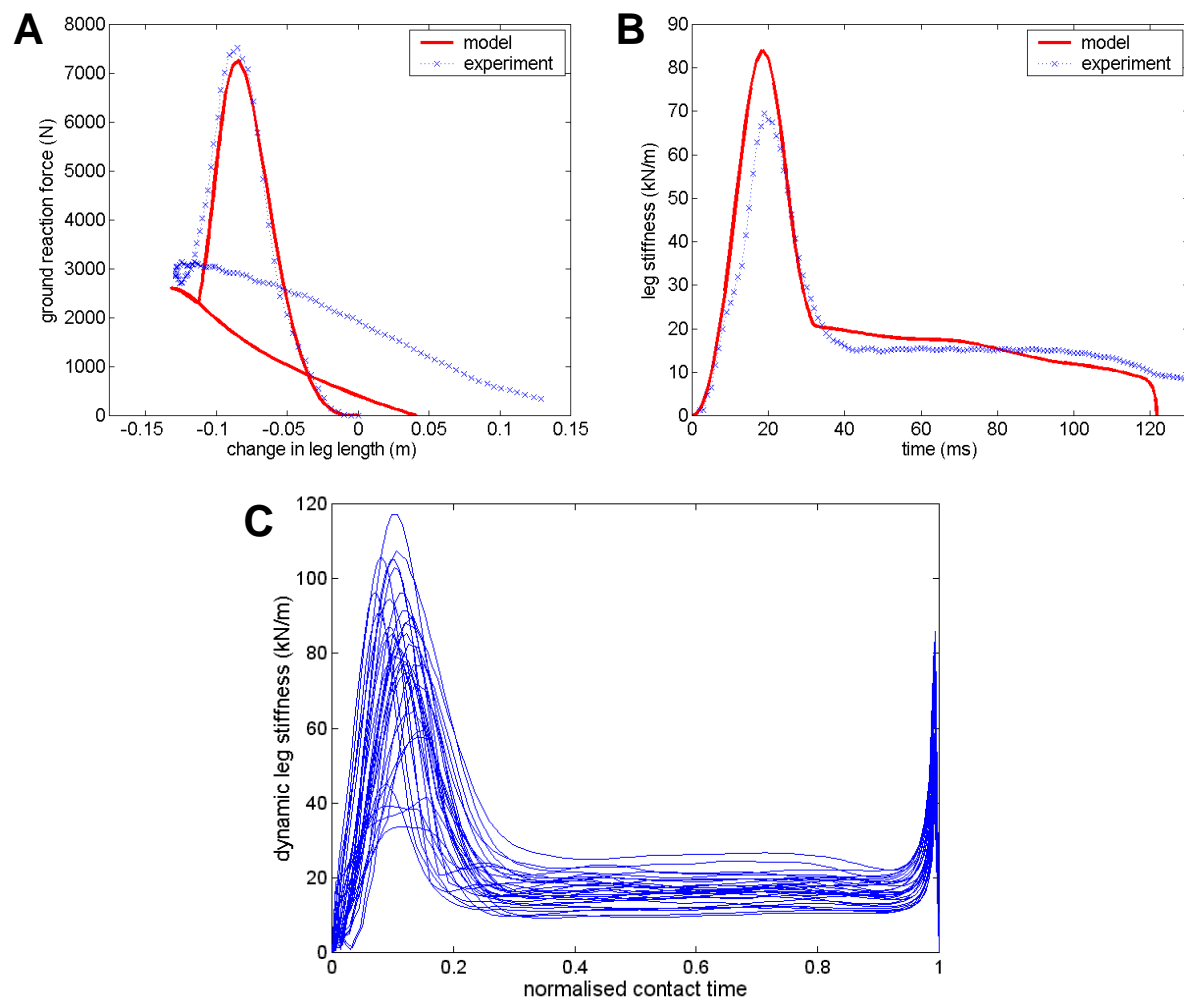

Fig. 3 (A) Leg force-leg length behaviour and (B) time series of the dynamic leg stiffness $k_{LEG}(t)$ predicted by the model ($k_{ACT} = 17.8$ kN/m, STV = 15.4%) compared to a measured tracing (experiment: $k_{ACT} = 16.4$ kN/m, STV = 2.8%) and (C) measured for 30 jumps of 18 athletes with a large variety of achieved distances (3.8 to 6.9 m). During active peak (0.3–0.9 t_C) an almost constant leg stiffnesses was observed ($k_{ACT} = 16.6 \pm 3.7$ kN/m, STV = 6.0 ± 3.4 %). The high stiffness values during the last milliseconds (C) are an artefact due to the gradual decrease of the experimental force tracings (Fig. 2).

The predicted leg force-length relationship was characterised by a limited ability of leg lengthening during the take-off (Fig. 3A). During the active phase a decrease in leg stiffness was present (Fig. 3B). During the active phase ($0.3 - 0.9$ t_C), the variation in leg stiffness (STV) took 15.4 % of the mean stiffness $k_{ACT} = 17.8$ kN/m. This was clearly more than observed experimentally (about 6.6 ± 3.7 %). An almost linear decrease in leg stiffness was found during the active phase (Fig. 3B).
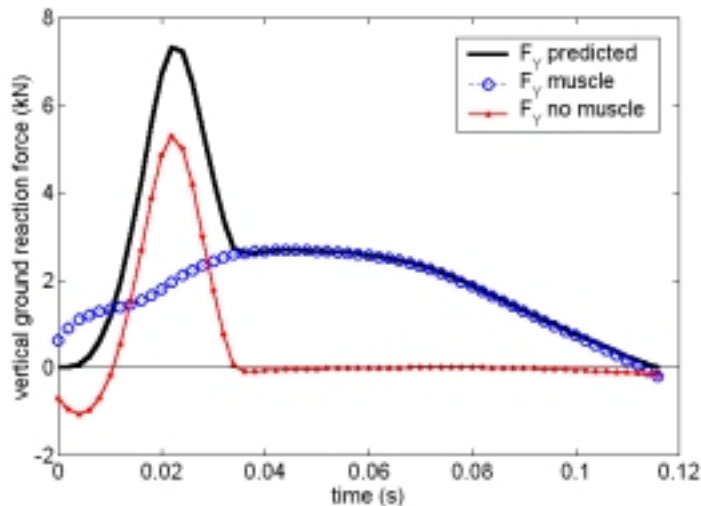

Fig. 4 Muscular contributions to the predicted vertical component of the ground reaction force F_Y. The force was recalculated by inverse dynamics using the predicted joint kinematics $\varphi_i(t)$ (Fig. 1) assuming either $M_{01} = 0$ and $\ddot{r}_B = 0$ ('muscle') or $M_{12} = M_{23} = M_{34} = 0$ ('no muscle').
Muscles (represented in M_{12}, M_{23}, M_{34}) were mainly responsible for the shape of the active peak. The passive peak was largely due to distal mass deceleration (external torque at ball M_{01} and foot deceleration $\ddot{r}_B$).

Muscular contributions to the first peak

In Fig. 4 the vertical component of the ground reaction force was calculated for given joint kinematics (Fig. 1C). Two different contributions to the centre of mass acceleration were separated: (1) the role of muscles represented by the joint torques M_{12}, M_{23} and M_{34}, and (2) the influence of the body deceleration due to the foot contact represented by the external torque M_{01} and the ball acceleration $\ddot{r}_B$. The ground reaction force was recalculated by neglecting either one or the other contributions (zero joint torques or zero external torque and no foot acceleration). This resulted in a clearly separated active peak due to muscle activity and a passive peak due to external forces. The passive force peak was largely (about 80%) due to ball torque M_{01} which corresponded to the heel pad deformation. In case (2), a negative force contribution was calculated at the beginning for the ground contact due to the inertial contributions (re-actio) corresponding to the muscle torques (actio). As the muscle torques were neglected, only the reaction remained resulting in pulling forces at the ground.

Dynamics of the muscle-tendon complexes (MTC)

The time series of the leg muscle forces contributing to the long jump (SOL, VAS, RF, GLM) is shown in Fig. 5. The monoarticular SOL and VAS produced their maximum forces at about half the contact time. RF had broad maximum of 2.6 kN (1.33 F_{MAX}) at 60 ms after touchdown.
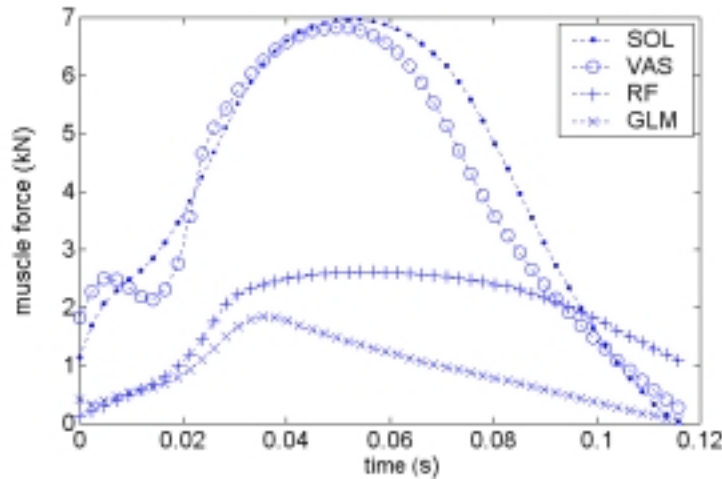

Fig. 5 Predicted muscle force of SOL, VAS, RF and GLM during stance phase. SOL and VAS muscles were characterised by an almost sinusoidal force pattern.
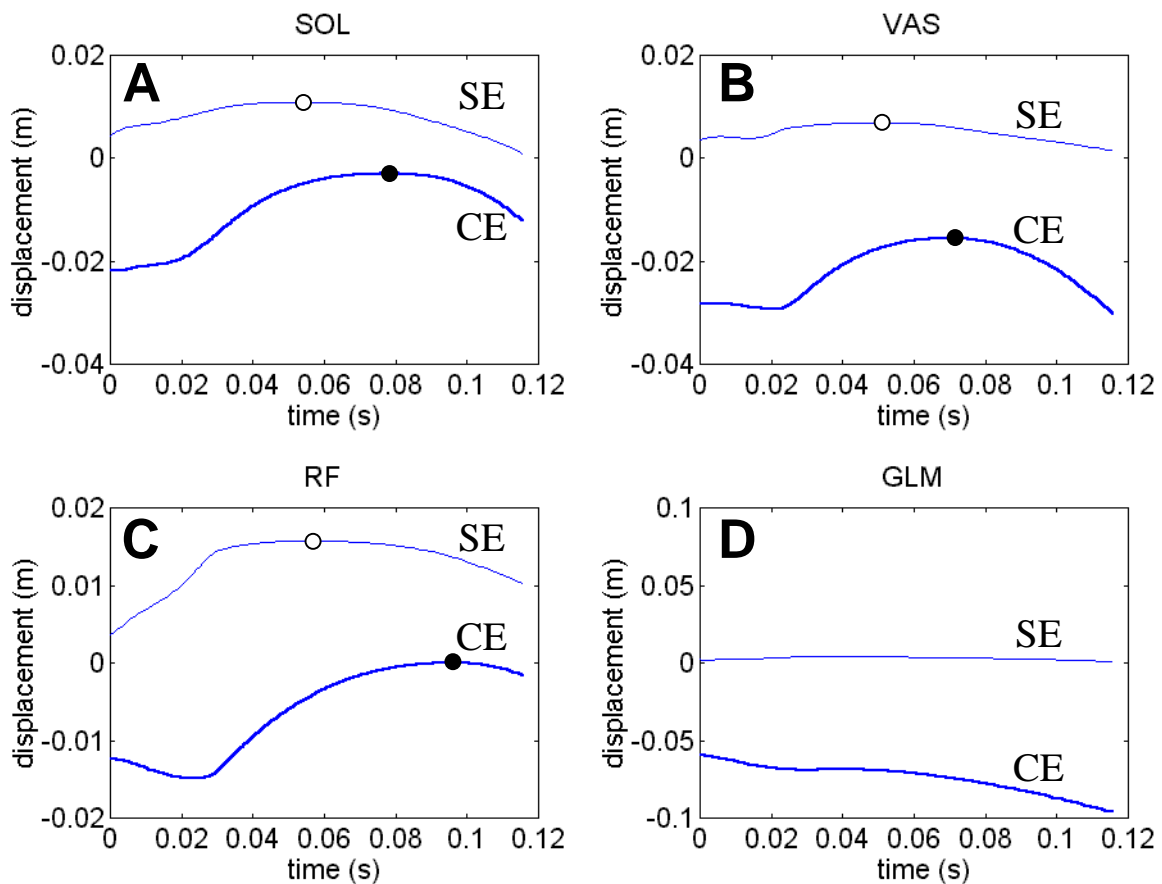
Fig. 6 Displacement of (A) SOL, (B) VAS, (C) RF and (D) GLM serial elastic (SE) and contractile elements (CE) during stance phase with respect to the tendon slack length $L_{SE,0}$ and the optimal fibre length $L_{CE,OPT}$. (A–C) In SOL, VAS and RF extension of the muscle fibres was delayed by about $20 - 30$ ms. About $20 - 40$ ms after maximum SE stretch (open circles) the CE reached the maximum displacement (filled circles). (D) In GLM muscle fibres (CE) were shortening during the whole contact phase.

The force shape of GLM was characterised by an early peak of about 1800 N (0.55 F_{MAX}) at 35 ms after touch-down followed by a steady descend. The highest forces were produced by SOL and VAS (almost 7000 N, 1.3 and 1.2 F_{MAX}). During the optimisation process these muscles became more and more synchronised and showed finally an almost identical sinusoidal force pattern.

Within the MTC's of SOL, VAS and RF the stretch occurred first in the serial elements (SE) with maximum displacements of about $0.4 - 1$ cm (Fig. 6). The contractile elements (CE) followed the stretch with a delay of $20 - 40$ ms and reach their maximum elongations (about $1.5 - 2$ cm) in the second half of the stance phase. In all four muscles, muscle fibres were operating below the optimal fibre length $\ell_{CE,OPT}$, i.e. at the ascending branch of the force-length relationship. The GLM was merely shortening during the whole ground contact.
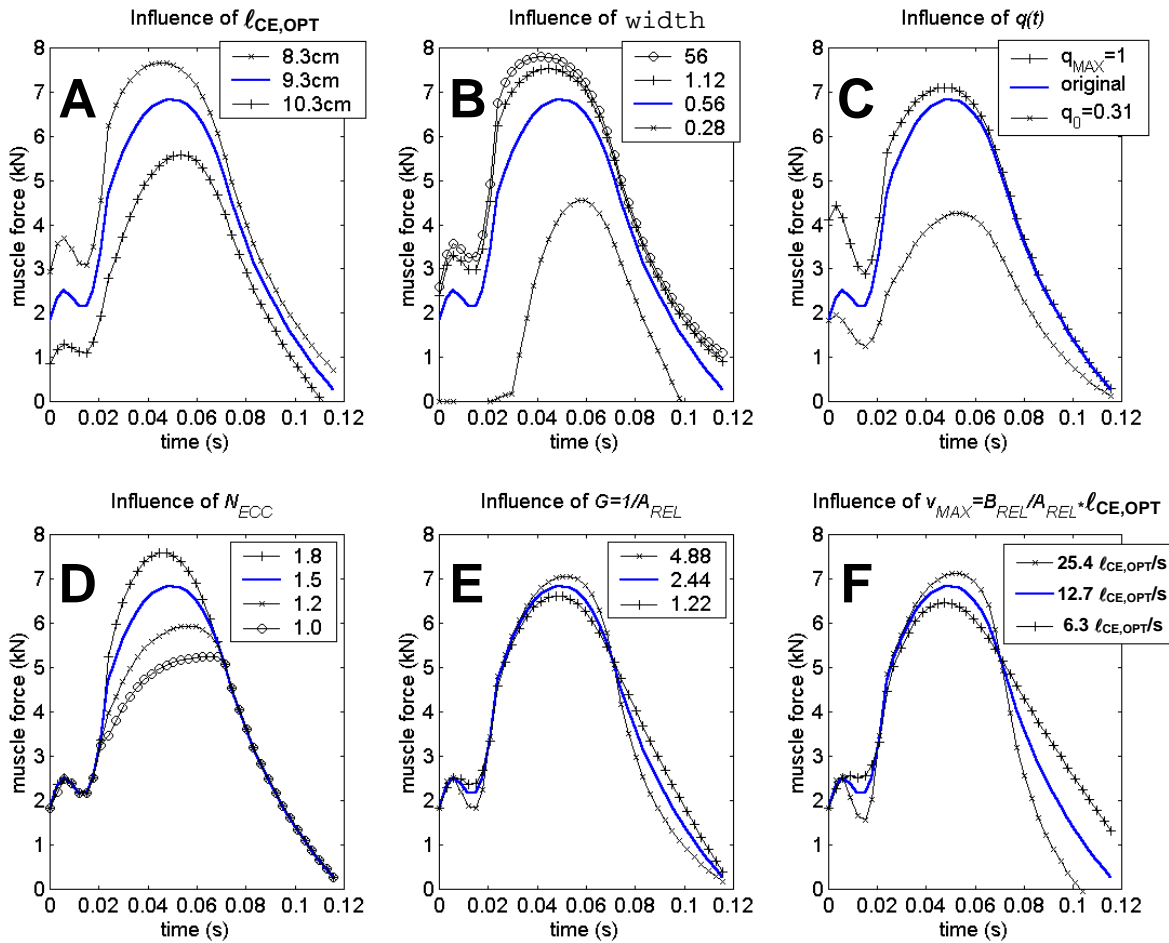
Fig. 7 Sensitivity of the predicted muscle (VAS) force pattern to (A) optimum fibre length $\ell_{CE,OPT}$, (B) `width` of the force-length relationship, (C) muscle activation q(t), (D) eccentric force enhancement N_{ECC}, (E) curvature G of the force-velocity function and (F) the maximum shortening velocity v_{MAX}. Hereby, the predicted fibre length $\ell_{CE}(t)$ and activation q(t) time sees of the optimised jump were used. The increase in muscle force and the instant of peak muscle force were mainly influenced by $\ell_{CE,OPT}$, `width`, q(t) and N_{ECC} (A–D). The shape of force descent was sensitive to G and v_{MAX} (E–F).

Sensitivity of muscle force to muscle properties (Fig. 7)

The predicted sinusoidal force pattern of the monoarticular SOL and VAS was a consequence of the chosen muscles parameters (for details: Van Soest and Bobbert, 1993; Van Soest 1992). To analyse the influence of the different muscle parameters on the predicted muscle force time series the forces of the VAS were recalculated using the tracings of the muscle fibre length $\ell_{CE}(t)$ and of the activation state q(t) obtained in the optimal solution.

The force build-up was mainly influenced by the force-length relationship ($\ell_{CE,OPT}$ and `width`), activation dynamics q(t) and eccentric force enhancement N_{ECC} (Fig. 7A-D). Within the force-length relationship larger optimal fibre lengths $\ell_{CE,OPT}$ and smaller `width` values may result in a steeper slope. Within the force time series (Fig. 7A: $\ell_{CE,OPT}$ = 10.3cm; Fig. 7B: `width` = 0.28) this could synchronise the force peak with the maximum joint flexion. In both cases a considerable loss in muscle force is observed. Working at the maximum of the force-length curve (smaller $\ell_{CE,OPT}$ or larger `width` value) increased the forces during leg shortening and midstance but had only little influence on muscle force during leg lengthening. The increasing activation level (q = 0.31 for t=0) till midstance (q ≈ 1) supported the continuos force increase during joint flexion. The level of eccentric force enhancement N_{ECC} (i.e. the ratio of maximum eccentric to maximum isometric force) had a strong influence of the shape of the muscle force during leg shortening and midstance. Obviously, the shape of the eccentric part of the force-velocity curve supported the almost sinusoidal form and the magnitude of the muscle force during this period. The first 20 ms no influence of N_{ECC} was found as the fibres were shortening.

The decrease in muscle force was largely influenced by the muscle's force-velocity characteristic represented by Hill's parameters A_{REL} and B_{REL} corresponding to the curvature G and the maximum muscle fibre shortening velocity v_{MAX} (detail in chapter IV; Fig. 7E,F). A steeper decent of the muscle force was observed for higher values for G and v_{MAX}. In contrast to Fig. 7E, different muscle forces were observed at the end of the ground contact for changes in the maximum shortening velocity v_{MAX}.
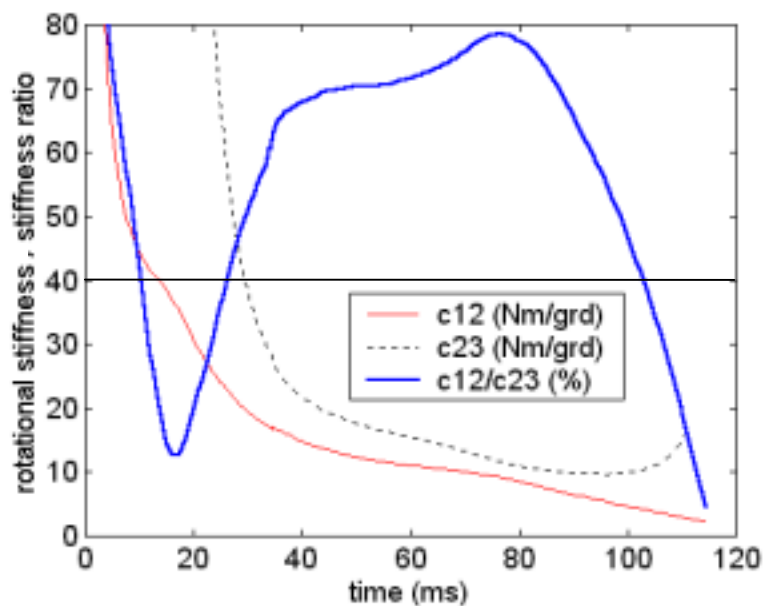
Fig. 8 Rotational stiffnesses at ankle (c_{12}) and knee (c_{23}) joint and stiffness ratio $R_C = c_{12} / c_{23}$. During active peak (0.3–0.9 t_C) the stiffness ratio R_C was well above 0.4.

Joint stiffness behaviour (Fig. 8)

At joint level, muscle preactivation resulted in high rotational stiffnesses at knee and ankle joint (c_{12}, c_{23}) during the first 10 ms after touch-down. After $30 - 40$ ms steadily descending stiffness values of less than 20 Nm/deg (1146 Nm/rad) were observed. During the active phase ($40 - 100$ ms) stiffness ratios R_C between 0.4 and 0.8 were observed. The first $10-30$ ms and at the end of the ground contact (last 10 ms) R_C values lower than 0.4 were found (Fig. 8).

DISCUSSION

In this study the mechanisms of leg stiffness in long jump were addressed. It was found, that leg stiffness originates from (1) quasi-elastically operating leg joints (due to muscle operation) and (2) a synchronised joint kinematics. According to the results of chapter III, this may result in a spring-like operation of the leg.

Muscle operation in the optimal solution

On knee and ankle joint the strongest monoarticular leg muscles (VAS and SOL) were active. To gain maximum performance, these muscles had to be fully activated during the whole stance phase. The level of preactivation at VAS was about 50% higher compared to SOL. The spring-like torque characteristics at knee and ankle joint were mainly due to the sinusoidal force pattern of these monoarticular muscles with maximum forces present at about

half the contact time (VAS 0.43 t_C, SOL 0.47 t_C). A comparable knee and ankle torque behaviour was found in an inverse dynamics analysis of the long jump by Stefanyshyn and Nigg (1998). They observed the highest torques at about midstance: for knee joint at $0.45 - 0.5$ t_C and for ankle joint at $0.5 - 0.6$ t_C. With regard to the net joint power curves (Fig. 7 in Stefanyshyn and Nigg, 1998) a similar quasi-elastic behaviour was found at knee and ankle joint with absorption during the first half and release in the second half.

The almost symmetric shape of the force patterns was associated with an synchronous flexion and extension of both joints. This resulted in comparable muscle lengthening tracings for SOL and VAS (Fig. 6). A similar timing of flexion and extension was found in experimental studies (Hay et al., 1999; Stefanyshyn and Nigg, 1998).

The biarticular muscles GAS and HAM were dropped out during the optimisation process. These muscles are less powerful compared to SOL and VAS. Furthermore, they are attributed to be responsible for the inter-segmental coordination (Van Ingen Schenau, 1989) which in the present study was completely controlled by the optimisation algorithm. Nevertheless, these muscles should be active during long jump (Kyröläinen et al., 1987). As shown in chapter III, a biarticular GAS could guarantee synchronous joint flexion at different landing conditions.

The action of the two remaining muscles RF and GLM was characterised by a lower level of preactivation and resulted in an almost parallel alignment of the upper body (HATL-segment) with the leg axis (Fig. 1C). As a result, only a moderate net power was predicted for the hip which agrees with the calculations of Stefanyshyn and Nigg (1998). A quasi-elastic operation was not present at the hip. As the ground reaction force was roughly pointing to the hip (due to the alignment of the HATL-segment) an existing hip stiffness could not contribute to the leg stiffness (Farley et al., 1998; chapter III).

The GLM was the only muscle which was only shortening during the ground contact and supplied energy at the hip joint. A part of this energy could by transferred to the knee by the biarticular RF which was slightly less preactivated than the GLM. This action of biarticular muscles could improve the quasi-elastic operation of the knee or ankle joint and should be investigated in more detail in future.

Importance of muscle and tendon properties on muscle force pattern

The symmetric shape of the force pattern of the monoarticular VAS was a consequence of the force-length relationship (Fig. 7A, B), the force-velocity relationship (Fig. 7D−F) and the activation dynamics q(t) (Fig. 7C). The muscle properties taken from the literature (Van Soest and Bobbert, 1993) proved to be suited to obtain the sinusoidal muscle force tracings.

The force generation was largely influenced by the force-length relationship, the activation dynamics and the shape of the eccentric force-velocity relationship. High muscle forces require to operate near to the optimum fibre length $\ell_{CE,OPT}$ and high eccentric forces. To obtain a symmetrical force pattern following situations were favourable:

(1) to operate slightly below the optimal fibre length,

(2) a `width` of about 0.5 in the force-length curve,

(3) approaching the maximum activation at about midstance,

(4) a considerable force enhancement (N_{ECC} about 1.5 or higher),

(5) to reach the maximum shortening velocity v_{MAX} (here 12.7 m/s) at take-off, and

(6) to adapt the curvature G (here 2.44) to the maximum shortening velocity.

The timing of the force peak was largely influenced by $\ell_{CE,OPT}$ (1) and the `width` (2) of the force-length curve. Furthermore, the instant of maximum lengthening velocity had a strong influence on the instant of maximum muscle force. A compliant serial elastic structure may delay the fibre lengthening (chapter IV).

The descent of muscle force was mainly influenced by the Hill-parameters (A_{REL} and B_{REL}) or the maximum shortening velocity and the curvature G, respectively, characterising the force-velocity relationship.

Requirements to the joint torque characteristics

Quasi-elastic joint operation requires maximum torque to occur at midstance and the same torques for equal joint configurations during loading and unloading. Monoarticular muscles are not able to work conservatively if maximum activation is assumed. Even by taking further serial elastic structure (e.g. aponeurosis) into account this problem can only be solved in part. As mentioned above, biarticular muscles could be used to transfer energy from more proximal joints to the knee and ankle joints. For instance, a delayed inset of biarticular GAS resulted in a reduced variance in leg stiffness, e.g. a more elastic behaviour.

The nonlinearity of the torque characteristic on joint level demanded in chapter III was mainly a consequence of the nonlinear tendon properties as shown in chapter IV. In this study a quadratic shape of the tendon stress-strain relationship was implemented. In fact, an exponent of about 1.7 would be necessary to result in a linear leg length – force relationship in the segmented system. The exponent of 2.0 resulted in a slightly curved descent (Fig. 3A). Nevertheless, there are other factors which might influence the exponent of the torque characteristic such as position dependent moment arms of the leg muscles and intrinsic muscle properties. For instance, the higher curvature (G = 5) used in chapter IV could compensate the lower exponent for the tendon stress-strain characteristics (1.75 or 1,

94

respectively) during leg lengthening (Fig. 7E). Finally, the action of biarticular muscles could imply a highly nonlinear increase of joint torque for unequal joint flexion or extension.

The leg stiffness in the optimal solution

The steady descent in the predicted leg stiffness $k_{LEG}(t)$ (Fig. 3B) was a consequence of the high eccentric work performed by the strongest monoarticular leg muscles (Figs. 5, 6). Although the length of the serial elastic elements (SE) was merely given by the tendon length and the contribution of the aponeurosis was neglected (Tab. 1: VAS $\ell_{SE,0} = 0.16$ m; in chapter IV: $\ell_{SE,0} = 0.42$ m) the previously predicted delay in CE stretch was still present (Fig. 6B). Nevertheless, the serial elastic structures within the muscle belly (aponeurosis) considered in chapter IV might explain the higher predicted variation in active leg stiffness STV (15.4%) in part. Recently, the mechanical properties of aponeurosis and tendon of the cat soleus muscle were found to be similar (Scott and Loeb, 1995). A doubled compliance of the serial elastic structures would reduce the stiffness variation below 10%. Especially the compliance of the most distal structures (like SOL) showed a strong influence on the stiffness variation (STV). This corresponds to elastic structures identified in the human foot which were not represented in this model (Ker et al., 1987).

Other origins of increased leg elasticity (lower STV values) could be biarticular muscles in the stance leg (see above) and movements of the remaining limbs with respect to the trunk. Contributions of the swing leg to jumping performance was studied in detail by Hildebrand and Prause (1988). According to their results, the acceleration of the swing leg leads to a prolonged ground contact and an increase in (kinetic) energy. Similar effects are assumable for the arm movement during the take-off phase of a long jump. Whether these effects are able to explain the predicted descent in the leg stiffness behaviour remains to be investigated.

Joint stiffness behaviour

The losses due to the eccentric muscle operation led to rotational stiffnesses (c_{12}, c_{23}) largely decreasing during the active peak (Fig. 8). In this period, the stiffness ratio R_C was in the range of the values predicted by the three segment-model (Fig. 11D in chapter III). Similar stiffness ratios were found in an inverse dynamics analysis of running (R_C about 0.5; Günther at al., in prep.). For equal knee and ankle joint angles, a stiffness ratio of 0.4 corresponds to an equal loading of both joint in a three-segmental leg. Due to the more flexed ankle joint position (about $25 - 30$ degree) with respect to the knee joint values of $0.5 - 0.8$ are required for a homogeneous joint loading (details in Chapter III). These values were present in the optimal solution during the active phase although the instantaneous joint stiffness values were

changing by a factor $2 - 3$. During the passive peak ($10 - 30$ ms), shortfall in ankle joint stiffness ($R_C < 0.4$) was compensated by heel contact which prevents ankle over-flexion.

Leg behaviour during the passive peak

Finally, the mechanisms of the first passive peak were addressed in this study. This was already done in chapter II (spring-mass model with a distal mass) and in chapter IV (two-segment model with one leg muscle). The four-segment model covers both contributions considered previously in separate studies: the effect of decelerated distal masses (chapter II) and the effect of high eccentric muscle forces together with an almost stretched leg immediately after touch-down. It was found, that the latter effect was of minor importance compared to the first one (Fig. 4). In contrast to the extended spring-mass model (chapter II), here the deceleration of rigid leg segments was modelled (no wobbling masses). This led to displacements of the contacting foot which were clearly larger than observed experimentally (predicted vertical displacement $\Delta y \approx 7$ cm).

The excursion of soft masses surrounding the rigid skeleton could explain this difference. These effects were neglected in this study. Thus, the description of the foot contact (Eq. 1a,b) is taking mechanical properties of the heel pad, foot deformation and wobbling masses (muscles, tendons, ligaments) of the stance leg into account. The mechanical properties of leg muscles could play an important role for the modulation of wobbling masses (first described by Gruber, 1987; Gruber et al., 1998). Therefore, the coupling parameters of the wobbling masses (swing mass in chapter II) are influenced by the activation state of the leg muscles. This would imply variations in the parameters of the force functions describing the foot contact in the present study (Eq. 1a,b).

GENERAL DISCUSSION AND CONCLUSION

VI

In this thesis the relationship between leg construction, leg performance and spring-like leg operation was addressed. The human long jump was taken as the movement of choice as a clear performance criterion exists.

The general dynamics of the long jump was investigated, first in a purely mechanical manner (chapter II), later taking muscle dynamics into account (chapter IV and V). Here the shape of the ground reaction force characterised by two clearly separated force peaks (passive and active peak) was guiding to an improved understanding.

The passive peak

The first peak was attributed to the deceleration of the distal segment masses in the stance leg. Thereby, the coupling of soft masses coupled to the skeleton had to be described by non-linear visco-elastic elements (chapter II). A neglect of this displacements would lead to unrealistic high forces after touch-down (Gruber, 1987; Gruber et al., 1998). Otherwise, a much more compliant (and larger) foot would be necessary to avoid the risk of joint damage.

This understanding of the passive peak contradicts the explanation given by Alexander (1990) who postulated that a highly activated extensor muscle could account for the first peak. In chapter IV his model was improved by a more realistic representation of the knee extensor muscle tendon complex. It was found, that the muscle's contribution to the passive peak could be moderate but clearly less than predicted previously. Finally, in chapter V, the origins of the passive peak were investigated taking muscle dynamics and distal segment masses into account. The contributions to the first peak could now be distinguished: The assumption in the first model (chapter II) was supported: the distal mass deceleration was the dominating effect. Nevertheless, the passive muscle properties could play an essential role for the shape of the passive peak. In fact, a main part of the soft masses in the leg segments consists of muscles. By changing the activation the mechanical properties of the muscles could be influenced (Meier and Blickhan, 1999). This would change coupling parameters in the nonlinear spring-damper element of the swing mass (chapter II).

The active peak

Despite the large variety in jumping style and performances observed experimentally, a surprisingly constant leg stiffness was found during the active peak (chapter II, V). Therefore, a linear spring was adequate to predict the shape of the ground reaction force (chapter II). But there are no springs in the leg which could account for the observed spring-like behaviour. A first approach was to identify the 'leg spring' within the zigzag of the leg segments (foot, shank, thigh; chapter III). This required to assume rotational springs at the joint. It was found how the rotational stiffnesses must be adjusted to the segment length design. Thereby nonlinear torque characteristics with exponents between 1.5 and 2.0 enhance the leg stability and result in an almost constant leg stiffness. This range seems to fit with experimental estimates of tendon properties which dominate the torque characteristics at excessive loading of the muscle-tendon complex (chapter IV). A higher exponent than 2.0 would improve leg stability for highly bent joint configurations (less than 40°). This exceeds the anatomical range of motion and would require more robust tissues (tendons, fibres, ligaments) to bear the increased loading rates.

Then, the elastic mechanisms of the structures surrounding the joints had to be identified. This was done first for one joint (knee: chapter IV) and finally for all major leg joints (ankle, knee, hip; chapter V). Torques had to rise continuously during leg shortening and to decrease smoothly during lengthening. It was shown that muscles can generate such a characteristic at a constant stimulation level at certain lengths due to the force-length, force-velocity and

activation characteristics (chapter V). At high loading rates, the nonlinear stress-strain property of the tendons may coin a nonlinearity in the joint torque characteristic (chapter IV).

Symmetrical operation of knee and ankle joint

A nonlinear torque characteristic forces the parallel operation of knee and ankle joint during leg loading (chapter III) and consequently results in an almost constant leg stiffness. Nevertheless, a proper adjustment of the rotational stiffnesses is still necessary to result in symmetrical loading configurations (chapter III). The optimisation procedure applied to the four-segment model was doing this almost perfectly by calculating the optimal stimulation pattern of the leg muscles. In reality, a considerable noise is present at the neural stimulation signals (Bobbert and van Zandwijk, 1999) and initial joint configurations. Under these circumstances biarticular muscles (depressed by the optimisation algorithm in chapter IV) could be of advantage. This was shown with the three-segmental spring-mass model in chapter III. The special design of the musculo-skeletal system provides stability on the single joint level (Wagner and Blickhan, 1999). This might also facilitate operation of multi joint systems.

The role of the foot

In chapter IV it was concluded that the missing foot required unrealistic high muscle forces to result in realistic ground reaction forces. This agrees with the statement noted above that the zigzag mode of leg loading realises the highest overall (leg) stiffness. On the other hand, introducing a redundant kinematic chain requires to generate torques at multiple joints. The high gain in leg stiffness is achieved by a relatively small foot which reduces the stiffness requirements at the ankle joint. The distance of the knee joint to the leg line of action can be reduced by a more flexed ankle joint (asymmetric loading). Nevertheless, a homogeneous loading of knee and ankle joint can be maintained by adapting the joint stiffnesses to the differences in joint angles. Here biarticular muscles and muscle-reflex circuits could support the stiffness regulation (Winters, 1995).

In contrast to the most vertical movements (hopping, countermovement jumps, drop jumps) where the foot orientation can be adjusted, in forward directed movements (like running) the foot position is mostly given by the heel contact in the first half of the contact phase. A foot fixed to the ground couples knee and ankle flexion. In a vertical movement, the flexion at ankle joint would be only half the flexion of the knee. This situation is not a symmetrical (or quasi-symmetrical) loading condition and is usually not realised.

In forward running or jumping the ankle flexion is about half the knee flexion plus the change in leg angle as long as the foot aligns with the ground. For symmetrical loading this fixes the relation between knee flexion and angle of attack.

The origins of leg lengthening

In chapter II the general dynamics of the long jump was described by a spring-mass model. To fit the experimental data the rest length of the leg spring had to be increased from touch-down to take-off. Mechanically this implies an additional supply of energy to the elastic energy of the spring which was subsequently released to the energy of the point mass. Where could this energy come from?

Starting on the joint level, a change in leg length could originate form different joint angles at touch-down and take-off. A change of the nominal joint angle could be realised by shifting the rest lengths (due to the force-length relationship) of antagonist muscles spanning the joint (Gielen et al., 1995). This could explain smooth changes in posture for some joint angles. Another way is to assume spring-like muscle properties as described by Feldman (1966) and supported by our findings in chapter V. Then the muscle force is characterised by a stiffness k and a threshold bias x which might be potentially controlled by neural commands to the muscle-reflex system (Winters, 1995).

In contrast to running or hopping, these strategies can not account for leg lengthening in long jump due to the almost stretched knee position and the relatively flat angle of attack at touch-down. Therefore, the movements of the remaining limbs (swing leg, arms) must be taken into account. The centre of mass moves forward and upward relative to the trunk as shown in Fig. 3 (chapter V). In fact, the acceleration of the swing leg (Hildebrand and Prause, 1988; Sørenson et al., 1999) and the arms (Hatze, 1981a) with respect to the body is an important technique to increase jumping performance as it allows to increase the amount and the angle of the take-off velocity. This corresponds to the low jumping distances of the model treated in chapter V where the masses of head, arms, trunk and swing leg were added to the rigid trunk segment.

How is spring-like leg operation related to leg performance?

Assuming a spring-like leg operation (chapter II) a minimal stiffness is necessary to achieve the maximum jumping distance for a given run-up speed (about 10 kN/m for a speed of 8.2 m/s). A further increase in leg stiffness will not improve the performance of the jump and requires a steeper angle of attack for maximum distance. Therefore, several strategies may

lead to the same distance. At the muscular level it was shown that maximising the leg performance may result in an almost linear leg stiffness (chapter IV and V). This was achieved by eccentrically operating (i.e. absorbing) leg extensor muscles. Therefore, for flatter angles of attack the energy absorption dominated due to higher loading speeds of the muscle (chapter IV). This led to an almost constant angle of attack (about 65°) predicted to result in maximum jumping performance for largely different run-up speeds ($6 - 12$ m/s). In our experiments about the same angle of attack was used by the subject independent of the jumping distance ($3.8 - 6.9$ m) and running speed ($6.5 - 9.1$ m/s).

The serial elastic structures connecting the muscle fibres to the skeleton support the quasi-elastic operation of the leg muscles by shifting the instant of maximum muscle lengthening velocity to about half the contact time (chapter IV and V). Spring-like operation requires to generate the highest forces at midstance. Due to the steep increase of the force-velocity relationship (eccentric force enhancement) maximal muscle stretching velocity and maximal muscle force occur almost simultaneously. For high stretching velocities a saturation in the eccentric force-velocity curve occurs at a critical muscle speed v_{Crit}. Therefore, the muscle stiffness is limited by the maximum eccentric force which can not be exceeded for fibre stretching velocities greater than the critical loading speed v_{Crit}. Higher muscle speeds would increase the energy losses dramatically with a decrease in muscle stiffness at further lengthening. A high increase in metabolic demands was found for running with an unusual amount of leg shortening (Groucho running: McMahon et al., 1987).

Finally, maximum performance requires a control that synchronises the joint movements (chapter III and V). Such a leg operation minimises the intermuscular energy exchange and results in the highest leg forces. Due to the predicted joint characteristics a spring-like leg operation was found to result in maximum jumping distance. Optimised segment kinematics with respect to minimal distances of the joints to the force line of action may lead to a maximised leg stiffness (chapter III). It remains for further investigations whether this explains e.g. the differences in aerobic demands observed in treadmill running for different leg stiffnesses (Dalleau et al., 1998; Heise and Martin, 1998) or changes of the leg kinematics during exhaustive exercises (e.g. distance running: Williams et al., 1991).

Further steps

In the future the focus will be on following three general directions:

- verification, adaptation and generalisation of the principles of spring-like legs for other types of movement (running, vertical hopping) and for animal locomotion including evolutionary and ontogenetic aspects of leg design;
- application to technical systems (robotics), ergonomics and prosthetics;
- integration of neuro-physiological and metabolic aspects of muscle operation.

Many strategies of leg construction and control presented in this study seem to fit to other types of human or animal motion. For instance, the three segment model was already successfully adapted to the hind limb of running cockroaches. As an approximation for the overall leg function the front and hind limbs of small mammals may be looked at as a z-shaped pantograph. Functionally, scapula, humerus and radius/ulna of the front limb of quadrupeds correspond to the femur, tibia/fibula and metatarsals of the hind limb (Fischer and Witte, 1998). Taking the most distal segments into account a four segmental representation with a z-shaped proximal and a bowed distal part seems to be more appropriate. In fast synchronous gaits, the pelvis significantly rotating against the lumbar vertebral column in the lumbar region is used as an additional proximal segment of the hind limb.

Currently, a physical model is build to illustrate the predicted mechanisms of stiffness adjustment of a multisegmental chain with variable segment lengths and exponents of the torque characteristic and a set of different springs (supported by C. Schilling, TU Ilmenau). With regard to technical applications the local implementation of muscle-like actuators is of general importance. At the muscle and joint level neuronal feedback mediated by muscle spindles and tendon organs can also result in a spring-like behaviour (Blickhan, 1996). The stiffness is largely determined by the gain within the reflex loop. Thus, suitable reflexes could also help to control multisegmental systems (Winters, 1995). This influence will be investigated in the next future.

Reflex control is not suitable for highly dynamic situations due to the synaptic delay and the time necessary for force generation. Certainly, any system with mechanical properties resulting by itself in a robust behaviour is much easier to control. Such solutions seem to be preferred by nature.

REFERENCES

VII

Alexander, R. McN. and Vernon, A. (1975). The dimensions of the knee and ankle muscles and the forces they exert. *J. Hum. Mov. Stud.* **1**, 115-123.

Alexander, R. McN., Bennett, M. B. and Ker, R.F. (1986). Mechanical properties and functions of the paw pads of some mammals. *J. Zool. A* **209**, 405-419.

Alexander, R. McN. (1988). *Elastic Mechanisms in Animal Movement.* Cambridge: University Press.

Alexander, R. McN. (1990) Optimum take-off techniques for high and long jumps. *Phil. Trans. R. Soc. Lond.* B **329**, 3-10.

Alexander, R. McN. (1995) Leg design and jumping technique for humans, other vertebrates and insects. *Philos. Trans. R.. Soc. Lond. B* **347**(1321), 235-48.

Bernstein, N. (1967) The coordination and regulation of movements. Oxford: Pergamon Press.

Blickhan, R. (1989) The spring-mass model for running and hopping. *J. Biomech.* **22**, 1217-1227.

Blickhan, R., Friedrichs, A., Rebhan, F., Schmalz, T., and Wank, V. (1995) Influence of speed, stiffness, and angle of attack on jumping distance. *Book of Abstracts.* XVth Congress of the International Society of Biomechanics (Jyväskylä), 108-109.

Blickhan, R. (1996) Motorische Systeme bei Vertebraten. In: *Neurowissenschaft: vom Molekül zur Kognition* (Hrsg. Dudel, J., Menzel, R., Schmidt, R. F.). Springer Verlag, Berlin, Heidelberg, New York. 191-213.

Bobbert, M. F. and van Soest, A. J. (1994) Effects of muscle strengthening on vertical jumps: a simulation study. *Med. Sci. Sports Exerc.* **27**, 1012-1020.

Bobbert, M. F. and van Zandwijk, J. P. (1994) Dependence of human maximum jump height on moment arms of the biarticular m.gastrocnemius; a simulation study. *Hum. Mov. Sci.* **13**, 697-716.

Bobbert, M. F. and van Zandwijk, J. P. (1999) Sensitivity of vertical jumping performance to changes in muscle stimulation onset times: a simulation study. *Biol. Cybern.* **81**, 101-108.

Bobbert, M. F., Gerritsen, K. G. M., Litjens, M. C. A., and Soest, A. J. van (1996) Why is countermovement jump height greater than squat jump height? *Med. Sci. Sports Exerc.* **29**, 1402-1412.

Close, R. I. (1972). Dynamic properties of mammalian skeletal muscles. *Physiol. Rev.* **52**, 129-197.

Dalleau, G., Belli, A., Bourdin, M. and Lacour, J. R. (1998) The spring-mass model and the energy cost of treadmill running. *Eur. J. Appl. Physiol.* **77**, 257-263.

Doorenbosch, C. A. M., Harlaar, J., Roebroeck, M. E. and Lankhorst, G. J. (1994) Two strategies of transferring from sit-to-stand; the activation of monoarticular and biarticular muscles. *J. Biomech.* **27**, 1299-1307.

Doorenbosch, C. A. M. and van Ingen Schenau, G. J. (1995) The role of mono- and biarticular muscles during contact control leg tasks in man. *Hum. Mov. Sci.* **14**, 279-300.

Dornay, M., Mussa-Ivaldi, F. A., McIntyre, J. and Bizzi, E. (1993) Stability constraints for the distributed control of motor behavior. *Neural Networks* **6**, 1045-1059.

Denoth, J. (1986) Load on the locomotor system and modelling. Chapter 3 in: Biomechanics of running shoes (ed. Nigg, B. M.) Human Kinetics Publishers, Champaign.

Ettema, G. J. C. (1996) Elastic length-force characteristics of the gastrocnemius of the hopping mouse (notomys alexis) and the rat (rattus norvegicus). *J. Exp. Biol.* **199**, 1277-1285.

Farley, C. T., Glasheen, J., and McMahon, T. A. (1993) Running springs: Speed and animal size. *J. Exp. Biol.* **185**, 71-86.

Farley, C. T. and González, O. (1996) Leg stiffness and stride frequency in human running. *J. Biomech.* **29**, 181-186.

Farley, C. T., Houdijk, H. H. P., van Strien, C. and Louie, M. (1998) Mechanisms of leg stiffness adjustment for hopping on surfaces of different stiffnesses. *J. Appl. Physiol.* **85(3)**, 1044-1055.

Farley, C. T. and Morgenroth (1999) Leg stiffness primarily depends on ankle stiffness during human hopping. *J. Biomech.* **32**, 267-273.

Feldman, A. G. (1966) Functional tuning of the nervous system during control of movement or maintenance of a steady posture. II. Controllable parameters of the muscle. *Biophyzika* **11**, 565-578.

Ferris, D. P. and Farley, C. T. (1997) Interaction of leg stiffness and surface stiffness during human hopping. *J. Appl. Physiol.* **82**, 15-22.

Fischer, M. S. and Witte, H. (1998) The functional morphology of the three-segmented limb of mammals and its specialities in small and medium-sized mammals.

Flash, T. (1987) The control of hand equilibrium trajectories in multi-joint arm movements in man. *Biol. Cybern.* **57**, 257-274.

Friedrichs, A., Seyfarth, A., Wank, V., and Blickhan, R. (in prep.) Spring-like behaviour in long jump – an experimental approach.

Full, R. J. and Tu, M. S. (1991) Mechanics of a rapid running insect: two-, four- and six-legged locomotion. *J. Exp. Biol.* **156**: 215-231.

Gielen, C. C. A. M., van Bolhuis, B. M. and Theeuwen, M. (1995) On the control of biologically and kinematically redundant manipulators. *Hum. Mov. Sci.* **14**, 487-509.

Gruber, K. (1987) „Entwicklung eines Modells zur Berechnung der Kräfte im Knie- und Hüftgelenk bei sportlichen Bewegungsabläufen mit hohen Beschleunigungen." *Dissertation* Universität Tübingen

Gruber, K., Ruder, H., Denoth, J., and Schneider, K. (1998) A comparative study of impact dynamics: wobbling mass model versus rigid body models. *J. Biomech.* **31**, 439-444.

Günther, M., Sholukha, V., Blickhan, R. (in prep.) Joint stiffness of the ankle and the knee in running – an inverse analysis and simulation approach.

Günther, M. (1997) Computersimulationen zur Synthetisierung des muskulär erzeugten menschlichen Gehens unter Verwendung eines biomechanischen Mehrkörpermodells. Dissertation, Tübingen.

Hatze, H. (1981a) A comprehensive model for human motion simulation and its application to the take-off phase of the long jump. *J. Biomech.* **14**, 135-142.

Hatze, H. (1981b) *Myocybernetic control models of skeletal muscle*. University of South Africa, Pretoria. pp 31-42.

Hay, J. G., Miller, J. A. and Canterna, R. W. (1986) The techniques of elite male long jumpers. *J. Biomech.* **19**, 855-866.

Hay, J. G. and Nohara, H. (1990) Techniques used by elite long jumpers in preparation for takeoff. *J. Biomech.* **23**, 229-239.

Hay, J. G. (1993) Citius, altius, longius (faster, higher, longer): The biomechanics of jumping for distance. *J. Biomech.* **26** (Suppl. 1), 7-22.

Hay, J. G., Thorson, E. M. and Kippenhan, B. C. (1999) Changes in muscle-tendon length during the take-off of a running long jump. *J. Sports Sci.* **17**, 159-172.

Heise G. D. and Martin P. E. (1998) "Leg spring" characteristics and the aerobic demand of running. *Med. Sci. Sports Exerc.* **30(5)**, 750-754.

Hildebrand, F. and Prause, K. D. (1988) Biomechanische Modellierung und Simulation der Absprungbewegung beim Weitsprung. *Theorie und Praxis des Leistungssports* **1-88**, 104-120.

Hollerbach, J. M. (1990) Fundamentals of motor behavior. In: D. N. Osherson, S. M. Kosslyn and J. M. Hollerbach (Eds.) Visual Cognition and Action: An Invitation to Cognitive Science, 151-182.

Ker, R. F. (1981) Dynamic tensile properties of the plantaris tendon of sheep (*Ovis aries*) *J. Exp. Biol.* **93**, 283-302.

Ker, R. F., Bennett, M. B., Bibby, S. R., Kester, R. C. and Alexander R. McN. (1987) The spring in the arch of the human foot. *Nature* **325**, 147-149.

Kovacs, I., Tihanyi, J., Devita, P., Racz, L., Barrier, J. and Hortobagyi, T. (1999) Foot placement modifies kinematics and kinetics during drop jumping. *Med. Sci. Sports Exerc.* **31(5)**:708-16.

Kyröläinen, H., Avela, J., Komi, P. V. and Gollhofer, A. (1987) Function of the neuromuscular system during the last two steps in the long jump. In: *Biomechanics XI-B*. (eds. de Groot, G., Hollander, A. P., Huijing, P. A., van Ingen Schenau, G. J) pp. 557-560. Amsterdam: Free University Press.

Lagarias, J.C., J. A. Reeds, M.H. Wright, and P. E. Wright (1997) "Convergence Properties of the Nelder-Mead Simplex Algorithm in Low Dimensions," May 1, 1997. To appear in the SIAM Journal of Optimisation.

Lees, A., Graham-Smith, P., and Fowler, N. (1994) A biomechanical analysis of the last stride, touchdown, and takeoff characteristics of the men's long jump. *J. Appl. Biomech.* **10**, 61-78.

Luhtanen, P. and Komi, P. V. (1979) Mechanical power and segmental contribution to force impulses in long jump take-off. *Eur. J. Appl. Physiol.* **41**, 267-274.

McMahon, T. A. and Greene, P. R. (1979) The influence of track compliance on running. *J. Biomech.* **12**, 893-904.

McMahon, T. A., Valiant, G. and Frederick, E. C. (1987) Groucho running. *J. Appl. Physiol.* **62**, 2326-2337.

McMahon, T. A. and Cheng, G. C. (1990) The mechanics of running: How does stiffness couple with speed? *J. Biomech.* **23**, Suppl. 1, 65-78.

Meier, P. and Blickhan, R. (2000) FEM-Simulation of skeletal muscle: The influence of inertia during activation and deactivation. Symposium on Skeletal Muscle Mechanics, Canmore (Alberta), 1999. Wiley & Sons. (to appear 2000).

Mussa-Ivaldi, F. A., Morasso, P. and Zaccaria, R. (1988) Kinematic networks. A distributed model for representing and regularizing motor redundancy. *Biological Cybernetics* **60**, 1-16.

Otten., E. (1987) A myocybernetic model of the jaw system of the rat. *J. Neurosci. Methods* **21**, 287-302.

Özgüven, H. N. and Berme, N. (1988) An experimental and analytical study of impact forces during human jumping. *J. Biomech.* **21**, 1061-1066.

Pandy, M. G., Zajac, F. E., Sim, E. and Levine, W.S. (1990). An optimal control model for the maximum-height human jumping. *J. Biomech.* **23**, 1185-1198.

Pierrynowski, M. R. (1985). A physiological model for the evaluation of muscular forces in human locomotion: theoretical aspects. *Math. Biosci.* **75**, 69-101.

Shadmer, R., Mussa-Ivaldi, F. A. and Bizzi, E. (1993) Postural force fields of the human arm and their role in generating multijoint movements. *J. Neurosci.* **13**, 45-62.

Scott, S. H. and Loeb, G. E. (1995) Mechanical properties of aponeurosis and tendon of the cat soleus muscle during whole-muscle isometric contractions. *J. Morphol*. 224(1),73-86.

Seyfarth, A., Friedrichs, A., Wank, V. and Blickhan, R. (1999) Dynamics of the long jump. *J. Biomech.* **32**, 1259-1267.

Seyfarth, A., Blickhan, R. and van Leeuwen, J. L. (2000) Optimum take-off techniques and muscle design for long jump. *J. Exp. Biol.* **203**, 741-750.

Smeets, J. B. J. (1994) Biarticular muscles and the accuracy of motor control. *Hum. Mov. Sci.* **13**, 587-600.

Sørenson, H., Simonsen, E. B., and van den Bogert, A. J. (1999) A simulation model of the long jump take-off. VIIth International Symposium on Computer Simulation in Biomechanics, University of Calgary.

Spector, S. A., Gardiner, P. F., Zernicke, R. F., Roy, R.R and Edgerton, V. R. (1980). Muscle architecture and force-velocity characteristics of cat soleus and medial gastrocnemius: implications for motor control. *J. Neurophys.* **44**, 951-960.

Stefanyshyn, D. J. and Nigg B. M. (1998). Contribution of the lower extremity to the mechanical energy in running vertical jumps and running long jumps. *J. Sport Sci.* **16**, 177-186.

Van Ingen Schenau, G. J. (1989). From rotation to translation: constraints on multi-joint movements and the unique action of biarticular muscles. *Hum. Mov. Sci.* **8**, 301-337.

Van Leeuwen, J. L. (1992). Muscle function in locomotion. In: *Advances in comparative and environmental physiology 11: Mechanics of Animal Locomotion.* (ed. R. McN. Alexander), pp. 191-242. Heidelberg, Berlin: Springer-Verlag.

Van Soest, A. J. (1992) Jumping from Structure to Control. A Simulation Study of Explosive Movements. PhD Dissertation, Free University Amsterdam. Thesis Publishers Amsterdam.

Van Soest, A. J. and Bobbert, M. F. (1993) The contributions of muscle properties in the control of explosive movements. *Biol. Cybern.* **69**, 195-204.

Wagner, H. and Blickhan, R. (1999) Stabilizing function of skeletal muscles: an analytical investigation. *J. Theor. Biol.* **199**, 163-179.

Williams, K. R., Snow, R. and Agruss, C. (1991) Changes in distance running kinematics with fatigue. *Int. J. Sport Biomech.* **7**, 138-162.

Winters, J. M. and Woo, S. L-Y. (1990) (eds.). Multiple Muscle Systems: Biomechanics and Movement Organization. New York: Springer Verlag.

Winters, J. M. (1995) How detailed should muscle models be to understand multi-joint movement coordination? *Hum. Mov. Sci.* **14**, 401-442.

Witters, J., Bohets, W. and Van Coppenolle, H. (1992). A model of the elastic take-off energy in the long jump. *J. Sport Sci.* **10**, 533-540.

Zajac, F. E. (1993). Muscle coordination of movement: a perspective. *J. Biomech.* **26** (Suppl. 1), 109-124.

ACKNOWLEDGEMENTS

IIX

ACKNOWLEDGEMENT

First of all I would like to thank my supervisors: Prof. Reinhard Blickhan directed my attention to the issues concerning the spring like leg operation. He supported this work during the whole time enormously by his guiding questions and suggestions.

During the work described in chapter II, Arnd Friedrichs and Prof. Gerhard Kluge were always available for discussions about the meaning and the realisation of the spring-mass model. Veit Wank and Thomas Schmalz were involved in the experimental studies.

The two-segment model addressed in chapter IV was largely supervised by Prof. Johan van Leeuwen at the University of Leiden. The discussions with him helped me a lot to become familiar with muscle dynamics.

The three-segment model introduced in chapter III was largely inspired by fruitful discussions with Dr. Michael Günther and Heiko Wagner. Especially Michael supported this work by his matter-of-fact way of thinking. His motivation helped enormously to understand all the tricky mechanisms of multi-segment legs.

Last not least the four-segment model presented in chapter V was created within a very intensive cooperation with Dr. Maarten Bobbert from the Faculty of Movement Science at the Free University Amsterdam. Only his experiences in simulating human body movements made it possible to develop such a model.

I would like to thank Prof. J. L. van Leeuwen (Wageningen), Prof. C. Farley and D. Ferris (both UC Berkeley) for useful comments on a draft of chapter II. G. Kluge helped to verify the equations of motion of the extended spring-mass system (chapter II). Professor R. F. Full (UC Berkeley) gave useful comments on a draft of chapter IV.